The role of *Grainyhead-like* Transcription Factors in Craniofacial Development and Tissue Fusion

A thesis submitted for the degree of Master of Science

Jarrad Nathan Fuller

Bachelor of Biomedical Science

Submitted in total fulfilment of the requirements of the degree Master of Science Department of Physiology, Anatomy and Microbiology,

College of Science, Health and Engineering

La Trobe University, Victoria, Australia

Submitted November 2021

Statement of Authorship

Except where reference is made in the text of the thesis, this thesis contains no material published elsewhere or extracted in whole or in part from a thesis accepted for the award of any other degree or diploma. No other person's work has been used without due acknowledgment in the main text of the thesis. This thesis has not been submitted for the award of any degree or diploma in any other tertiary institution

All research procedures reported in this thesis were approved by the relevant ethics committee.

This work was supported by an Australian Government Research Training Program Scholarship.

Jarrad Fuller, 20/11/2021

COVID-19 impact statement

Due to the events of COVID-19, various obvious avenues for further investigation were not able to be pursued (for example the use of additional in-situ hybridisation riboprobes, particularly *dlx2, dlx3, edn1* and *hand2*) and optimisation of antibodies (pSMAD 1/5/8 and *Noggin*) in Western blot/immunohistochemistry experiments.

Additionally, existing data produced by Dr. Seb Dworkin, during his time as a post-doctoral research scientist in the lab of Prof. Stephen Jane, Monash University, between 2011-2014 was provided during 2020 to facilitate the honours project which formed the 1st year of this Master's degree. Both qualitative and quantitative data were provided (raw data only), and all statistical analyses, figure generation and interpretation of these data were performed by Jarrad. The data provided forms sections 3.2.1-3.2.3 of this thesis.

Abbreviations

Abbreviation	Full term
bh	Basihyal
bmp	Bone morphogenetic protein
cb	Ceratobranchial
ch	ceratohyal
cl	Cleft lip
cldn	claudin
cp	Cleft palate
edn1	Endothelin 1
EMT	Epithelial-mesenchymal transition
ep	Ethmoid plate
fgf	Fibroblast growth factor
fgfr	Fibroblast growth factor receptor
GRHL/Grhl/grhl	Grainyhead-like (human/mouse/zebrafish orthologues)
gsc	Goosecoid
hs	Hyosymplectic
HYB-	Prehybridisation buffer
HYB+	Hybridisation buffer
mc	Meckel's cartilage
NBT	Nitro Blue Tetrazolium Chloride
NCC	Neural crest cell
Os	Optic stalk
Ov	Otic vesicles
NT/NTD	Neural tube/neural tube defect
PA	Pharyngeal arches
PCP	Planar cell polarity
PBST	Phosphate buffered saline with Tween
pch	Parachordial cartilage
pq	Palatoquadrate
Shh	*Sonic Hedgehog*
TGF- β	Transforming growth factor beta
VWS	Van-Der Woude syndrome
WISH	Whole-mount In-situ hybridisation

Acknowledgements

I would like to thank a number of people, without whom I could not have made it through this year. First and foremost, I want to thank my supervisor Dr. Sebastian Dworkin for everything you have done to make sure my year was a success. Despite the challenges posed by the pandemic, you always found time to help me with my endless list of questions and provided me with the encouragement I needed to make it through this year. I really couldn't have asked for a better supervisor. I also want to thank PhD candidates Jemma Gasperoni and Nishanthi Mathiyalagan for their help in guiding me through my time in the lab, and patience in putting up with my questionable lab skills. I'm also incredibly grateful for the work of the staff at the La Trobe Animal Research and Training Facility – In particular Tanmay Shekhar for providing me with excellent training in zebrafish handling, as well as Dr Marina Carpinelli and Dr Tariq Butt at the Australian centre for blood diseases for providing me with invaluable samples when I needed them most. Lastly, I want to thank my fellow master's students, particularly Jeremy Neylon, Daniel Couch, Tayla Gibson-Hughes, Buddhila Wickramasinghe and Liana Theodoridis for making this year such a great experience for me.

Abstract

Craniofacial defects are amongst the most common birth defects worldwide, with malformations of the head or face affecting approximately 1 in 250 live births and often necessitating invasive surgery. Despite their widespread impact, the aetiology of over 50% of birth defects remains unknown. This project aims to investigate the roles played by *the Grainyhead-like* transcription factor family, as well as its' putative target genes *tmem54a tmem54b, pvrl4* and *noggin,* using both zebrafish (*Danio rerio*) and mouse models. This project also aims to identify additional putative target genes. *grhl*3, tmem54 and *pvrl4* gene expression was inhibited in zebrafish and resulted in a variety of craniofacial defects, which revealed defects in rhombomere and 1st pharyngeal arch (PA1) development using Whole-mount In-Situ Hybridisation (WISH). Taken together, these results demonstrated roles for the *grhl3*-dependent transcriptional network in craniofacial development. The expression of genes previously implicated in the aetiology craniofacial defects, including genes from the Shh pathway, Fgfr2 and Ovol1 were investigated in *Grhl2*$^{-/-}$ mice. Differential expression of Shh pathway genes Gli1, Gli2 and Gli3, as well as Fgfr2 and Ovol1 was detected in some, but not all, tissues extracted from the facial prominences and PA1 of developing *Grhl2*$^{-/-}$ mouse embryos. These results suggest a role for Shh, Fgfr2 and Ovol1 in *Grhl2* signaling in the developing murine face and cranium. An approach for the investigation of the Bmp antagonist and *Grhl2* target gene *Noggin* in *Grhl2*-related defects was demonstrated using Immunohistochemistry (IHC) and Western blotting. The identification of *Grhl* target genes and subsequent investigation of their functions in craniofacial defects, aids in the understanding of the mechanisms that lead to craniofacial disease.

Table of Contents

Chapter 1

Introduction

1.1 The costs and burdens of birth defects

Birth defects represent a significant burden, to both sufferers and the healthcare system. Common birth defects such as neural tube defects, cleft palate and congenital heart defects are associated with poorer quality of life, shorter lifespans and are difficult to rectify medically (Oster et al., 2013). Moreover, studies suggest that a number of corrective surgeries may also result in further developmental complications, including aberrant growth of the maxilla (Hsieh, Ko, Chen, & Huang, 2010; Richardson, Krishna, & Khandeparker, 2018). Additionally, congenital malformations are the most common cause of death amongst infants worldwide, contributing to 20% of infant mortality and thus representing a widespread and important target for research (Xu, Kochanek, Murphy, & Arias, 2014).

The cost of rectifying congenital abnormalities is immense, even in developed countries. In the United States, the total cost of birth defects has been estimated to exceed $22.9 billion annually (Arth et al., 2017). Many of the most common birth defects are also the most costly; congenital cardiovascular defects are both the most common and most expensive defects – affecting 1 in 100 births and costing over $5.5 billion each year (Botto, 2015). Further, in cases where congenital defects may be left untreated such as cleft lip and palate, the financial ramifications over the individual's lifetime due to communication disorders could exceed $2,500 per person per year. Clearly, congenital defects represent a significant financial burden on the healthcare system and those individuals who suffer from them.

However many of the most common birth defects also carry a significant burden psychologically and socially for sufferers and their families. Defects such as cleft lip and palate can necessitate both invasive and expensive surgery, as well as ongoing speech therapy (Burg, Chai, Yao, Magee, & Figueiredo, 2016; Harding & Grunwell, 1996). Multiple studies have associated these conditions with psychological and social challenges, particularly in adolescents and children (Hunt, Burden, Hepper, Stevenson, & Johnston, 2006), with one study even linking facial clefts with higher rates of suicide (Christensen, Juel, Herskind, & Murray, 2004). The immense cost both financially and socially on the healthcare system and sufferers of congenital defects, necessitates further research which can potentially limit the incidence and severity of these conditions.

1.2 Birth defect prevalence

The incidence of congenital defects globally, varies significantly from region to region, often as a result of economic factors, diet and genetics. Income plays a significant role in the epidemiology of birth defects globally (Cubitt, Hodges, Van Lierde, & Swan, 2014). 60% of birth defects occur in low-income countries, as do 72% of all early deaths in infants, while low-income countries comprise only 55% of overall births annually (March of Dimes, 2006). The overall contribution of congenital defects to death amongst children under 5 is 7% (WHO, 2004). This figure also varies significantly between regions, in Africa only 5% of under 5 deaths are due to congenital defects, whilst in Europe 19% of under 5 deaths are due to congenital defects (WHO, 2020). The relatively low contribution of congenital defects to overall mortality in children under 5 in Africa is undoubtedly due to pathogen and malnutrition-induced diseases that are largely treatable or rare in developed countries. However, the relatively high contribution of birth defects toward child mortality in Europe indicates a lack of preventative and curative therapies and highlights the need for a greater understanding of the risk factors influencing congenital defects and how to mitigate them.

The disproportionate rate of congenital defects in the third world suggests that malnourishment is clearly a key contributor in low income regions. A number of studies have linked nutrient deficiencies to higher rates of birth defects, particularly Vitamin D, B12 and folate (Hernández-Díaz, Werler, Walker, & Mitchell, 2000; Mulligan, Felton, Riek, & Bernal-Mizrachi, 2010; Pitkin, 2007; Refsum, 2001). Further, wealthier countries are able to avoid the potential effects of these deficiencies through fortification of foodstuffs and early diagnoses facilitated by more effective public health systems (Lassi et al., 2020). Folic acid deficiency is implicated in up to 70% of neural tube defects (Wald, 1991), and consequently, fortification of foodstuffs with folate has been mandated in many countries (Atta et al., 2015). This has been successful in decreasing the prevalence of neural tube defects - in the United States, folate fortification was mandated in 1998, and subsequently a 19% drop in neural tube defects was observed (Honein, Paulozzi, Mathews, Erickson, & Wong, 2001). The efficacy of fortification programs demonstrates both the role of non-genetic factors in birth defects, as well as the importance of identifying causative factors and implementing preventative measures.

In third world countries however, deficiency still plays a significant role in the prevalence of congenital abnormalities and premature deaths (Ţarcă et al., 2021). Nutrient deficiency and malnourishment are associated with low birth weight and in turn, low birth weight is associated with a myriad of defects both at birth and later in development (Basnet, Gauchan, Shrestha, & Jha, 2021). Third world countries account for the vast majority of low birth weight infants, with

incidences in some South Asian countries exceeding 30% (de Wilde, van Buuren, & Middelkoop, 2013). As a result, malnutrition and the low birth weight that can result, influence the proportion of birth defects present in developing countries. The intake of various teratogens have also contributed to severe birth defects both in developing and developed countries. The effects of thalidomide use during pregnancy and the resulting limb defects observed in the 1960's are a well-known example of the potentially deleterious effects of chemicals with regard to birth defects (Webb, 1963). Similarly, a plethora of evidence suggests that prenatal smoking and alcohol intake lead to complications and defects during pregnancy (Malik et al., 2008). The influence of malnutrition and teratogen exposure on birth defect incidence provides further evidence of the importance of preventative measures in lowering defect incidence.

The potential mechanisms through which the teratogens act to produce defects can include chemical-gene interactions. A number of gene pathways have been identified as potentially being dysregulated by thalidomide and contributing to limb defects. Increased expression of *Bmp* and *Dkk* genes was identified in response to thalidomide exposure, and given that these genes have known pro-apoptosis roles, are likely involved in the stunted development of limbs in thalidomide-exposed embryos (Knobloch & Rüther, 2008). Teratogens found in tobacco smoke are known to influence the incidence of cleft palate in embryos (Knopik, Maccani, Francazio, & McGeary, 2012). In particular, binding to the aryl hydrocarbon receptor leads to aberrant expression of both the detoxifying gene CYP1A1 as well as TGF-β genes, both of which are important in palate fusion (Knopik et al., 2012). The effects of these substances on embryonic development underscores the various aetiologies implicated in congenital defects, as well as the importance of investigating the pathways that lead to birth defects so as to prevent their occurrence.

While gene-environment interactions play significant roles in congenital defects, gene mutations represent the primary underlying cause of birth defects (Hall & Solehdin, 1998). It has been estimated that as many as 20% of all birth defects are due solely to genetic mutation (Feldkamp, Carey, Byrne, Krikov, & Botto, 2017), although ~75% of all defects have a genetic contribution. Many genes involved in early development have widespread and varied functions throughout the body. As a result, mutations in one gene can result in defects in seemingly unrelated areas. For example, edn1 mutations can lead to heart defects including ventricular defects, as well as defects in the pharyngeal arches which lead to lower jaw malformations (C. T. Miller, Schilling, Lee, Parker, & Kimmel, 2000). Similarly, members of the TGF-β family such as BMP genes, are highly expressed throughout the developing embryo and defects in these genes have been demonstrated to induce defects ranging from skeletal and cartilaginous defects to heart and

craniofacial defects (Nie, Luukko, & Kettunen, 2006). Investigating the genetic mechanisms behind embryological development is thus vital to understanding how congenital defects occur and how best to prevent and treat them.

1.3 The Neural tube in embryonic development

Occurring from the 17th day of embryonic development onward, neurulation is a key event in early development which is required for the proper formation of the brain, spinal cord, vertebrae and cranium. The neural tube itself forms from the neural plate, which is composed of neural ectoderm, and this process is termed neurulation (Rifat et al., 2010). The beginning of neurulation is marked by bending of the flat neural plate into the medial hingepoint and the elevation of the neural folds on either side of the neural ectoderm (fig 1.1b). Following this, two further bends, known as the dorso-lateral hingepoints, form and re-orientate each side of the neural ectoderm to grow toward the midline where they will eventually meet (Rifat et al., 2010). Signals from the notochord and non-neural ectoderm promote folding of the ventral area of the neural plate and the fusion of the neural ectoderm at the midline of the neural tube finalises neural tube formation (Copp & Greene, 2010). Along with the neural tube, the neural crest is formed from tissue that lies on the border of the neural and non-neural ectoderm and delaminates following neural tube fusion. Critically, at more caudal levels, the process of neurulation differs. In contrast to that of primary neurulation which occurs in the more rostral areas of the neural tube, secondary neurulation contains no neural crest and no subsequent folding (Copp & Greene, 2010). Rather, mesenchymal cell populations in the tail bud condense to form a tube without the involvement of the neural plate, and dorsal aspects undergo a mesenchymal to epithelial transition (Copp & Greene, 2010). Ultimately however, the neural tubes created via primary and secondary neurulation remain largely continuous.

The morphological changes that the neural tube undergo require a number of cellular changes. Cell polarity is influential in the shaping of the neural plate and neural crest. During neurulation, cells undergo a process termed ‘contraction-extension’ characterised by antero-posterior extension and contraction of medial-lateral cells (Copp, Greene, & Murdoch, 2003). The medial lateral condensation of cells requires specialised filopodia which extend along the axis and allow for the cells to contract and intercalate (Ciruna, Jenny, Lee, Mlodzik, & Schier, 2006). Migratory cells during and after neurulation also display specialised filopodia which protrude along the trajectory of the migrating cell, contacting neighbouring migratory cells which subsequently move towards the lead cell, forming ‘streams’. Cell projections are also displayed by the leading-edge cells of the neural ectoderm prior to their meeting and fusion at the anterior midline of

what will become the neural tube (Colas & Schoenwolf, 2001). The roles of cell projections and cell polarity in neurulation are evidence of the complexity of the process, not just from the perspective of gross morphological changes, but also on the cellular level.

The non-neural surface ectoderm, like the notochord, provides signals that guide neural tube closure. Non-neural ectoderm derived signals such as the transcription factor *Grhl3*, are critical to the final stages of neural tube closure. In particular, these signals appear to regulate cellular protrusions and cellular organisation that are critical to late stages of neurulation. *Grhl3* was demonstrated to be critical in the formation of distinctive 'rosette' cellular formations and F-actin protrusions which are necessary for posterior neural tube closure (Zhou et al., 2020) (fig 1.1). Additionally, the above-mentioned cell projections which present from the neural ectoderm prior to closure, may also be derived from the non-neural ectoderm. Evidently, investigation of neural tube development requires a focus on both the tissues that directly form the neural tube, as well as the signals derived from tissues surrounding it.

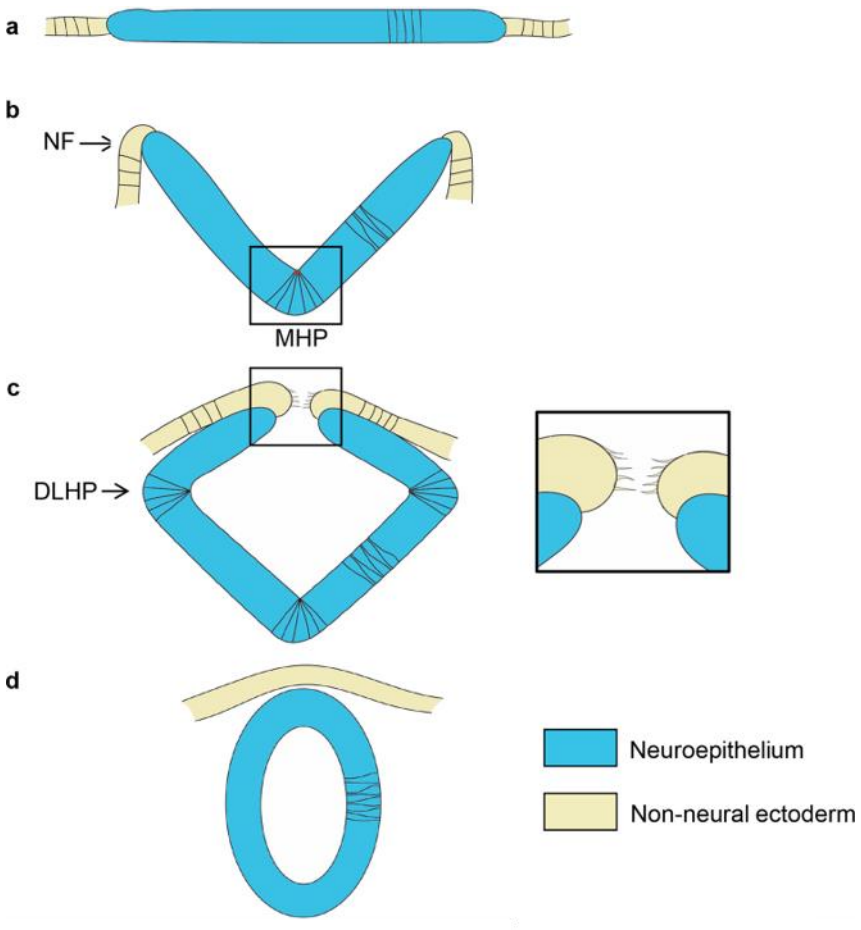

Figure 1.1 The neuroepithelium and the non-neural ectoderm contribute to neural tube fusion. **A)** the neurulation begins with the neural plate composed of neuroepithelium (blue) which is

flanked by non-neural ectoderm (white). **b)** Neural tube folding begins with the formation of the medial hinge point (MHP). **c)** The dorso-lateral hingepoints (DLHP) are formed prior to neural tube fusion. The neuroepithelium and overlying non-neural ectoderm are now opposed, apical projections from the non-neural ectoderm facilitate the fusion process between either side of the presumptive neural tube. **d)** The neuroepithelium-derived neural tissue has fused to form the neural tube, and the non-neural ectoderm has fused and overlies the neural tube dorsally adapted from Werner et al. (2021).

1.5 Neural Tube defects

The proper fusion of the neural tube is critical to avoiding potentially severe defects. The incidence of NTD is estimated at approximately 0.5-2 per 1000 births worldwide (Salih et al., 2014), and although the causes are multifactorial, it is thought that 80% of cases are genetically influenced (Greene, Stanier, & Copp, 2009). NTD are generally termed based on the position on the rostral/caudal axis that is left open following neurulation (fig 1.2).

The most common neural tube defect is spina bifida which affects approximately 4.6 in every 10,000 births and can vary in its severity from being mild and often undiagnosed, to resulting in gross malformation and an inability to walk. Spina bifida occurs when the dorsal neural tube at the caudal end of the embryo (fig 1.2) fails to fuse, the resulting opening potentially affecting the later development of the spinal vertebrae, spinal cord and meninges (Northrup & Volcik, 2000). The most common form of spina bifida, *spina bifida occulta* is often asymptomatic, while the most severe form of spina bifida is *myelocele* which is characterised by an exposed spinal cord which protrudes dorsally in the absence of both the vertebrae and meninges. In contrast to occulta, the effects of myelocele are debilitating and can include serious complications. The protrusion of the spinal cord dorsally can lead to bacterial infection of the nerve tissue and consequently, secondary conditions such as lower limb paralysis (Northrup & Volcik, 2000). Individuals born with spina bifida often suffer from spinal cord tethering, wherein the spinal cord becomes attached to structures surrounding the spinal cord canal and leading to pain later in life (Lapsiwala & Iskandar, 2004). Importantly, the neural tube is not only responsible for development of the spinal cord and lower vertebrae but is also critical to the formation of the upper vertebrae and cranium (Lapsiwala & Iskandar, 2004). Defects affecting the fusion of the neural tube at this level of the rostral-caudal axis are invariably severe.

Anencephaly is an example of failure in fusion of the rostral neural tube, and results in still births or infants that are born without significant portions of the brain and cranium (Greene & Copp, 2014). Such is the severity of this condition; if they survive to birth, these infants invariably die within the first year of life. Anencephaly results from an open rostral neuropore and in humans occurs around the 26th day post conception (Greene & Copp, 2014). Craniorachischisis, which results when the entirety of the neural tube is unfused, is even more severe. Craniorachischisis is typically linked to defects in the Planar Cell Polarity (PCP) pathway, due to the apparent failure in cell-polarity which is thought to cause the condition (Greene & Copp, 2014; Robinson et al., 2012).

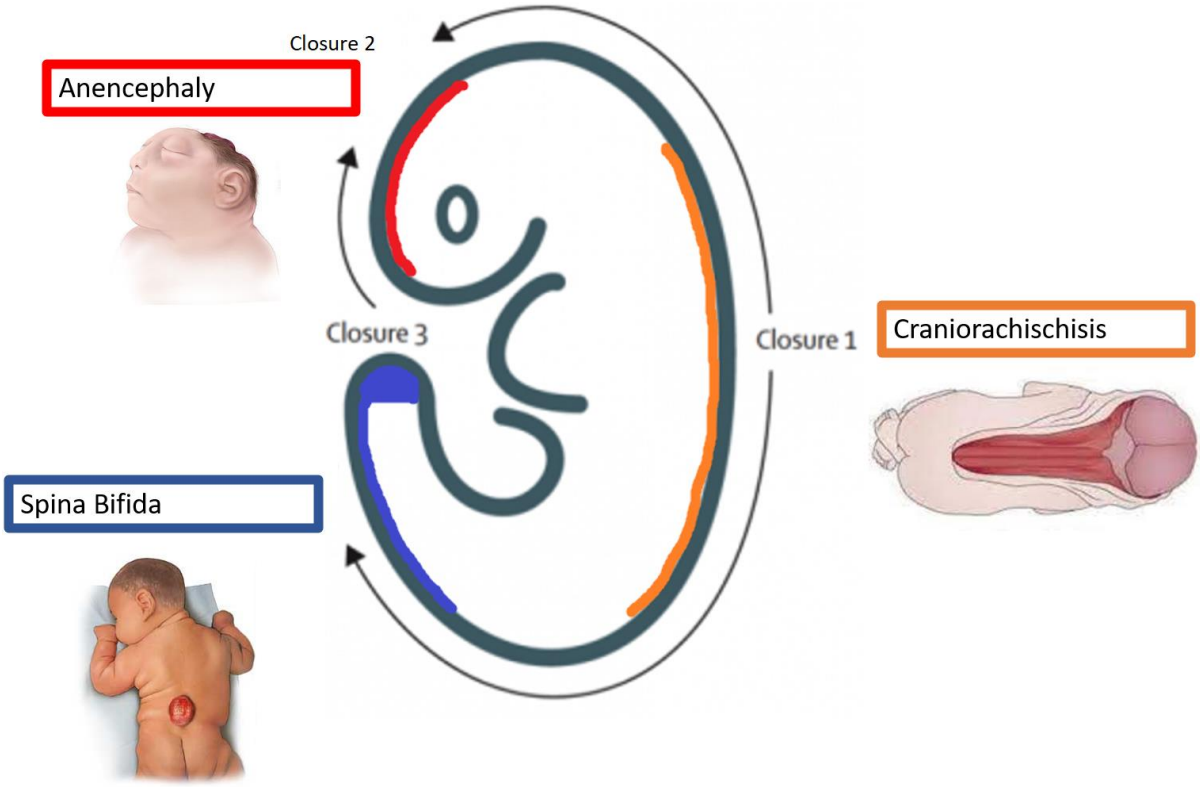

Figure 1.2: Neural Tube defects and the areas from which they arise. The specific neural tube defect which arises following defects in neural tube fusion is dependent on the area of the neural tube affected. Failure of neural tube fusion at closure point 3 in the rostral forebrain and closure point 2 in the hindbrain/cervical boundary may lead to anencephaly. Defects occurring during closure of the neural tube along its length (orange, closure point 1) may lead to craniorachischisis, while the rostral forebrain, (red, closure point 2) results in defects to the brain and skull (anencephaly). Failure at the the posterior neuropore (blue) is characterised by spina bifida.

Whilst NTD vary in their severity, the incidence of all subtypes is multifactorial, including genetic, environmental, and chromosomal factors. Further, NTD collectively account for a significant portion of congenital defects and contribute significantly to child mortality worldwide Salih et al. (2014).

1.6 Craniofacial Development

The early development of the face and cranium, as with many other areas of the body, relies upon the function of Neural Crest Cells (NCC), which delaminate from the dorsal-most fusion point of the neural tube and migrate ventrally to populate various areas of the body, including the pharyngeal arches (PA) and cranium (Cordero et al., 2011). It is through the differentiation of cranial neural crest cells (CNCC) within PA1 that the majority of the structures of the face will form (Cordero et al., 2011).

The signals that determine the fate of each NCC population, as well as at what point cell fate is determined, are still unclear. Traditionally, NCC induction was thought to occur around the time of neural tube closure, however more recent studies have demonstrated that this may occur during gastrulation and be dependent on further signals later in development (Basch, Bronner-Fraser, & García-Castro, 2006). Among the many putative signals in NCC induction, the WNT and BMP gene families have been demonstrated as being critical during the process of establishing the three germ layers (ectoderm, endoderm and mesoderm) known as gastrulation. Early induction requires the upregulation of WNT genes and inhibition of BMP, however later stages appear to require the upregulation of BMP also (Steventon, Araya, Linker, Kuriyama, & Mayor, 2009). Additionally, FGF and MAPK signalling prior to gastrulation are critical for neural crest induction (Stuhlmiller & García-Castro, 2012). These major pathways and the necessity of their expression prior to and during gastrulation underscore how signals received prior to neurulation itself, can be essential to the development of the neural crest and by extension, neural crest cells. Following their population of the pharyngeal arches, CNCCs will differentiate into various cell types within the face and skull in order to form the recognisable structures of the face.

The first pharyngeal arch is significant for craniofacial development as it is specifically responsible for the formation of the ventral portion of the vertebrate skull. In particular, the ventral aspect of the first pharyngeal arch contributes to the mandible (lower jaw) and maxilla (upper jaw) in mammals and gill structures in fish. Each of the pharyngeal arches is composed of

a tubular core of paraxial mesoderm, covered by a lining of ectoderm and endoderm on either side (Fig. 1.3). The shape of these arches also create endodermal pouches on the interior, and ectodermal clefts on their exterior, some of which are also responsible for tissue patterning during development (Graham & Richardson, 2012). The pouches of the 1st and 2nd arches give rise to the auditory canal and structures of the middle ear, whilst the ectodermal clefts pattern the development of the external auditory meatus (Lambert & Dodson, 1996).

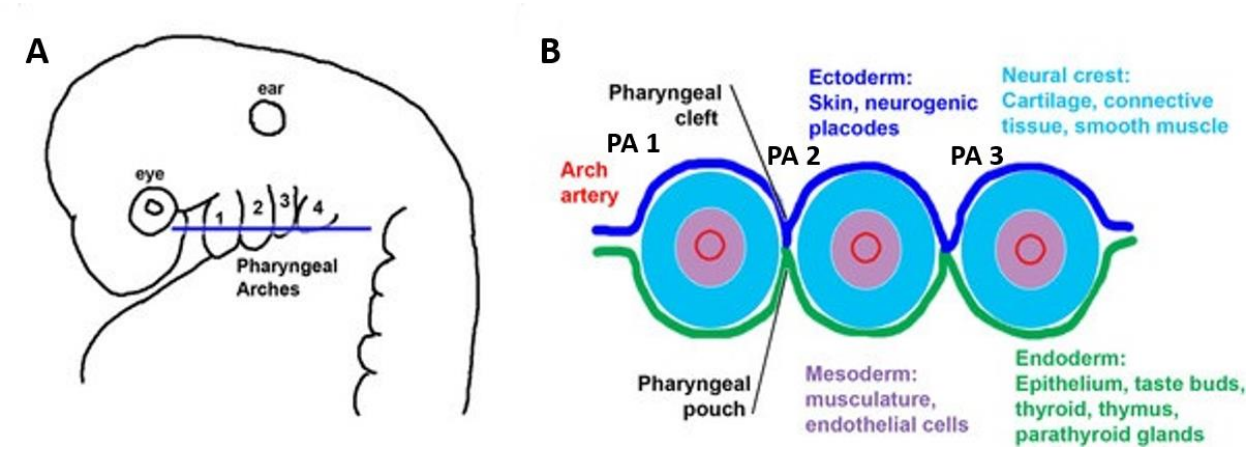

Figure 1.3: Coronal view of pharyngeal arches showing their structure and composition. A) developing vertebrate embryo depicting pharyngeal arches (1-4), eye and ear (blue line represents level of cross-section. B) A core of mesoderm (purple) is surrounded by neural crest cells (light blue), which are further surrounded by ectoderm distally (dark blue), and endoderm proximally (green). The areas between each arch form endodermal pouches and ectodermal clefts respectively. Various structures of the head and neck are derived from these tissues in the pharyngeal arches. Adapted from Graham & Richardson, (2012).

NCC streams originate along the length of the neural tube, from defined segments termed 'rhombomeres'. NCCs which pattern craniofacial development are derived from the first and second rhombomere, and migrate ventrally from them to populate the first pharyngeal arch (Minoux & Rijli, 2010) (fig. 1.4). The mechanisms underlying NCC streams include areas which are NCC free surrounding rhombomeres 3 and 5, which are the result of mesenchyme which prevents NCC survival in these areas. The neuroepithelium and surface ectoderm at rhombomeres 3 and 5 have been shown to repulse NCC migration in the associated areas via the action of *Msx* and *Bmp* families of genes which induce apoptosis of premigratory NCCs (Farlie et al., 1999).

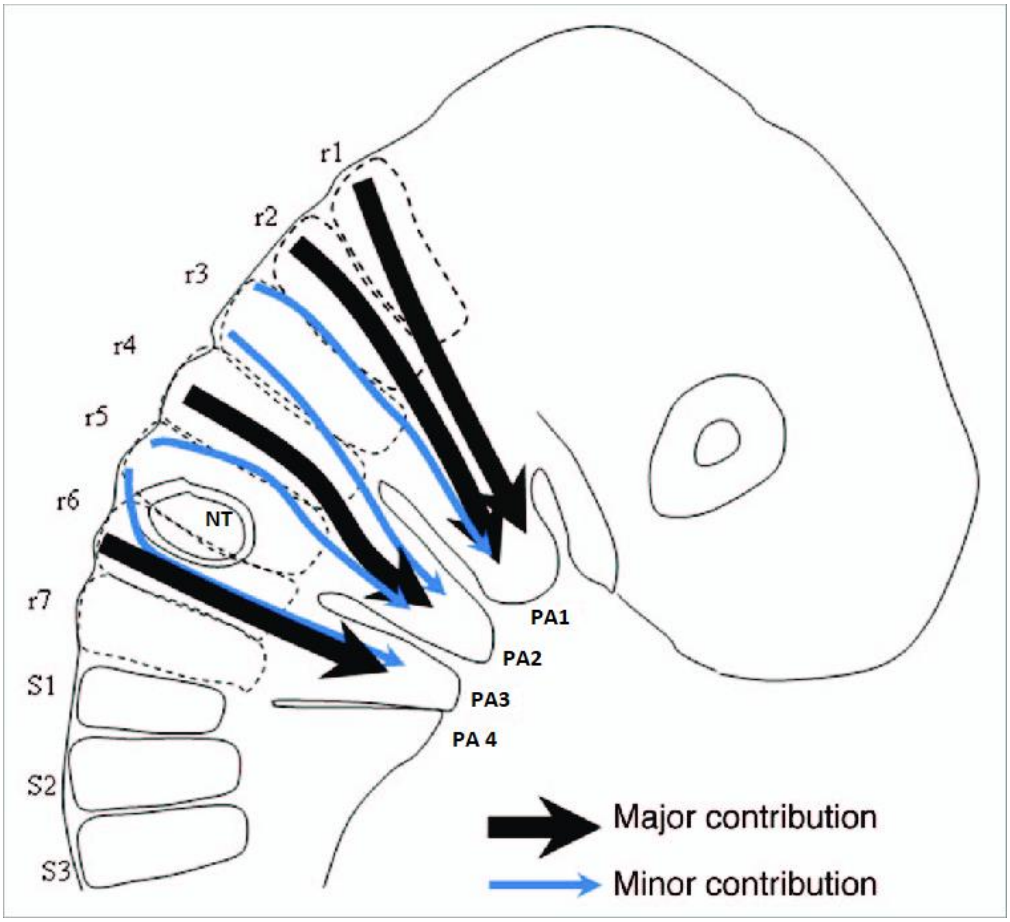

Figure 1.4*:* Neural crest cell (NCC) migration into the pharyngeal arches. PA1, PA2, PA3 and PA4 represent the pharyngeal arches, r1-r6 and S1-3 represent the rhombomeres of the developing embryos respectively. The black arrows represent NCC streams from rhombomeres 1,2,4 and 6 which contribute significantly to Pharyngeal arch development, whilst blue arrows represent smaller streams of NCCs from rhombomeres 3 and 5 which contribute minimally. NCCs originating from the dorsal neural tube (NT) following NT fusion to form the brain and spinal cord, migrate into the pharyngeal arches in 'streams' of cells after undergoing an Epithelial to Mesenchymal Transition (EMT). Various cadherins anchor the NCCs prior to EMT, which are downregulated and cleaved in order to induce NCC migration (Pla et al., 2001). Following the EMT and subsequent delamination of NCCs from the NT, NCCs begin migrating in streams towards the pharyngeal arches. Adapted from Kuo & Erickson, (2010)

NCC migration into PA1 ends with cellular differentiation, the mechanisms of which involve both pre-programmed (cell-intrinsic) instructions and environmental cues at their destination (Schneider & Helms, 2003) (Shah & Anderson, 1997). Following migration and differentiation, NCCs will ultimately form the jaws, facial and cranial bones.

In humans, the external face begins to form around the 5th week of embryological development (Kurjak, Azumendi, Andonotopo, & Salihagic-Kadic, 2007). During this period of growth, the face is comprised of facial prominences from which the major distinguishable features of the face will form (fig. 1.5). The fronto-nasal prominence comprises the facial midline from the forehead to the tip of the nose (Kurjak et al., 2007). The precursor to the nasal openings - the nasal pits - are formed by paired medial and lateral nasal prominences. Inferior to the nasal buds, paired maxillary prominences form the primordial maxilla and the palatal shelves, whilst the mandibular prominences initially surround the maxillary prominences medial and inferior aspects (Kurjak et al., 2007).

Critical to the proper development of the face is the fusion of these prominences. Cell adhesion and cell to cell communication genes are necessary for the fusion of each process, however whilst these signals are required to some extent throughout the developing face during fusion of the prominences, the specific genes involved differ between tissues. Analysis of the transcriptome of tissue from each prominence has shown, for example, that while members of the claudin (cldn) family are generally expressed throughout the developing face during tissue fusion, the more inferior prominences display higher expression of cldn1 whilst the remaining prominences exhibit increases in the expression of claudin 3, claudin 6, claudin 7 and claudin 9 (Brunskill et al., 2014). In this way, the genes required for tissue fusion can vary between tissues even within the same family of genes.

The claudin gene family has been shown to interact with a number genes known to govern tissue fusion elsewhere. Claudin 6 is inhibited by the BMP antagonist Noggin, which itself plays significant roles in regulating tissue fusion in the developing palate and neural tube. Consistent with this finding, other members of the claudin family also interact with Wnt-1 and B-catenin, which are in turn involved in BMP expression (Turksen & Troy, 2001). Similarly, *Shroom3* expression was significantly increased in the frontonasal prominence specifically. Shroom3 deficiency has been linked to various tissue fusion-related defects including spina bifida myelomeningocele, anencephaly, and cleft palate. Further, Shroom3 is a downstream target of the highly influential PCP pathway discussed previously as being involved in convergence extension in neural tube development which is significant given that signals that promote the growth and fusion of the facial prominences are also derived from the neural tube and facial ectoderm (McGreevy, Vijayraghavan, Davidson, & Hildebrand, 2015). Evidently, craniofacial development relies upon a sophisticated web of interacting genes, the expression of which varies even amongst seemingly related tissues.

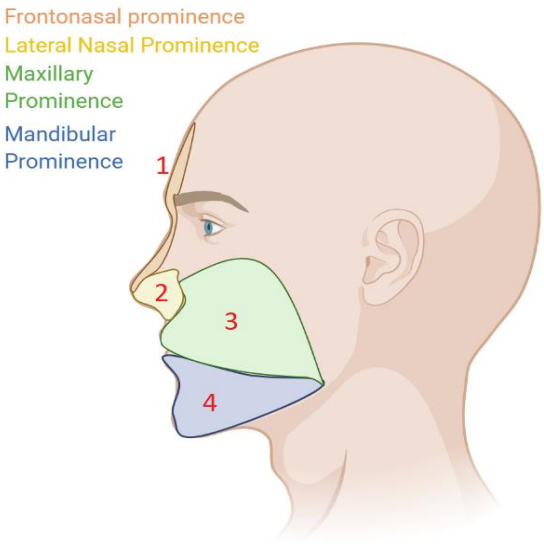

Figure 1.5: Facial prominences after fusion form the recognizable structures of the face. Cranial neural crest cells that have migrated into the first pharyngeal arch differentiate to form the frontonasal (1), lateral nasal (2), maxillary (3) and mandibular (4) prominences, which then fuse later in development to form facial structures.

1.7 Development of the primary and secondary palate

Palate development begins with the primary palate, which forms from the fronto-nasal prominence beginning in the 5th week of embryonic development. The primary palate comprises a relatively small area at the roof of the oral cavity wherein the four incisor teeth attach. The secondary palate originates from the maxillary processes during the 6th and 7th weeks post-conception (Bender, 2000). Outgrowths of the maxillary processes on either side of the tongue – known as palatal shelves - initially grow vertically downward. During the eighth week, the growth of the mandibular prominence creates room for the tongue to depress and subsequently, for the palatal shelves to re-orient and grow horizontally above it (Bender, 2000). Each palatal shelf, as well as the primary palate and the nasal septum, will fuse to separate the nasal and oral cavities (figure 1.6).

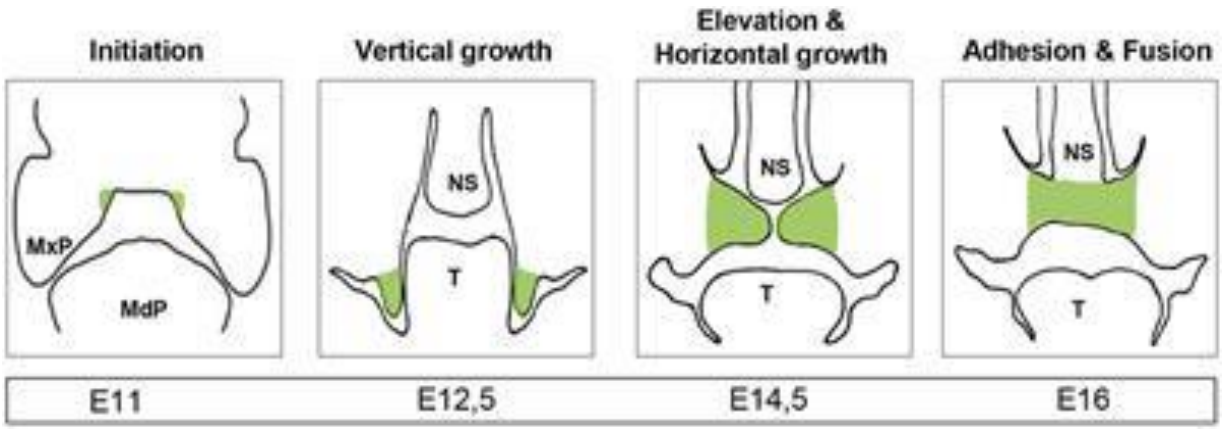

Figure 1.6: The development of the palatal shelves in mice. The palatal shelves (green) arise from the maxillary prominence (mxp) beginning at E11 in mice. By E12.5, the palatal shelves have grown vertically on either side of the tongue. By E14.5 the tongue has depressed to allow the palatal shelves to elevate horizontally and approximate at the midline of the mouth. Fusion of the palatal shelves occurs at E16 and thus forms the oral and nasal cavities. Adapted from Schoen et al. (2017).

The tissues which constitute the palatal shelves undergo several changes before, during and after fusion at the midline. The palatal shelves are primarily composed of mesenchymal and epithelial cells. The fusion of the palatal shelves begins initially with the fusion of the medial epithelial cells of each shelf which form a midline 'seam' (Nawshad, 2008). The seam is transient, as it exists only until the medial epithelial cells which fused are disintegrated. Three theories exist as to the fate of the epithelial cells – either the epithelial cells undergo apoptosis, migrate away from the seam, or undergo epithelial-to-mesenchymal transition and become part of the surrounding mesenchyme (Nawshad, 2008). In any case, the midline seam is replaced with a continuous area of mesenchyme. The palatal epithelium in the nasal cavity, in line with its role in the respiratory tract, differentiates into pseudostratified columnar ciliary cells while the epithelial cells in the oral cavity differentiate into non-keratinizing stratified squamous cells. Thus, the end result of palatal shelf fusion is a confluent palatal midline, and the successful separation of the nasal and oral cavities (figure 1.7).

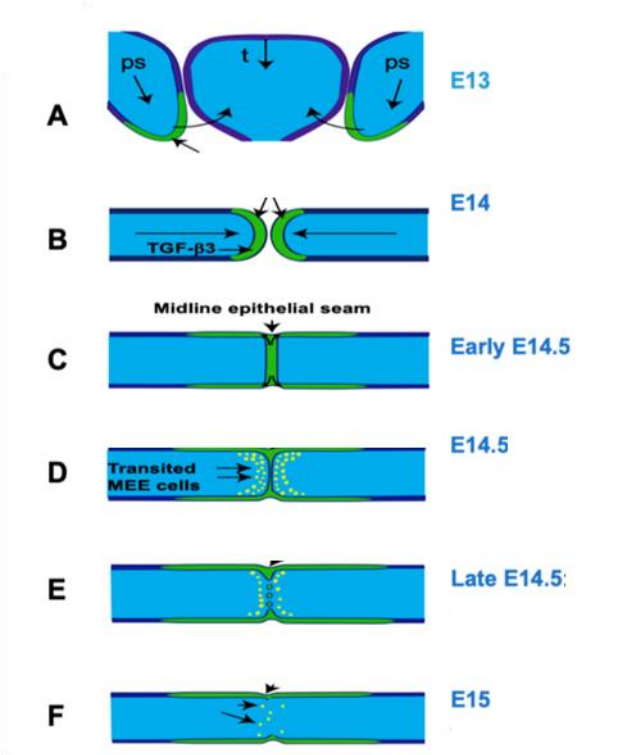

Figure 1.7: The fusion of the midline seam. **A**) the palatal shelves change orientation to grow horizontally toward the midline (arrows). **B)** At E14, the epithelium (green) of the palatal shelves, driven by signals from TGF-β, meet at the midline. **C)** the epithelium of each shelf begins to fuse. **D)** Midline epithelial cells begin to transit away from the seam, and as epithelial cells are removed, they are replaced with mesenchyme (**E, F)** until the tissue is confluent. Adapted from Nakajima, F. Shuler, Gulka, and Hanai (2018).

The development of the human palate is evidently a sophisticated and highly regulated event, involving a multitude of cell types and requiring extensive morphological changes within the developing embryo. The steps that prove most problematic in this sequence are the fusion events that occur between each of the palatal shelves (Dudas, Li, Kim, Yang, & Kaartinen, 2007). Wherein the palatal shelves fail to fuse at the midline, a cleft will remain in the roof of the oral cavity. The resulting condition – cleft palate – is among the most common birth defects. Investigating the morphological processes and genes underpinning this defect is an important focus of this project.

1.8 Craniofacial defects

Craniofacial defects are second only to cardiac defects in prevalence (Parker et al., 2010). Mutations in any number of complex gene pathways contribute to craniofacial abnormalities. Further, the identification of disease-causing gene mutations allows for the screening and genetic counselling of individuals at-risk of conceiving affected children. There are more than 275 craniofacial syndromes directly associated with the mutation of a single gene (E. J. Leslie & Marazita, 2013). For this reason, characterizing the role that gene mutations and polymorphisms play in craniofacial development is critical to our understanding of craniofacial defects.

1.9 Craniosynostosis

Craniosynostosis is a craniofacial anomaly affecting the skull, caused by premature fusion of the cranial sutures, leading to the outgrowth of the bones, increased intracranial pressure and associated cognitive issues as a consequence (fig. 1.6) (Yagnik et al., 2012). Craniosynostosis can be categorized as syndromic or non-syndromic based on whether it presents with other related aberrations (Yagnik et al., 2012).

Crouzon syndrome occurs as a result of premature cranial fissure fusion (craniosynostosis), which subsequently induces defects elsewhere in the face (Ahmed & Afzal, 2009). In this way, mutations affecting one gene or tissue can lead to secondary defects throughout the embryo. Conversely craniosynostosis can occur 'non-syndromically' wherein the premature fusion of the sagittal fissure is the only defect present (Boyadjiev, 2007). Many genes involved in craniosynostosis are inherited in an autosomal dominant fashion, meaning if one pregnancy is affected, there is a 50% likelihood for each subsequent pregnancy that the child will be born with craniosynostosis (Bowling & Burstein, 2006). Understanding and diagnosing the genetic cause of craniosynostosis in a given child can thus allow for genetic counselling of parents who may be at risk of giving birth to another affected child and is an example of the potential benefits of genetic counselling.

Gain of function mutations in the *FGFR* group of genes which code for receptors that regulate cell growth as well as loss of function in *TWIST1* transcription factors responsible for suppressing *FGFR*, represent the most common gene mutations in syndromic craniosynostosis (Bessenyei et al., 2015). Mutations in the FGFR family, in particular *FGFR1*, *FGFR2* and *FGFR3* account for approximately 1 in 4 cases of craniosynostosis and advances in the understanding of FGFRs roles in craniosynostosis have also allowed for novel pharmacological interventions to be considered (Ketwaroo, Robson, & Estroff, 2015). Small molecule inhibitors that have proven effective in combatting FGFR mediated cancer have been suggested as potential treatments for

craniosynostosis prenatally (Eswarakumar et al., 2006). Further, RNA-based interventions have proven successful in mouse models of apert syndrome, by introducing small hairpin RNA molecules which are able to target the dominant mutant *FGFR* gene specifically (Shukla, Coumoul, Wang, Kim, & Deng, 2007). These treatments underscore the potential impact on clinical outcomes that may result from a greater understanding of the genes involved in tissue fusion, particularly in the context of craniofacial defects.

1.10 Orofacial clefts

Cleft lip and cleft palate – collectively known as orofacial clefts – represent the second most common birth defect worldwide (Kirby, 2017). Treatment options for infants born with orofacial clefts are currently limited to surgical intervention, which itself can lead to adverse medical outcomes, including airway complications (Jackson et al., 2013). The causes of orofacial clefts in humans remain largely unknown, the incidence of cleft palate varies significantly based on ethnicity and gender suggesting a strong genetic component (Setó-Salvia & Stanier, 2014). As is the case with man other congenital defects, orofacial clefts can occur in addition to other symptoms (syndromically) or individually (non-syndromically). Additionally, orofacial clefts may manifest as either cleft lip, cleft lip with cleft palate, or cleft palate only.

Orofacial clefts result from defective fusion of the secondary palate and will present as openings in the roof of the mouth, in either the hard or soft regions of the palate (Bush & Jiang, 2012). Given the complex series of cellular and morphological events required to form the palate, ectopic expression of any of genes in any number of pathways can potentially contribute to orofacial clefts. The most common orofacial cleft related syndromes are Van Der Woude syndrome, affecting some 2% of cleft palate cases, and Di George syndrome (Tehranchi et al., 2017). Most Van Der Woude (VWS) cases are due to reduced IRF6 expression, generally resulting from gene mutation-induced haploinsuffiency (Ferrero et al., 2009; E. J. Leslie et al., 2013). In contrast to VWS however, Di George syndrome is the result of a chromosomal deletion affecting the 22Q11.2 locus (McDonald-McGinn & Sullivan, 2011). Di George syndrome sufferers suffer from cleft lip and palate as well as cardiac defects, and maxillary hypomorphism amongst other phenotypes. Many of the affected structures are reliant on the function of NCC for development, which is consistent with a loss of the TBX1 gene which usually lies within the 22Q11.2 locus and regulates NCC migration and the development of the pharyngeal arches (Hannah et al., 2014). Similarly, The FGFR2 receptor responsible for both apert syndrome (which also presents with craniosynostosis) and Crouzon syndrome, also contributes to regulating cellular proliferation and patterning of the developing pharyngeal region (Larbuisson, Dalcq, Martial, & Muller, 2013).

More recently, *FGFR* genes have been linked to the migration of trunk NCC, defects in this process could produce defects in NCC derived tissues including those seen in cleft palate and craniosynostosis (Dunkel, Chaverra, Bradley, & Lefcort, 2020). Whether or not this extends to Cranial NCC however, has not yet been elucidated. These syndromes underscore the importance of regulating and patterning pharyngeal arches and NCC development, and how defects to one gene amongst the many regulatory factors involved, may produce a range of potential defects.

Whilst mutations to individual genes are capable of causing orofacial defects, mutations in multiple genes within the same pathway are capable of modifying the defective phenotype observed in vivo. Members of the 'homeobox' gene family, in particular *Dlx1* and *Dlx2*, have been identified as necessary for various stages of craniofacial, pharyngeal arch and NCC function and development (Talbot, Johnson, & Kimmel, 2010). Knockout of *Dlx1* in mouse models leads to mild cranial defects, whilst knockout of *Dlx2* leads to mild clefting of the palate amongst other craniofacial symptoms (Jeong et al., 2012). When both genes were knocked out the palatal clefting was fully penetrant. The amplification of the defect as a result of simultaneous knockout of both dlx genes, is indicative of potential functional overlap and redundancy between genes. Further, examples like the *Dlx* gene family, underscore the role of genetic interaction and regulation which is vital for proper palatal development.

Despite the relatively high incidence of cleft palate, as well as the lack of pharmacological alternatives to traditional surgical treatment for sufferers, there remains significant uncertainty regarding the genetic basis for cleft palate. For this reason, investigating genetic interactions and contribution to orofacial clefts is vital for providing better alternatives for treating those affected by these conditions.

1.11 *Grhl* family

The *Grainyhead-like (Grhl)* family of transcription factors are an evolutionarily conserved genes with numerous roles in craniofacial, and neural tube development. Originally identified in *Drosophila*, "*grainyhead*" was so named for the disrupted and 'grainy' appearance of *Drosophila* heads in *grhl* mutants. The *grainyhead-like* family has 3 mammalian orthologues: *Grhl1*, *Grhl2* and *Grhl3*, each play varying roles in embryological development, with some functional overlap (Carpinelli, de Vries, Jane, & Dworkin, 2017). Given their function as transcription factors, the *Grhl* family regulate the transcription of hundreds of downstream target genes and are expressed almost exclusively in epithelial tissues (Auden et al., 2006a; Dworkin et al., 2017).

1.12 Conservation of gene function

The evolutionary conservation of *Grhl* genes is indicative of their important function in a number of developmental processes. *Grhl* genes are present in all vertebrates, as well as some invertebrates and fungi, and the presence of *Grhl* genes has been dated back to over 700 million years ago (Venkatesan, McManus, Mello, Smith, & Hansen, 2003) still, each *Grhl* member retains the same conserved binding site (Mathiyalagan et al., 2019).

Though *Grhl* genes are largely evolutionarily conserved and all share a consensus binding site, the function of individual *Grhl* family genes is complex. In mammals, *Grhl1* is important for the attachment of skin cells to each other, as well as to hair (Mlacki, Darido, Jane, & Wilanowski, 2014). As such, mutations in *Grhl1* tend to result in epithelial defects and hairlessness. In mice *grhl2* is associated with craniofacial development, particularly in the palate and facial prominences, whereas *Grhl3* is associated with epithelial wound healing (Carpinelli et al., 2020; Moussian & Uv, 2005). Conversely, the development of craniofacial structures in zebrafish appear to rely primarily on *Grhl3*, whilst *Grhl2* is associated with otic development and maintenance of the midbrain-hindbrain boundary (Dworkin et al., 2012). However, both *grhl2* and *grhl3* are implicated in cleft palate and neural tube defects, demonstrating a degree of functional overlap (Juriloff & Harris, 2018). Despite overlap in function and the conserved DNA binding site, *Grhl2* and *Grhl3* functional redundancy varies depending on the tissue and process involved. In neural tube defect mouse models, the only region in which *Grhl2* and *Grhl3* appeared to work co-operatively was in the fusion of the mid-thoracic neural tube (Juriloff & Harris, 2018). However, *Grhl2* is able to compensate for loss of *Grhl3* in wound repair, but not in maintenance of the epithelium (Auden et al., 2006b). Additionally, while *Grhl2* and *Grhl3* are thought to contribute to NT fusion through independent mechanisms, they have also demonstrated heterodimerization, highlighting a degree of genetic interaction, the purpose of which has not yet been elucidated. Evidently, the extent of *Grhl* functional overlap, and their interaction with each other, is incredibly complex and not entirely understood.

1.13 *Grhl2* in Human defects

The *Grhl* family of genes have long been linked to skin defects, particularly through the contribution of *Grhl1* to epidermal maintenance and the role of *Grhl3* in epidermal wound repair in animals as well as in human skin cancer (Kikulska et al., 2018). However, *GRHL2* too has been linked to skin development through its association with ectodermal dysplasia. In the affected family, ectodermal dysplasia presented as skin and nail dystrophy, tongue pigmentation, short stature and hypodontia (Petrof et al., 2014). Despite the obvious ectodermal defects associated

with this *GRHL2* variant, none of the affected individuals showed spina bifida or any symptoms of neural tube defects, despite the lack of *GRHL2* in the surface ectoderm to contribute to the neural tube during development, suggesting that neural tube development is not reliant on *GRHL2* in humans.

Though clinical cases of *GRHL2* mutations affecting palatal development have not been identified, *GRHL2* has been linked to hearing loss (Kim et al., 2015). The variants causing hearing loss tend to result from the insertion of a premature stop codon, resulting in a shortened gene transcript. In the clinical setting, this produces hearing loss that is slow and progressive, but not congenital as seen in defects arising from other members of the *Grhl* family in other areas of the body.

1.14 *Grhl2* in Animal models

Grhl2 is expressed in the developing murine palate and in the epithelium overlying the neural tube amongst other places its' presence underpins the organisation of cells in the epithelium (Carpinelli et al., 2020). Several murine knockout models exist that have characterised the functions of *Grhl2* in murine embryonic development. *Grhl2*$^{-/-}$ mouse embryos are embryonic lethal at E10.5, due to an array of severe defects. At E10.5, whilst the palatal shelves have not yet formed, *Grhl2*$^{-/-}$ embryos display a unique 'split-face' phenotype wherein the entire maxillary prominence is cleft at the midline. Analysis of MXP tissue from *Grhl2*$^{-/-}$ embryos via histological sectioning, shows a distinct change in the cellular identity of epithelial tissues. The distinct and organised epithelium usually seen in wild type MXP tissue is replaced with a disorganised layer of cells with both epithelial and mesenchymal cell traits. Furthermore, this change is underpinned by decreases in the expression of the epithelial marker E-cadherin and increases in the mesenchymal marker Vimentin. These changes are consistent with the known role of *Grhl2* as a driver of epithelial cell identity, as well as its role in regulating Epithelial to mesenchymal transition in other settings, particularly in cancer biology (Xiang, Fu, Ran, & Wang, 2017). In colorectal cancer studies, *grhl2* knockdown was shown to contribute to EMT in cancer cells, and the injection of *Grhl2* and genes upstream of *Grhl2* including *ZEB1*, were shown to maintain epithelial cell types (Hu, He, Sun, & Rong, 2019). Conditional knockouts, wherein *Grhl2* expression was inhibited in craniofacial tissues, exhibited significant hypomorphism of the lower jaw, a characteristic shared with mutations in human *GRHL2*. Clearly, the degree to which human *GRHL2* and murine *Grhl2* functionally overlap in craniofacial development is complicated and as of yet, not fully explored.

Interestingly, despite not being expressed within the neuroectoderm which forms the neural tube, one key phenotype present in *Grhl2*$^{-/-}$ mouse embryos is the failure of neural tube fusion which is responsible for the embryonic lethality observed in mice around E10.5. Each of the closure points along the length of the developing neural tube require differing contributions from *Grhl2* and *Grhl3* (Rifat et al., 2010). Closure site 1 does not rely on *Grhl* expression of any kind and is regulated instead by the PCP pathway. Closure site 2 however requires the expression of either *Grhl2* and *Grhl3*, and is instead dependent on *Grhl* dosage rather than the expression of either *Grhl2* or *Grhl3* specifically (Rifat et al., 2010). Neural tube closure at the caudal neuropore however is reliant entirely on the expression of *Grhl2*. Given that closure point 2 is at the rostral end of the embryo, failure of NT formation here will result in anencephaly or exencephaly, both of which are observed commonly in *Grhl2*$^{-/-}$ embryos. Despite the stark differences in the roles of *Grhl2* and other *Grhl* genes in murine craniofacial development, their roles overlap in terms of the development of the neural tube.

Multiple studies have demonstrated that both loss of expression and overexpression of *Grhl2* result in defects (Brouns et al., 2011; J. He et al., 2020). In particular, the axial defects (axd) mouse model demonstrated that the *axd* mutation led to overexpression of *Grhl2* and ultimately to spina bifida, whilst loss of *Grhl2* resulted in the aforementioned cranial and lumbosacral NTDs (Brouns et al., 2011). *Grhl2* heterozygotes however, in both the *axd* model and in embryos with one wild type allele, do not display defects at a rate higher than *Grhl2*$^{+/+}$ embryos. It can thus be inferred that both over expression and total loss of *Grhl2* results in defects, however even a single wild type *Grhl2* allele is adequate to prevent *Grhl2* induced NTD. It is clear that *Grhl2* plays a significant role in Neural tube development, as evidenced by the plethora of murine models which have characterised the consequences of *Grhl2* expression. Further, the clinical evidence that exists currently highlights the importance of *Grhl2* in humans. The mechanism through which *Grhl2* dosage contributes to defects, and the significance of this to human clinical defects however, still remain to be explored.

In Zebrafish, two orthologues of the *grhl*2 gene exist, *grhl2a* and *grhl2b*. Studies of *grhl2b* have shown a role in convergence-extension processes in zebrafish, however this requires co-operation with *grhl*3, as knockdown of either gene alone will not result in defects to this function (Miles, Darido, et al., 2017). *grhl*2 is also functional during later periods of zebrafish development, as the introduction of *grhl*2 mutations known to affect hearing loss in humans has shown similar effects on the otic vesicles of fish, demonstrating a conserved role in hearing across species (Han et al., 2011). Thus, *grhl*2 associated hearing loss underscores not only the importance of *grhl*2 in clinical settings, but that mutations in genes that function early in development can manifest in tissue and organ defects much later in life.

1.15 *Grhl*3 in Human defects

Given the widely conserved nature of *Grhl* genes, as well as their widespread distribution in the epithelium of various embryonic tissues during development, several distinct tissue fusion defects have been associated with this family of genes in humans. In particular, *Grhl*3 related human defects are generally linked to the role of *Grhl*3 in neurulation, and thus comprise defects relating to failures in neural tube fusion and tissues derived from NCC.

Perhaps the most well-established human defect associated with *GRHL*3 is that of Van Der Woude syndrome. Although 70% of cases of VWS are attributed to mutation in the gene IRF6, 5% of all cases are due to mutation in *GRHL*3 (Peyrard-Janvid et al., 2014b). Both *IRF6* and *GRHL*3 play roles in the development of the oral periderm, and mouse models have shown that *Irf6* mutation induced periderm defects can be partially rescued by expression of *Grhl*3. Further, mouse models comparing *Grhl*3$^{-/-}$ and *Irf6*$^{-/-}$ embryos displayed similar characteristics oral characteristics in addition to cleft palate (Peyrard-Janvid et al., 2014b). Adhesion affecting the palatal shelves, maxillary and mandibular surfaces was present in both *Grhl3*$^{-/-}$ and *Irf6*$^{-/-}$ embryos, suggesting that these genes contribute to palatal development in a similar manner. The role of *GRHL*3 mutations in palatal defects is further supported by studies which have identified *GRHL*3, as a causative gene in non-syndromic cleft palate in various populations (Azevedo et al., 2020; Eshete et al., 2018). In zebrafish and mouse models, *Grhl*3 exists downstream of *Irf6* in epidermal permeability and periderm differentiation (de la Garza et al., 2013). Given that periderm serves to separate epithelia and prevent fusion of epithelial tissues, it is feasible that defects such as cleft palate may occur if a defect in either *IRF6* or *GRHL*3 is present, should they indeed interact in regulation of palatal periderm. In neural tube development, *GRHL*3 is a putative downstream regulator of *TFAP2A* and *IRF6*, all of which are critical for palatogenesis and which also present with similar defects when inhibited (Kousa et al., 2019). These results highlight the importance of *GRHL*3 expression in VWS, its potential relationship to *IRF6*, and the critical role that *GRHL* factors play in clinical birth defects in humans.

The importance of *GRHL*3 expression in neurulation and human spina bifida has been noted in numerous studies, however the specific mechanisms through which *GRHL*3 causes NTD are unclear. Mutations in *GRHL*3 have been identified in both familial and sporadic cases of spina bifida (Lemay et al., 2017). The mechanism through which human *GRHL*3 may influence neural tube defects in humans is unknown. Experiments using mouse models have noted that mutations in *Grhl*3 cause defects in cell projections which are necessary during the fusion of the neural crest during the final steps of neurulation (Jaffe & Niswander, 2021). An additional

proposed mechanism suggests that loss of *GRHL*3 expression may affect epidermal migration via the putative partner protein LMO4, a process upon which neural tube development also depends (Hislop et al., 2008). Yet while *Grhl* genes are widely conserved amongst vertebrates, the specific effects mediated by loss of these genes makes establishing definitive mechanisms and generalisations towards human defects complicated. Further complicating this, is that overexpression of *Grhl*3 in mice causes defects, a phenomenon not yet established in human patients, and hypomethylation of *GRHL*3 which doesn't require changes to the *GRHL*3 sequence at all, is also associated with defects (Tian et al., 2018). Evidently, there is a clear link between NTD and abnormal Grhl3 expression, as well as numerous potential pathways and mechanisms with which Grhl3 has been associated that may cause NT abnormalities.

1.16 *Grhl*3 in Animal models

Studies of *Grhl*3 function *in vivo* focus largely on its' function in mice and zebrafish, wherein the impacts of ectopic *Grhl*3 expression have differing effects on the development of the organism.

Similarly to *Grhl*2, *Grhl*3 has known roles in the incidence of craniofacial and neural tube defects in mice. Importantly however, these defects are largely mild by comparison to the substantial morphological changes that follow the loss of *Grhl*2 expression (Goldie et al., 2016). Despite the severe clefting affecting the *Grhl*2 null mouse embryos, craniofacial defects in *Grhl*3 mice appear to be restricted largely to the cranium, wherein premature apposition of the parietal and frontal bones and smaller brain cavities in *Grhl*3$^{+/-}$ mice. This does not, however, suggest that *Grhl*3 is not a critical gene for the development of the mouse embryo, as *Grhl*3$^{-/-}$ mice die pre-natally. This embryonic lethality is likely the result of severe thoraco-lumbar spina bifida associated with these null embryos. *Grhl*3$^{-/-}$ induced spina bifida is also resistant to rescue from folate and inositol which rescue neural tube defects in some other instances (Ting et al., 2003). The well characterised *curly tail* mouse phenotype is used to model spina bifida in mice and is associated with a hypomorphic *Grhl*3 allele (De Castro et al., 2010). As mentioned above, the mechanisms through which loss of *Grhl*3 lead to those phenotypes is not well known but may involve defects in cell projections and epidermal migration which prevent the proper fusion of tissue in important events including neurulation and palatal shelf fusion.

Conversely, zebrafish models demonstrate a far more involved function for *Grhl*3 in craniofacial and neural tube development. Morpholino induced knockdown experiments on *grhl*3 expression in zebrafish demonstrate hypomorphic development of the craniofacial structures of the developing zebrafish embryo (Miles, Darido, et al., 2017). This defect is notable for its resemblance to *Grhl*2 hypomorphism in the lower jaw, further highlighting the similarity

between *Grhl*2 in mice and *grhl*3 in zebrafish (de Vries *et al*, 2021). These *grhl*3 defects are thought to involve edn1, due to similarities in the craniofacial structures demonstrated in the *sucker* mutant which was identified as being the consequence of a mutation in edn1 (C. T. Miller et al., 2000). Further analysis showed that *grhl*3 hypomorphism was the result of NCC cell death in the pharyngeal arches, and that edn1 was a downstream target of *grhl*3 and likely a mediator of *grhl*3 function. The process through which edn1 was identified as being a target gene of *grhl*3 and a key gene governing craniofacial development, is evidence of the value of zebrafish as a model, and an example of a potential approach to identifying target genes of *grhl*3 in craniofacial development.

Table 1.1: *Grhl*2 and *Grhl*3 defects and functions across species

Model organism	***Grhl*2**	***Grhl*3**
Human	Hearing loss Ectodermal dysplasia	Van Der Woude syndrome
Mouse	Cleft face (Craniofacial Defects) Open Neural tube	Spina bifida Skin barrier formation Epidermal wound healing defects
Zebrafish	Convergence-Extension defects Otic vesicle development impairment	Hypomorphic Jaw structures (Craniofacial defects)

1.17 Identification of target genes

The investigation of genes that cause defective phenotypes in organisms has traditionally used one of two approaches – forward or reverse genetics. Forward genetics begins with the identification of a phenotype and seeks to investigate the causative gene through mutagenesis and genetic screens. Conversely, reverse genetics begins with an established gene, and uses techniques to reduce or eliminate expression of the gene and observe the effect that this has on a developing organism.

The identification of *Grhl* genes has primarily involved a reverse genetics approach using various experimental approaches to refine the roles of *Grhl*2 and *Grhl*3 and its targets in tissue fusion. RNA sequencing experiments allow for the generation of lists of genes which may be affected by changes in *Grhl* expression (Skromne & Prince, 2008). These experiments are, however, limited

in terms of the conclusions that may be drawn from them. RNA sequencing does not establish whether the identified genes are directly regulated by *Grhl*, nor does it suggest that downregulation of a given gene is associated with the phenotype or any potential mechanism. Chromatin Immunoprecipitation (ChIP) provides evidence of binding between an upstream gene (*Grhl*) and its downstream effectors, and as such is an important step in establishing the direct regulation of transcription factors to their targets (Carey, Peterson, & Smale, 2009).

Neither of the above methods, are able to establish a relationship between the differentially regulated genes and abnormal phenotypes. These phenotypes, and the underlying genetic causes, need to be modelled in animals to provide evidence of their roles in development and disease. The literature surrounding *Grhl* target genes has primarily utilized mice and zebrafish studies to investigate candidate genes and establish their relevance to developmental defects. Given the well conserved nature of the *Grhl* family, even morphologically and evolutionarily distant organisms including teleosts (of which zebrafish are an example) can yield relevant findings for human developmental defects.

This project will utilise both mouse and zebrafish models to identify and characterize the roles of, *Grhl*2 and *grhl*3 target genes and their roles in tissue fusion and craniofacial development.

1.18 Aims

To determine whether *grhl*3 and the predicted *grhl*3 target genes *tmem54* and *pvrl4* regulate craniofacial development in zebrafish

To identify downregulated gene pathways in the primordial craniofacial tissues of *Grhl*2$^{-/-}$ mice

To investigate the molecular changes that result from deregulation of the *Grhl*2-*Noggin* pathway

Chapter 2

Methods

2.1 Animal ethics

All mouse conduct and experimentation was conducted in compliance with the standard protocols for the La Trobe Animal Research and Training Facility (LARTF), and approved by La Trobe ethics board (AEC-21-001).

2.2 Zebrafish housing, maintenance and husbandry

Zebrafish were housed at the LARTF at a temperature of 28^{o}C with 12 hour light/dark cycles between 8pm and 8am. Zebrafish breeding was conducted using sloped breeding tanks (Tecniplast UK). Males and females were separated the day before embryo collection, and then allowed to mate for 15 minutes the following morning. Embryos were collected immediately and injected whilst at the 1-2 cell stage.

2.3 Animal line derivation

*Grhl*2$^{+/-}$ Noggin$^{+/-}$ mice were re-derived from frozen sperm samples in C57-BL/6 strain mice at the Australian Phenomics facility at the Australian National University. *Grhl*2 mutants contain a LacZ sequence region in place of exon 3 and the mBOM12 primer sequence in Exon 2. Double heterozygote (*Grhl*2$^{+/-}$ Nog$^{+/-}$) progeny were selected for maintenance of the colony. single heterozygotes (*Grhl*2$^{+/-}$,Nog$^{+/+}$ or *Grhl*2$^{+/+}$, Nog$^{+/-}$) and double heterozygotes, were utilised for breeding to produce the desired progeny.

2.4 Mouse housing

Mouse colonies were housed initially at the Australian Phenomics facility until approximately 9 weeks of age, and then transferred to the Specific Pathogen Free (SPF) zone at LARTF, to minimise exposure to foreign pathogens.

2.5 Mouse embryo extraction

Pregnant mice were transferred from the SPF area and culled using CO2 asphyxiation at a displacement rate of 20% of chamber volume per minute (in accordance with LARTF culling procedures). Secondary cull methods included decapitation and cervical dislocation. Dissected samples of maxillary prominence, genotyping material and whole embryo specimens were transported on ice and stored at -20°C until use. Samples collected for RNA extraction were transported using liquid nitrogen to avoid degradation. Dissection of facial prominence and pharyngeal arch epithelium/mesenchyme for qPCR analysis was performed by Dr. Marina Carpinelli at the Australian Centre for Blood Diseases.

2.6 Genotyping

Genotyping of adult mouse samples utilised ear clips, whilst embryo genotyping utilised either yolk sack or limb bud tissue. In all instances, the HotShot method of DNA extraction was used: specimens were incubated in 50mM NaOH for 40 mins at 100°C. Samples were cooled on ice and neutralised with 1M Tris-HCl using 1:10 the volume of NaOH. Samples were centrifuged at 13,000 x g for 5 minutes, and the supernatant was used for PCR. Samples were stored at 4°C for less than a week before being transferred to -20°C freezers.

1µl of the supernatant containing extracted DNA was added to 1µl of each primer (listed below), 10µl of GoTaq G2 DNA polymerase (Promega) and 6 µl of MilliQ water to a total volume of 20µl. A Bio-Rad C1000 thermocycler using settings outlined below (table 2.1) was utilised for PCR.

Table 2.1: *Grhl*2 and Noggin genotyping primers

Gene	Primers	PCR settings
*Grhl*2	mBOM11 mBOM12 LacZ promoter	95°C – 5 mins 95°C – 30s 60°C – 30s 72°C – 1 min 72°C – 7 mins 10°C – until gel loading
Noggin	P1 P2 P3	94°C – 5 min 94°C – 45 sec 65°C – 30 sec 72°C – 1 min 72°C – 7 mins 10°C – until gel loading

PCR products were run on a 2% agarose gel with SYBR safe (Invitrogen) used at a dilution of 1:25 v/v. The gels were run for 75 minutes at 110V. Imaging of agarose gels was completed using a BioRad Chemi-Doc XRS+ gel imager and analysed via Chemilab imaging software.

2.7 Paraffin embedding and sectioning

Slides for use in Immunohistochemistry (IHC) were prepared by embedding whole E9.5 and E10.5 embryos in paraffin wax. Following embryo extraction, samples were initially stored in 4% PFA in PBS for at least 60 mins at 4°C. embryos were then transferred to 70% ethanol and stored

at 4°C until embedding. Tissue was dehydrated in alcohol before transfer to a Leica TP1020 paraffin processor. Settings for paraffin processing are outlined in table below (fig 2.2). Samples were then transferred to a paraffin sample mould and immersed in paraffin wax. Sample moulds were then cooled and sectioned using a Leica RM2045 microtome in 10 µm sections. Sections were immersed in a water bath at 55°C before transfer to slides.

2.8 Immunohistochemistry

Slides were incubated at 60°C for 45 minutes to melt paraffin wax and assist section adherence, prior to rehydration. Slides were then washed in Histolene for 2 x 4mins, and rehydrated via 4 x 1min washes in 100% ethanol, 1 x 1min wash in 70% ethanol, before immersion in H_2O for 10 minutes at room temperature. Antigen unmasking utilised a sodium citrate buffer (0.018M citric acid, 0.082M $Na_3C_6H_5O_7$, pH 6). The sodium citrate buffer was boiled using a microwave oven, slides were then immersed in the buffer and placed in the microwave on a high setting for 3 minutes, agitated, and then boiled for a further 3 minutes before allowing the buffer to cool to RT for ~30 mins. The slides were then removed from citrate buffer and washed for 3 x 5mins using PBS to remove excess buffer. To maintain a humid environment and thus prevent drying out, a humid chamber was created using a slide box with wet paper towel to provide moisture. 3% H_2O_2 was then added for 30 mins to block endogenous peroxidases.

Anti-Noggin primary antibodies (BIOSS-2975R, Bioss antibodies) were diluted to 1:250 (4 picogram per µl) and Anti- pSMAD5 antibodies (Rabbit mAb, ab92698, abcam) were diluted to 1:500. For analysis of epithelial/mesenchymal signals, Anti-Vimentin (Rabbit mAb, #5741, Cell Signalling Technology) and Anti E-cadherin (Rabbit mAb, #3195, Cell Signalling Technology) at 1:500 dilutions were used. 80µl of primary antibody in PBS was added to each section, and slides were incubated overnight at 4°C in the humid chamber.

Primary antibody was removed using 1 x 10min, followed by 2 x 5 min PBS washes. 80µl of biotinylated universal anti-rabbit secondary antibody diluted to 1:1000 in PBS, was added to each section. Slides with secondary antibody were incubated for 50 minutes at room temperature in a humidified chamber. During incubation, a streptavidin/biotin (ABC) detection solution was prepared (ABC Vectastain Elite, Vector Laboratories) using 1:50 dilution of Vectastain solutions A and B (as specified by manufacturer). Secondary antibody was then removed with 3 x 5 min PBS washes and the ABC kit detection solution was added for 30 mins at RT. The ABC solution was then removed using 3 x 5min PBS washes. 3,3'-diaminobenzidine tetrachloride (DAB)(DAB substrate kit, peroxidase, SK-4100 - Vector Laboratories) was added to visualize HRP according to manufacturer's instructions. When brown precipitate became visible

(approximately 5 minutes) slides were placed in PBS to halt the reaction. Slides were washed for 30 mins in H2O, air dried for 12 hours and coverslipped using 200 µl of Distyrene/plasticisiser/xylene (DPX, sigma). Slides were imaged using a Leica DMRBE brightfield microscope and DFC 290 camera.

2.9 Protein extraction

Protease and phosphatase inhibitor cocktails (sigma) were diluted to 1:10 in RIPA buffer. Tissue samples were thawed and suspended in either 50µl, 100µl, 200µl, or 300µl of the RIPA buffer + inhibitors and placed on ice. The Tissue samples were homogenized using a disposable polypropylene pestle and placed on ice for 15-20 minutes to allow for the sample to dissolve. The dissolved tissue sample was then centrifuged at 4°C, and 13,200 G for 15 mins to pellet undigested material. The supernatant was then removed and stored at -80°C until use.

2.10 BCA assay

To determine protein concentration from tissue extracts, BCA assays were performed using Pierce BCA protein assay kit (Thermofisher scientific, USA). Kit reagent B was diluted 1:50 in reagent A to create a working reagent for each sample. 25µl of protein sample was added to each well and all samples were run in triplicate. To establish a standard curve, a blank sample, 25 µg/ml, 50µg/ml, 125µg/ml, 500µg/ml, 1,000µg/ml and 2,000µg/ml standards were produced using Bovine serum albumin diluted in the same RIPA Buffer + protease/phosphatase inhibitor mixture used for protein samples. 200µl of working reagent was added per well to begin the reaction, after which the plate was incubated in the dark at 37°C for 30 mins. The plates were then allowed to cool to room temperature and the absorbance was measured using a Thermofisher multiskan spectrophotometer at 562 nm.

2.11 Western Blot analysis

The extracted protein samples detailed above were diluted to ensure that all samples contained equal total protein concentrations. 15µl of each sample was mixed with 5µl of western loading dye and boiled at 95°C for 5 minutes, cooled, and were run on a 10% SDS PAGE gel (table 2.2) with a (Precision Plus Protein™ Kaleidoscope™ Prestained ladder #1610375) at 140v for 60 mins. Gels were run in running buffer composed of 50% Tris glycine buffer in distilled H_2O.

Figure 2.2: Main and stacking gel components for SDS page gels

Main gel (5ml) components	**Concentration**
Distilled H2O	40% of final volume
30% acrylamide mix	35% of final volume
1.5M Tris pH 8.8	7.5mM final concentration
10% SDS	0.01% final concentration
10% ammonium persulfate	0.01% final concentration
Tetramethylethylenediamine (TEMED)	0.004% final volume

Stacking gel (1ml) components	**Concentration**
Distilled H2O	0.68% of final volume
30% acrylamide mix	0.17% of final volume
1.0M Tris pH 6.8	1mM final concentration
10% SDS	0.0001% final concentration
10% ammonium persulfate	0.0001% final concentration
Tetramethylethylenediamine (TEMED)	0.1% final volume

Concurrently, a transfer buffer composed of 20% methanol, 14.41 g/L glycine, 3.03 g/L Tris in distilled H2O was made for later use. Next, the gel was removed and placed on a nitrocellulose membrane with filter paper either side and placed into a bio rad transfer apparatus. The transfer apparatus was then immersed in transfer buffer and run for 1 hour at 100v.

Following the transfer, the membrane was blocked using 5% skim milk powder in TBS-t for 1 hour. Anti-Noggin antibodies were then diluted to 1:1000 in 1% skim milk, whilst anti-β-actin antibodies were diluted to 1:10,000. Membranes were then cut vertically so that β-actin and *noggin* could be probed separately and placed in their respective antibody overnight at 4°C.

The membranes were then washed 3 x 5mins in TBS-t to remove unbound primary antibody, and Horse Radish Peroxidase conjugated secondary antibodies (goat anti-rabbit and Goat anti-mouse) were diluted to 1:10,000 in 1% skim milk/TBS-t. Membranes were incubated in secondary antibody for 1 hour at room temperature before 5 x 10min washes in TBS-t to remove unbound secondary antibody.

Detection of bound secondary antibodies utilised Develop with Clarity western ECL substrates (bio rad). Substrates A and B were mixed 1:1 on a flat surface, and the membrane was placed

face down on the mixed substrate and left to incubate in the dark for 5 mins. Imaging of the membranes was performed using a Bio-Rad Gel-doc chemiluminescent imager.

2.12 Morpholino Microinjection

Approximately 2nl of Morpholino oligonucleotide was micro-injected into zebrafish embryos no later than the two-cell stage (~30 minutes post-fertilisation; Kimmel, Warga and Kane, 1994). Embryos were monitored at 6 hpf, then subsequently every 24 hours. Data derived from using both ATG- and splice-blocking morpholinos to inhibit *grhl3* were analysed. Sequences of all morpholinos are provided in Table 2.3.

Table 2.3: Candidate and control genes, morpholino sequence and type.

Gene	**Site**	**Morpholino type**
MO:*grhl*3	5' TGAGAGCCTCAATCTCCTTGGTCAT	ATG-blocking/splice blocking
MO:*tmem54a*	5'-GGCCTTCTTTCGGATTAAGTCATAA-3'	ATG-blocking
MO:*tmem54b*	5'-GCAACACAACCCTGAAGTACCCATC-3'	ATG-blocking
MO:*pvrl4*	5'-CATGTTGCTGCTTAATTCACACGTT-3'	ATG-blocking
Control	5'-TGTTACTCTCTCTCTCCTCTGAGAT-3'	5-Pair mismatch

2.13 Alcian Blue staining

At 96 hours post fertilization (hpf), zebrafish larvae specimens were euthanized in Benzocaine, and fixed in 4% paraformaldehyde for 24 hours at 4°C. Specimens were subsequently dehydrated in acid alcohol for 30 mins at 50%, 70% and 90% EtOH, before staining with 0.1% w/v Alcian blue for 16 hours in 4:1 ethanol:acetic acid at room temperature. Specimens were then rehydrated for 30 mins in an ethanol series with concentrations of 90%, 80%, and 70% acid alcohol, before being transferred to PBST.

Specimens were bleached in Hydrogen peroxide for 1 hour, and washed twice in PBST before being stored in 70% glycerol at 4°C.

2.14 Generating DNA templates from plasmid vectors

Anti-sense RNA riboprobes for ISH use were generated from vectors containing the DNA template encoding each respective riboprobe. These were: *edn1 , snai1* & *sox9b* (Cheung et al., 2005; C. T. Miller et al., 2000)*, gsc* (Jung et al., 2020)*, dlx2 & dlx3 (*D. Wang et al., 2019) and *hand2* (Angelo et al., 2000), *krox20*, *tfap2a* and *pax2a* (Dworkin et al., 2012; Dworkin et al., 2007; Dworkin et al., 2014).

To linearise the plasmids, 5μg of plasmid was linearised by incubating with 1 μl *XhoI* restriction enzyme, 0.2μl BSA, 2μl restriction enzyme buffer in a final volume of 20μl with nuclease-free water for 37^{o}C for 3 hours, before incubation at 65°C for 15 minutes to inactivate the Xho1. Linearized DNA was precipitated using 10μl NaOAc and 500μl 100% ethanol via benchtop centrifugation at 13,000 rpm for 30 minutes at 4°C. The pellet was then washed in 70% ethanol and spun for 5 minutes at 4^{o}C and resuspended in double distilled water (DDW).

2.15 Generating RNA riboprobes

In order to generate riboprobes, 1μg of linearised plasmid was incubated with 2μl 10x DIG labelling mix (Roche), 4μl 5x Transcription Buffer (Promega), 2μl DTT (Promega), 1μl RNAsin (Promega), 2μl T7 RNA and DDW to a final volume of 20μl for 2.5 hours at 37^{o}C. Next, 1μl RNase free DNase was added and the riboprobe incubated for 12 mins to remove the plasmid. The riboprobe was precipitated by addition of 4μl 1M LiCl and 75μl 100% ethanol, incubation at -70°C for 2 hours and centrifugation at 13,000rpm for 30 minutes at 4°C. The supernatant was removed, and the pellet was then washed in 70% ethanol, spun for 5 minutes and resuspended in 50μl water. An aliquot (5μl) was removed to assess concentration using a spectrophotometer. A working solution of riboprobe was made by diluting the stock to 1ng/μl in HYB+ solution.

2.16 In Situ Hybridisation

Dechorionated embryos were fixed in 4% paraformaldehyde overnight at 4^{o}C, then washed 3 x 10 minutes in PBST. Fixed embryos were dehydrated using a methanol series (25% methanol/75% PBST, 50% methanol/50% PBST, 75% methanol/25% PBST, 2 x 100% methanol, 10 min per wash, at room temperature). Following the series, embryos were stored overnight in 100% methanol at -20°C.

Rehydration of the zebrafish embryos was achieved by reversing the methanol series above, culminating in 2 x 10 min washes in PBST, re-fixation with 4% paraformaldehyde for 20 mins, and a further 2 x 10 min washes in PBST. Next, embryos were digested in a 500µl solution of 20µg/ml proteinase K/PBST for 25 minutes and rinsed with PBST.

Prehybridisation steps required embryos to be separated into riboprobe specific batches. PBST was replaced with HYB- solutions and incubated at 70^{o}C for 15 minutes. The solution was then replaced with HYB+ and incubated for 4-6 hours at 70^{o}C.

Riboprobe RNA secondary structures were removed by heating the solution for 10 mins at 68^{o}C. The HYB+ solution was then replaced with riboprobe solution and incubated overnight at 70^{o}C. In a hybridisation oven, the riboprobe solution was removed and the embryos were washed for 30 minutes at 70^{o}C with 50% formamide/2x SSCT. Afterwards, embryos were washed 3 times for ten minutes at 37^{o}C in 2xSSCT, 10 minutes at 37^{o}C in PBST and digested with 20µL/ml RNAse for 30 minutes at 37^{o}C. Following RNAse digestion, the embryos were washed in 2X SSCT for 10 minutes, 50% formamide/2xSSCT at 70^{o}C for 1 hour, 2x SSCT for 15 minutes and 0.2x SSCT for 15 minutes twice.

For detection of target mRNA, embryos were washed 3 times for 5 minutes in PBST, blocked for 2 hours in blocking reagent (see section 2.3), and incubated overnight at 4^{o}C in a blocking solution with Anti-DIG and Fab-AP antibody fragments

To develop colour in riboprobe-labelled embryos, 4 washes for 30 mins with PBST, followed by three 5-minute washes with staining buffer were used. Staining buffer was then replaced with staining substrate and placed in the dark at room temperature to develop, for a period of 15 minutes to three hours, depending on probe intensity. Stained embryos were visualised using a Zeiss light microscope.

2.17 RNA extraction and cDNA synthesis

Pharyngeal arch and maxillary prominence samples were collected from E9.5 mouse embryos and immediately placed in 800µl of Trisure and stored at -80°C. Samples in Trisure were homogenized manually using plastic pestles and chloroform was added to 20% of the volume of Trisure used. Samples were shaken for 15 seconds and allowed to rest on ice for 5 minutes before centrifugation at 13,000 rpm for 15 minutes at 4°C. Centrifuging produced phase separation, and the top phase containing the RNA was removed. To this, an equal volume of isopropanol and 4ul of analytical grade glycogen was added and the samples were placed at -80° for approximately 90 minutes to precipitate RNA. Following this, the samples were thawed and

centrifuged for 30 minutes at 13,000rpm for 30 minutes at 4°C to pellet nucleic acids. The supernatant was then removed and replaced with 75% ethanol, centrifuged for 8 minutes at 7700 rpm at 4°C, and dried for 30-60 minutes. Dried samples were resuspended in nuclease-free water and their purity and concentration checked using a nanodrop spectrophotometer.

2μg of RNA was added to a mix contains 0.25μg random hexamers, 0.83mM di-Nucleotide Triphosphate, and diluted with H_2O to 12μl final volume. This solution was incubated for 5 minutes at 65°C and subsequently placed on ice until the addition of the reverse-transcriptase mixture containing 4μl of 5x first-strand buffer, 2μl of 1M Dithiothreitol, 20μg of RNAsin and 40μg of Superscript III reverse transcriptase, to a final volume of 6.9μl added to each RNA template mixture. This mix remained at room temperature for 10 minutes following addition of the reverse transcriptase mix, and then incubated at 50°C for 90 minutes. The superscript was then inactivated by incubation at 70°C for 15 minutes, and the samples were stored at 4°C for up to a week and -20°C for longer term storage.

2.18 Quantitative PCR

A master mix of 0.4μl cDNA, 4μl BioRad Sso Advanced Universal SYBR Green Supermix, and 3.6μl of nuclease-free water per well was created. A working stock of each primer (table 2.5) was created and diluted 1:10 in nuclease-free water. From this stock, 2μl of the appropriate primer working stock was added to each well and 8μl of the cDNA master mix was added, for a final volume of 10μl per well. Each sample was run either in duplicate or triplicate, and blanks utilised 4ul of nuclease free water, 4μl of SYBR green supermix, and 2μl of the respective primer. Hprt was used as a housekeeping gene as it was not expected to differ between experimental and control conditions. qPCR settings and primer sequences are outlined below (table 2.4, table 2.5).

Table 2.4: Forward and Reverse primer sequences for qPCR

Gene	**Forward primer**	**Reverse primer**
Sonic Hedgehog	5’ GAAGGGAAGATCACAAGAAACTCC	5’ ACTTGTCTTTGCACCTCTGAGTC
Gli1	5’ CCCTGTGTACCAGACTCTACTC	5’ ACCATATCCAGCTCTGACTTC
Gli2	5’ ATATGGAGCACTACCTCCGGTCT	5’ CTAAAGAGTCCCCTCTCTTTCAGA
Gli3	5’ AGTTCCTTGCAGTTATGCAGTAGG	5’ TACTTGAGACACATCCCAATCAGG
Fgfr2	5’ CCTCTGGACAACACAGCTTATTTAT	5’ TTAGATTCAGAAAGTCCTCACCTTG
Ovol1	5’ CGAACCAAGATGAAGGTGAC	5’ GTAGGGCCGCACACCAGT
Hprt	5’ GCTGGTGAAAAGGACCTCT	5’ CACAFFACTAGAACACCTGC

Table 2.5: qPCR settings

Step	Settings	Repeat
Denaturation	95°C for 3:00 minutes	X1
Denaturation	95°C for 10 seconds	X40
Annealing	60°C for 10 seconds (plate read)	X40
Melt Curve	65°C - 95°C, 0.5°C increment	1x

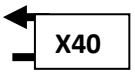

2.19 Acridine Orange staining

Live zebrafish were treated with 0.006% PTU/DMSO in e3 media at 8hpf to prevent pigmentation. At 72hpf, larvae were collected and allowed to swim in 10μg/ml acridine orange in e3 media for 30 minutes at room temperature in the dark. Following this, embryos were anaesthetized using AQUI-S fish anaesthetic, diluted 1:20 in e3 media. Live embryos were then imaged using a fluorescent microscope with a FITC filter.

2.20 Statistical Analysis

Statistical analysis of phenotypic incidence was conducted using a Welch's t-test, comparing control morpholino-injected embryos with experimental morpholinos, while a students' t-test was utilised for analysis for the comparison of fluorescent cells in acridine orange staining. Q-PCR results detailed in chapter 2 were analysed using the ΔCT method, whereby the average difference incycle-threshold values of target genes and the housekeeper gene were calculated, and then null-genotype samples subtracted from control (+/+) samples. These results were then analysed for statistical significance using a students' t-test.

Chapter 3: zebrafish *grhl3* and its putative target genes

3.1 Introduction

3.1.1 *grhl*3 as a regulator of zebrafish craniofacial development

The well-conserved nature of the *Grhl* family of transcription factors allows for the accurate modelling of *grhl* associated disease in organisms as morphologically dissimilar as mice and zebrafish. Despite the well-conserved nature of these genes as a family, the distinct roles of each *Grhl* orthologue across species do appear to vary, as outlined above. In zebrafish, *grhl*3 in particular is key to a number of developmental processes, including facial and spinal development. Knockdown of *Grhl*3 has been identified as leading to hypoplasia of facial cartilages in the early development of zebrafish larvae (Dworkin et al., 2014). Additionally, knockdown was associated with axial extension defects. The pathway through which these defects are manifested in zebrafish embryos is, however, unknown. *Edn1* is a downstream effector of *Grhl*3 signalling and loss of edn1 in pharyngeal signalling was the underlying cause of craniofacial defects in the absence of *grhl*3. The identification of edn1 in the *grhl*3 signalling pathway and the techniques which facilitated its identification, provide evidence for the use of the efficacy of zebrafish knockdown experiments in identifying and characterising craniofacial target genes.

3.1.2 Identification of putative target genes by in silico and meta-analysis

Using RNA sequencing, quantitative PCR and ChIP, many putative target genes have been identified in the literature thus far, including *cldn23*, *ppl* and *prom2*. Mathiyalagan (2019) provided a comprehensive list of differentially regulated genes from *grhl*2 knockout datasets in various model organisms as well as human samples. Predicted target genes (based off of the presence of the conserved *Grhl* binding sequence) were compared to differentially regulated genes in *Grhl*2$^{-/-}$ models to generate a list of candidate genes. The genes *Transmembrane 54* (Tmem54) and *Polio-virus receptor like 4* (Pvrl4) were identified as being differentially regulated in two microarray data sets: *Walentin et al* (2015) which examined differentially expressed genes in the placenta of *Grhl*2$^{-/-}$ mice at E9.5, and *Aue et al* (2015) which examined gene expression in kidney samples of E15.5 mice. Further, these genes were found to be directly regulated by *Grhl*2 in mice as evidenced by ChIP experiments which found their locus bound by *Grhl*2 (Chung et al., 2019). These data provided the basis for further investigation into the role of these genes in other models, for example zebrafish, based on the evolutionarily conserved characteristics of *Grhl* pathways in craniofacial development.

3.1.3 Investigating craniofacial candidate genes in zebrafish

Much of the literature regarding Tmem54 focusses on its role in oncogenesis. However even within the existing cancer biology literature, Tmem54 has only been identified as being differentially regulated in various carcinomas, with no direct evidence or animal/cell lines having been established to study its' function. In mice, ectopic *Tmem54* expression was linked to hepatic tumours following arsenite exposure, however its most relevant function appears to be its ability to regulate micro RNA (miRNA) (Luo et al., 2012). The exact method through which *Tmem54* regulates miRNA and its' involvement in hepatic tumours is unknown, however *Grhl* genes have been linked to similar functions in miRNA regulation and hepatic tumours (Darido et al., 2011; Nishino et al., 2017). This function was identified in the context of nasopharyngeal carcinoma, where *Tmem54* was identified as a potential regulator of miRNA sequences involved in the progression of this disease. The importance of this putative function is twofold: firstly, it presents a role for Tmem54 in the pharyngeal region, which (as mentioned above) is implicated in the development of the face, although the exact expression patterns of Tmem54 in the pharyngeal regions during embryonic development still remain to be investigated. Secondly, members of the *Grhl* family are known to both regulate transcription of miRNA's themselves and to act downstream of the influence of various miRNAs (Satishchandran et al., 2018; Yu et al., 2017). Even amongst the relatively scant literature surrounding Tmem54, there appears to be some overlap in the phenotypic and regulatory contributions of Tmem54 and *Grhl* genes.

When compared to *Tmem54*, *Pvrl4* function is better characterised. Much of the existing literature surrounding *Pvrl4* focusses on its role as an entry point for polio and measles viruses, as well as its association with nectinopathies. The latter role is particularly significant, as Pvrl4 codes for Nectin 4 and nectinopathies frequently result in cleft lip/cleft palate (Brancati et al., 2010). In particular, loss of *Pvrl4* is causative in ectodermal-dysplasia syndactyly syndrome, where loss of function in *Pvrl4* appears to affect cell junction formation via a loss of Pvrl4 receptors in keratinocytes. It appears that *Pvrl4* and *Grhl*2 overlap in terms to some degree, as *Grhl*2 has been linked to keratinocyte function and ectodermal dysplasia (Chen et al., 2012; Petrof et al., 2014). Further, both *Grhl*2 and *Tmem54* are differentially regulated in various tumour lines, and both are directly regulated by the tumour suppressor p63 (Mehrazarin et al., 2015; Mollo et al., 2015). Despite the notable similarities in terms of function and genetic regulation between *Grhl* genes and *Pvrl4*, no direct link between *Pvrl4* and craniofacial development has yet been established.

This study will focus on characterising the role of *Grhl*3 and its putative downstream genes *Tmem54* and *Pvrl4* in the craniofacial development of zebrafish, through the transient knockdown of their zebrafish orthologues. Additionally, the mechanisms through which these

genes may regulate NCC function will be investigated in order to further elucidate the genetic mechanisms behind facial development.

3.2 Results

3.2.1 *grhl3* inhibition results in craniofacial defects in zebrafish

grhl3 morphant embryos display defects in a number of skeletal structures throughout the face, resulting in a significantly reduced lower jaw (fig. 3.1). Defects in the lower jaw of morphant zebrafish are characterized by hypoplasia of Meckel's cartilage (MC) in which the distal portions are absent in the morphant embryos (B,D) (fig3.3). The palatoquadrate (PQ) cartilage of morphant embryos also developed abnormally (B), in a position more proximal than is seen in wild type embryos. The hyosymplectic, which exists posteriorly to both the Meckel's cartilage and upper jaw structures, remained in its expected position, but was significantly reduced in size.

Abnormal development of facial structures extends to several other structures outside the zebrafish jaw. The ceratobranchial bones (cb) are part of a second set of jaws found in zebrafish (amongst other fish) and in *grhl3* morphants were entirely absent when compared to wild types (A, B respectively). Further, the ethmoid plate (ep), part of the neurocranium of the zebrafish, was also affected by knockdown of *grhl3* as it displayed significant hypoplasia and did not extend as far ventrally in *grhl3* morphants when compared to controls.

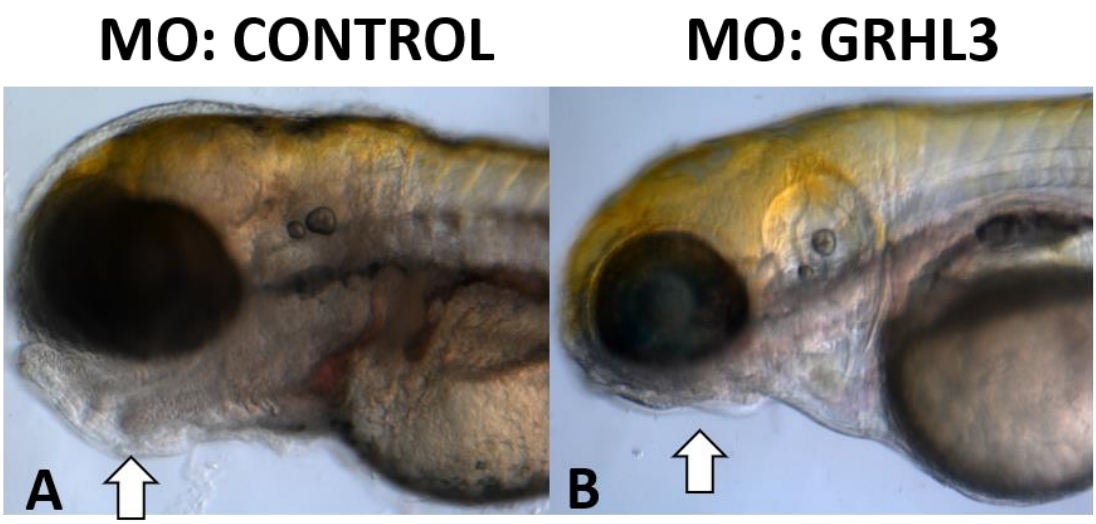

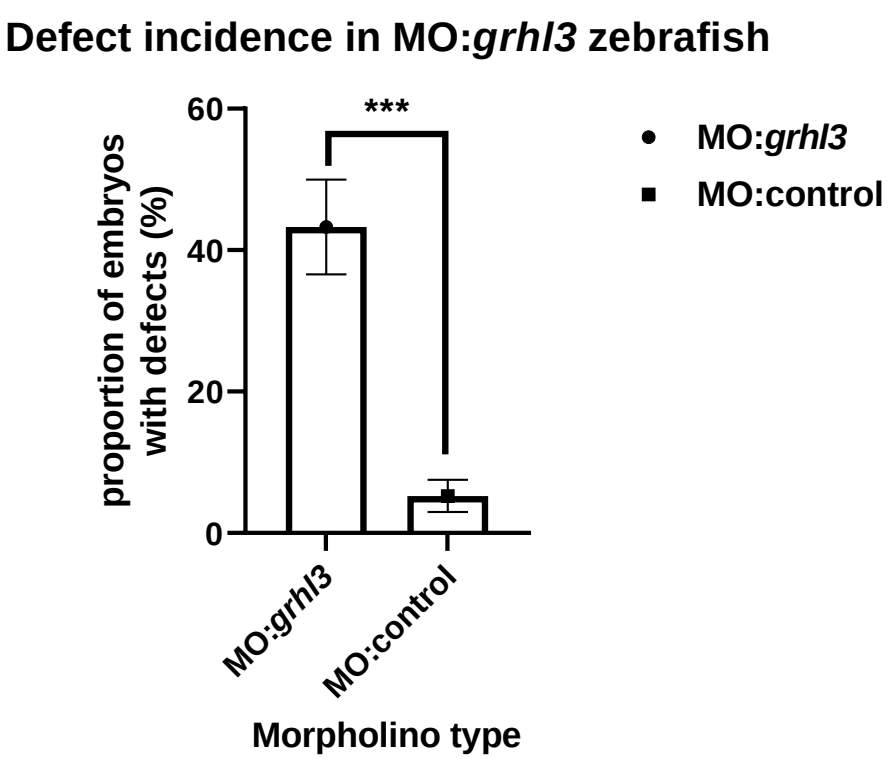

Figure 3.1: Facial phenotypes of *grhl3*-morphants at 5dpf. MO:*grhl3* embryos (B) display defects in the development of the ventral face, particularly the lower jaw when compared to controls (white arrows) (A). Of surviving embryos, those injected with the *grhl3* morpholino displayed a greater number of morphant phenotypes (43.27% +/- 6.89%; n=164/382) than those injected with a control morpholino (5.24% +/- 2.29%; n= 22/298; p = 0.0006 by Welch's t-test).

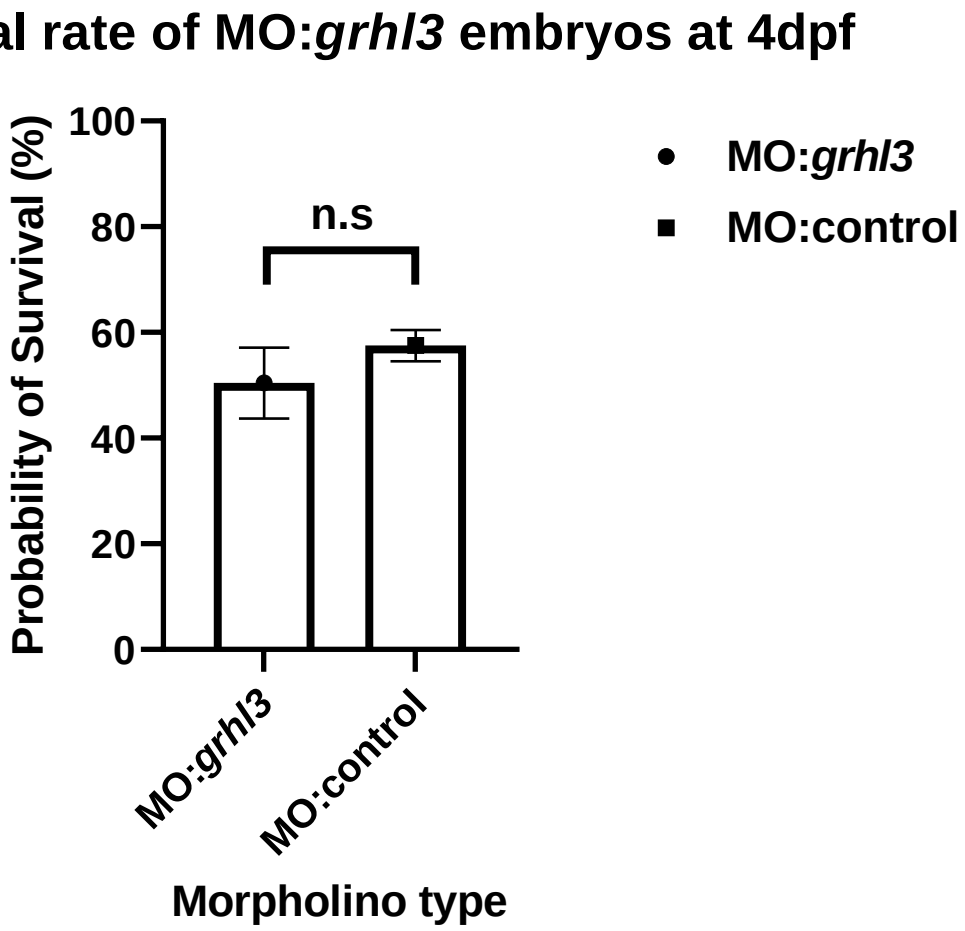

Figure 3.2: Overall survival rate following morpholino injection. The survival rate of MO:*grhl3* zebrafish embryos was 50.42%+/-6.71%, while the survival rate of MO:control embryos was 57.51% +/-2.98%. There is no statistically significant difference in survival between *grhl3* morpholino and control morpholino injection. MO:*grhl3* n= 382, MO:control n=298.

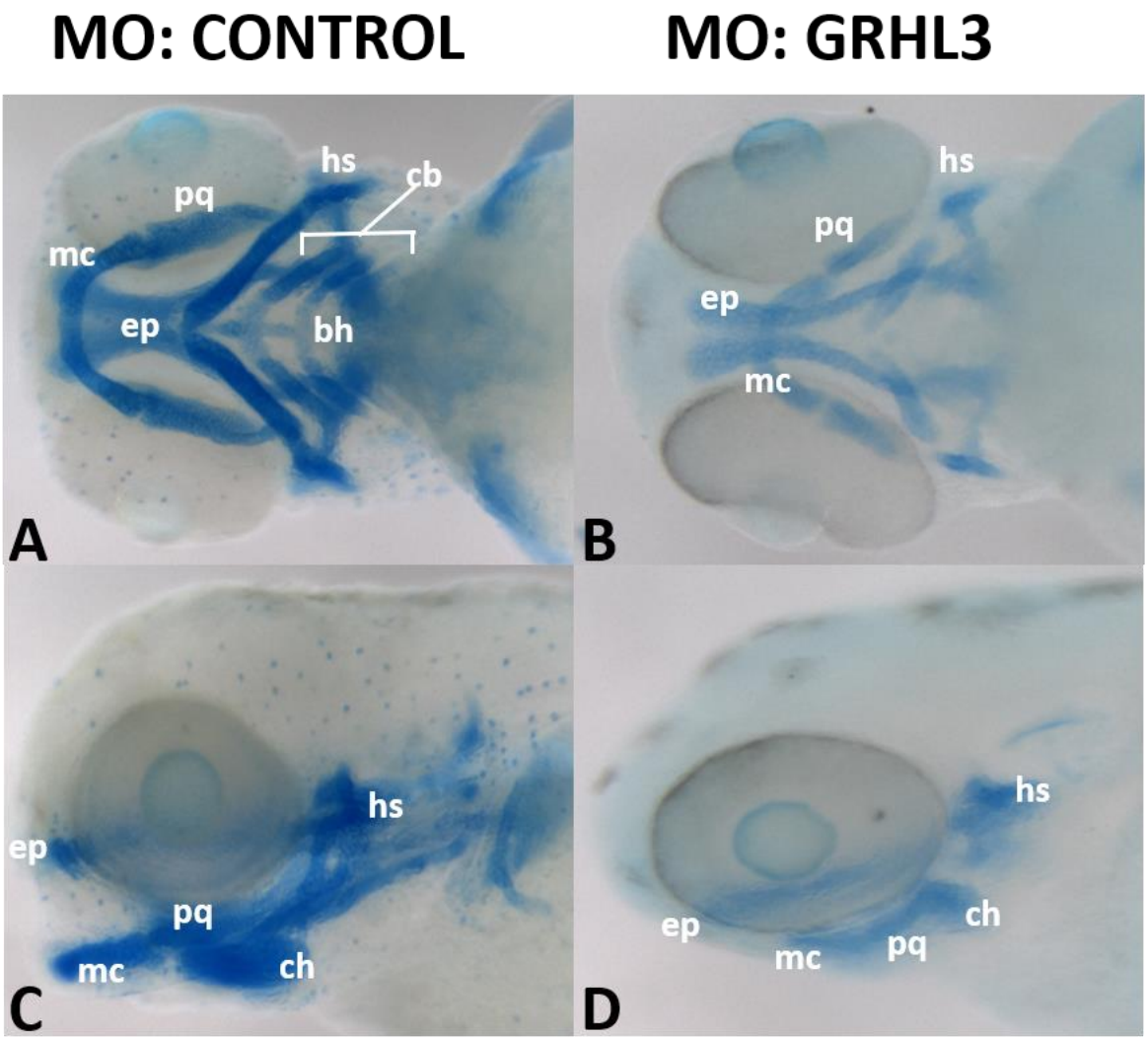

Figure 3.3: Zebrafish craniofacial alcian blue stain. *Grhl3* morphants display a characteristic phenotype presenting with a markedly reduced lower jaw. Alcian Blue staining shows hypoplasia of Meckel's cartilage in stained *grhl3* morphant specimens (B, D) when compared to wild type specimens (A, C). Abnormal development of the ethmoid plate and absence of the ceratobranchial cartilages is also shown in *grhl3* morphant specimens (B, D). (A, B: dorsal view of wild type and *grhl3* zebrafish respectively stained with alcian blue) (C, D: lateral view of wild type and *grhl3* zebrafish respectively stained with alcian blue). Mc: Meckel's cartilage, ep: ethmoid plate, pq: palatoquadrate, ch: ceratohyal, hs: hyosymplectic, cb: ceratobranchial, bh: basihyal.

3.2.2 *grhl3* expression regulates pathways involved in mandibular development.

In order to ascertain which aspects of lower jaw development were regulated by *grhl3*, marker genes with known functions in jaw development were assayed for mRNA expression. The *edn1*-dlx-*hand2* pathway is a pathway with known functions in the development of the lower jaw. *Edn1* and *hand2* are involved in the growth of the pharyngeal arches, and in particular the

development of ventral skeletal structures including the jaw (Craig T. Miller, Yelon, Stainier, & Kimmel, 2003). *Dlx3* is a component of this pathway that is expressed in the ventral portion of the pharyngeal arch, and its' expression is driven by *edn1* and downregulated by *hand2* (Sasaki, Nichols and Kimmel, 2013).

WISH of zebrafish embryos (24hpf) was used to determine mRNA expression of genes in the *edn1-dlx-hand2* pathway following morpholino-induced knockdown of *grhl3* (Fig. 3.4). *Edn1*, *dlx3* and *hand2* all displayed significantly aberrant mRNA expression in *grhl3* morphant embryos (Fig. 3.4 B, D, F). *Edn1* and *dlx3* mRNA expression was significantly downregulated in the first and second pharyngeal arches (B, D), when compared both to control embryos (A, C) and relative to unaffected expression within the otic vesicles (ov). *Hand2* mRNA expression remained strong within the second pharyngeal arch (F), however expression in the first pharyngeal arch (responsible for lower jaw development), was entirely absent. Outside the pharyngeal arches, *hand2* expression persisted in the heart. These results suggest that the knockdown of *grhl3* has subsequent effects on the expression of genes in the *edn1-dlx-hand2* pathway, and that the downregulation of these genes is specific to areas of the pharyngeal arches to craniofacial development.

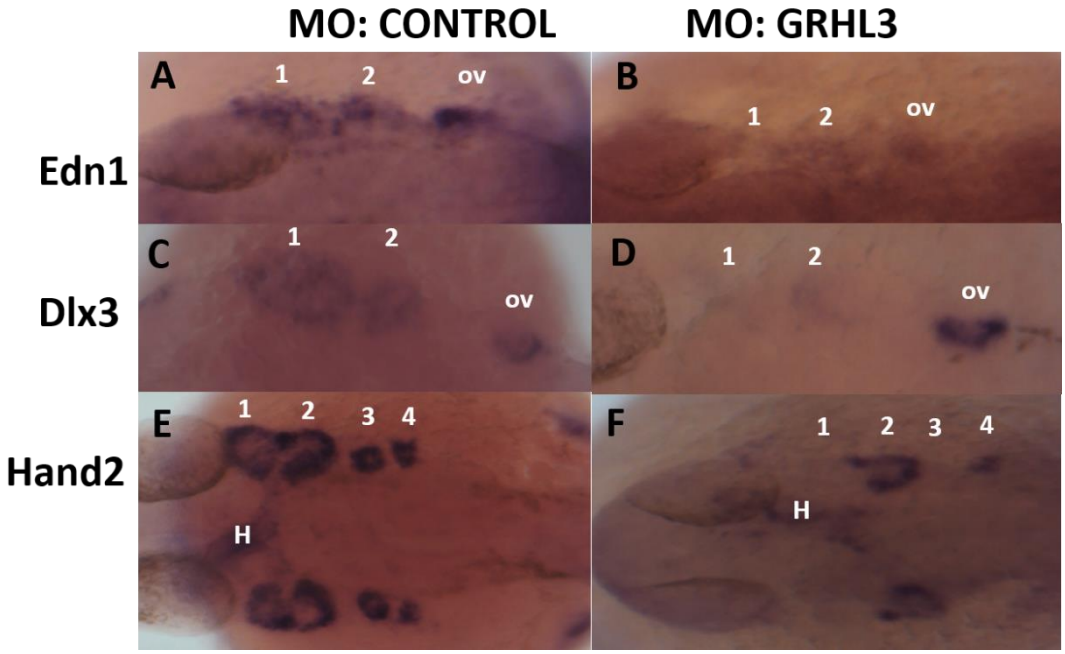

Figure 3.4: Lower jaw development marker gene expression is downregulated in MO:*grhl*3-injected embryos embryos. Expression of *edn1* in pharyngeal arches 1 and 2 was entirely absent, however expression was evident in the otic vesicles when compared to controls. Similarly, *dlx3* mRNA expression was significantly reduced in pharyngeal arches 1 and 2. *Hand2* mRNA expression was absent in the first pharyngeal arch, but not in the second pharyngeal arch or

heart. Control embryos were injected with 5 pair-mismatch morpholinos and showed no aberrant expression of lower jaw marker genes. (1-4; pharyngeal arches 1-4, ov; otic vesicles)

3.2.3 *grhl3* regulation of *dlx* genes is specific to the ventral pharyngeal arch.

The specificity of *grhl3* regulation of pharyngeal arch development was investigated using *dlx2* and *dlx3* as marker genes in a WISH experiment. At 24hpf, *dlx2* is expressed specifically in the dorsal aspect of the pharyngeal arches, whilst *dlx3* is expressed in the ventral portion of the pharyngeal arch that is generally associated with development of the lower jaw.

Dlx2 mRNA expression in the dorsal pharyngeal arches of MO:*grhl3* embryos was unchanged compared to controls (Fig. 3.5: A,B). Conversely, *dlx3* mRNA expression in *grhl3* knockdown embryos was absent in the first and second pharyngeal arches (Fig. 3.5: C, D). These data suggest that the regulation of genes by *grhl3* is specific to the ventral pharyngeal arch and does not affect patterning in the dorsal aspect of the pharyngeal arch. Additionally, the ceratobranchial bones that are notably absent in MO:*grhl3* injected embryos are responsible for a second set of jaws present in many species of fish, including zebrafish. These bones are formed from the same processes and pathways as the Meckel's cartilage, which too was absent. This lends credence to the idea that the effects of *grhl3* regulation are specific to lower jaw development.

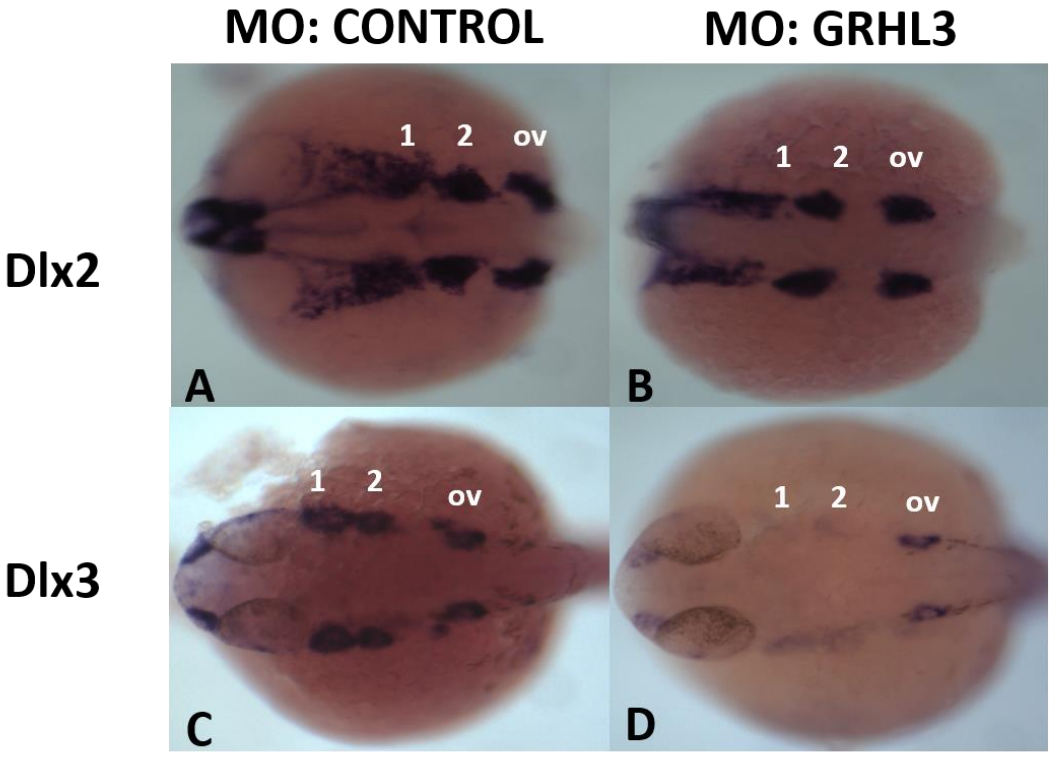

Figure 3.5: *grhl3* inhibition exhibits no effect on *dlx2* expression (A-B), whilst downregulating *dlx3* expression in PA 1 and 2 (C-D). Whole-mount In-Situ Hybridisation of *dlx2* and *dlx3* in embryos treated with *grhl3*-blocking morpholinos and control morpholinos embryos at 24hpf. *dlx2* mRNA expression in the dorsal pharyngeal arches was unaffected compared to controls. Conversely, *dlx3* mRNA expression in the pharyngeal arches is absent. Expression of both *dlx2* and *dlx3* persists outside of the pharyngeal arches in the otic vesicles of both MO:*grhl3* and MO:control embryos. (A) *dlx2* expression in control embryo (B) *dlx2* mRNA expression in *grhl3* knockdown embryo (C) *dlx3* expression in control embryo (D) *dlx3* mRNA expression in *grhl3* knockdown embryo.

To examine the effects of *grhl3* in terms of its' impact on the NCCs prior to those cells populating the pharyngeal arches, marker genes expressed during premigratory NCC specification (Sox9b) and migration (Snai1) were tested for expression in *grhl3* knockdown embryos at 10hpf and 16hpf respectively (Fig. 3.6: A-D). No significant difference was observed in terms of expression of Sox9b or Snai1 when *grhl3* knockdown embryos were compared to controls (Fig. 3.6: A-D). These results suggest that *grhl3* exerts its effect after NCC migration to the pharyngeal arches has been completed. This is also consistent with the observation that NCC derivatives outside of the pharyngeal arches, such as the cardiac neural crest cells, are unaffected.

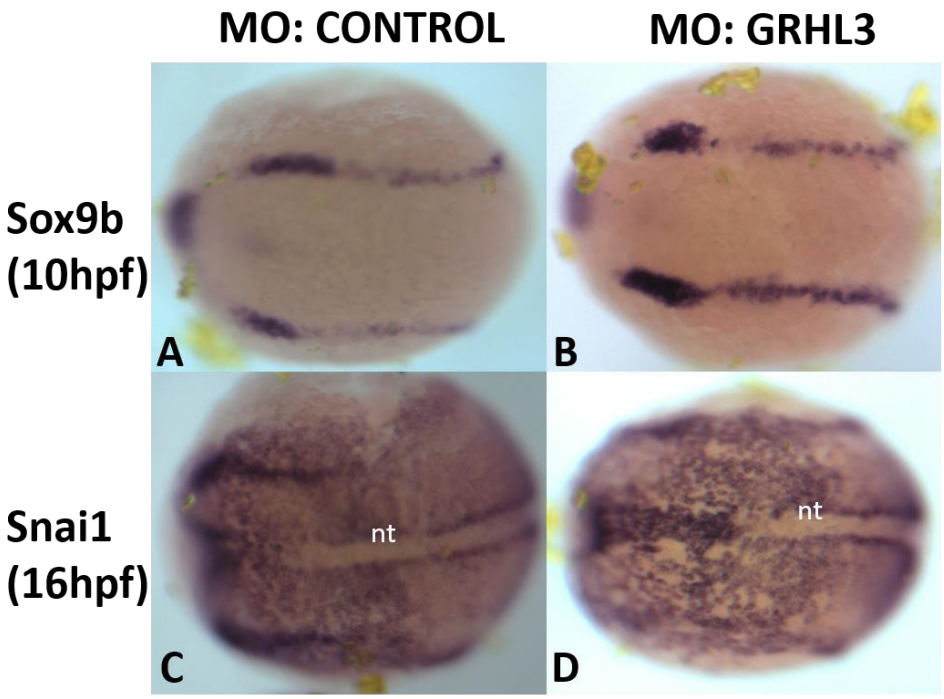

Figure 3.6: Neural Crest Cell (NCC) establishment and migration is unaffected by *grhl3* knockdown. Whole-Mount In-situ hybridisation of Sox9b (10hpf) and Snai1 (16hpf) in *grhl3* knockdown and control embryos shows no significant difference between *grhl3* knockdown and

controls. This test suggests that genes expressed in pre-migratory (sox9b) and migratory (snai1) NCCs are unaffected by knockdown of *grhl3*.

To further investigate the specificity of *grhl3*-dependent regulation of NCCs, the effects of *grhl3* inhibition on cranial NCCs and cardiac NCCs were compared. *Hand2* is a marker of NCCs in both the pharyngeal arches and the heart. Comparing expression of *hand2* following *grhl3* knockdown thus allows the differences between the maintenance of these two respective NCC populations to be determined. Using WISH, it was found that at 24hpf, *hand2* expression was absent in the pharyngeal arches (fig. 3.7, 1-4), whilst no difference in expression was visible in the heart (fig. 3.7, H). These data show that cardiac NCCs are unaffected by loss of *grhl3* and provides further evidence that *grhl3* regulation is limited only to post-migratory NCCs that have entered the 1st pharyngeal arch. Additionally, this is consistent with the observation that the defects which arise in MO: *grhl3* injected embryos are restricted to the lower jaw.

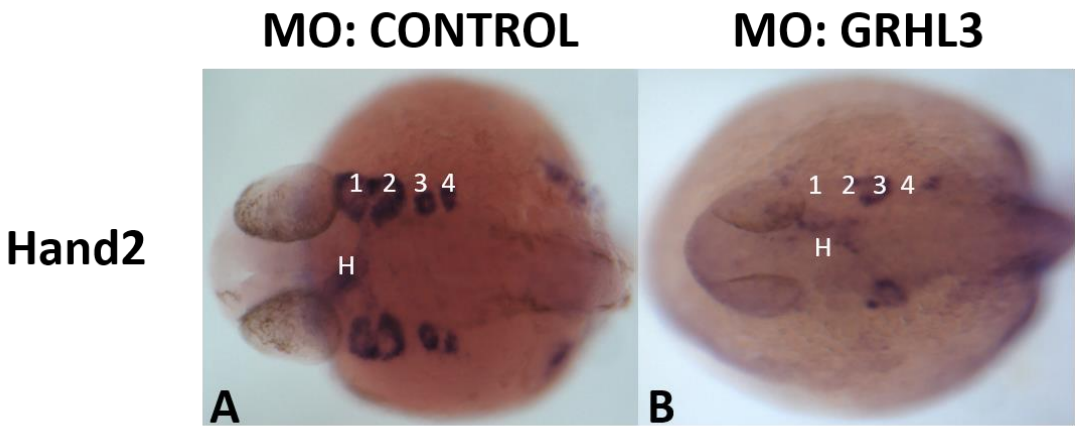

Figure 3.7: *Hand2* expression is unchanged in the heart (H) of *grhl3* knockdown embryos. In-Situ Hybridisation shows that following knockdown of *grhl3*, embryos at 24hpf display unchanged expression of *hand2* in the developing heart (H), despite an absence of *hand2* expression in the first (1), second (2) and fourth (4) pharyngeal arches.

The pharyngeal mesoderm and ectoderm also play important roles in craniofacial development. Goosecoid (*gsc*) is a gene that drives mesoderm induction, and cells that express gsc eventually comprise the pharyngeal endoderm and head mesoderm (Rivera-Perez *et al,* 1995). We tested *gsc* expression to confirm that the effects of *grhl3* knockdown are confined to neural crest derived structures (NCC), and not due to effects on mesodermal tissues. WISH was conducted at 6 hpf to examine expression of *gsc* following *grhl3* knockdown (fig 3.8). Expression was unchanged compared to controls, suggesting that *grhl3* knockdown does not impact on differentiation of endoderm or mesoderm in the pharynx, suggesting that the only cells affected

in the context of craniofacial development are the NCCs that populate the ventral pharyngeal arch.

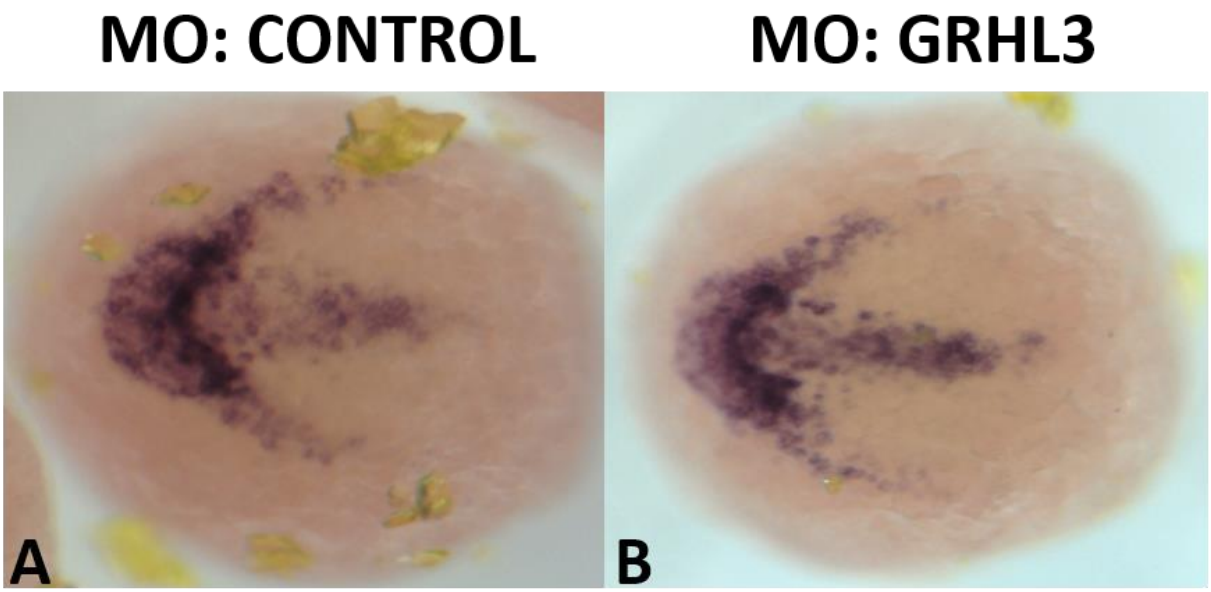

Figure 3.8: *Gsc* is unaffected by *grhl3* knockdown. Whole-Mount In-Situ Hybridisation (WISH) of *Gsc* following injection of *grhl3* and control morpholinos at 6 hours post-fertilisation. *Gsc* expression is limited to the mesoderm in early development and is thus unaffected by *grhl3* knockdown. (A) *gsc* expression following control morpholino injection. (B) *gsc* expression following *grhl3* injection.

3.2.4 *tmem54a* inhibition leads to severe axial and craniofacial defects

As previously mentioned, the gene *Tmem54* was identified as being differentially regulated in the kidney and placenta in of *Grhl2*$^{-/-}$ mice/embryos. Given the conserved function of *Grhl* family genes across species, the role of *tmem54* in zebrafish was investigated. Due to a genome duplication event in the evolutionary history of teleosts, zebrafish contain duplicate orthologues of many genes (Glasauer & Neuhauss, 2014). *tmem54* is included among these genes and as such contains the orthologues *tmem54a* and *tmem54b*, both of which are investigated in this chapter.

Inhibition of gene function was achieved using morpholino knockdown, a technique well validated among zebrafish developmental studies (Nasevicius & Ekker, 2000). A 200μm concentration of morpholino was used, as this was validated by validated by previous pilot experiments as causing phenotypes without producing toxicity. A distinctive phenotype characterised by the obvious loss of the lower jaw and axial defects wherein the tail of the fish is

curved downward. The severity of tail phenotypes was variable, ranging from mild curvature (fig. 3.9: A) to more severe curvature (fig 3.9: B).

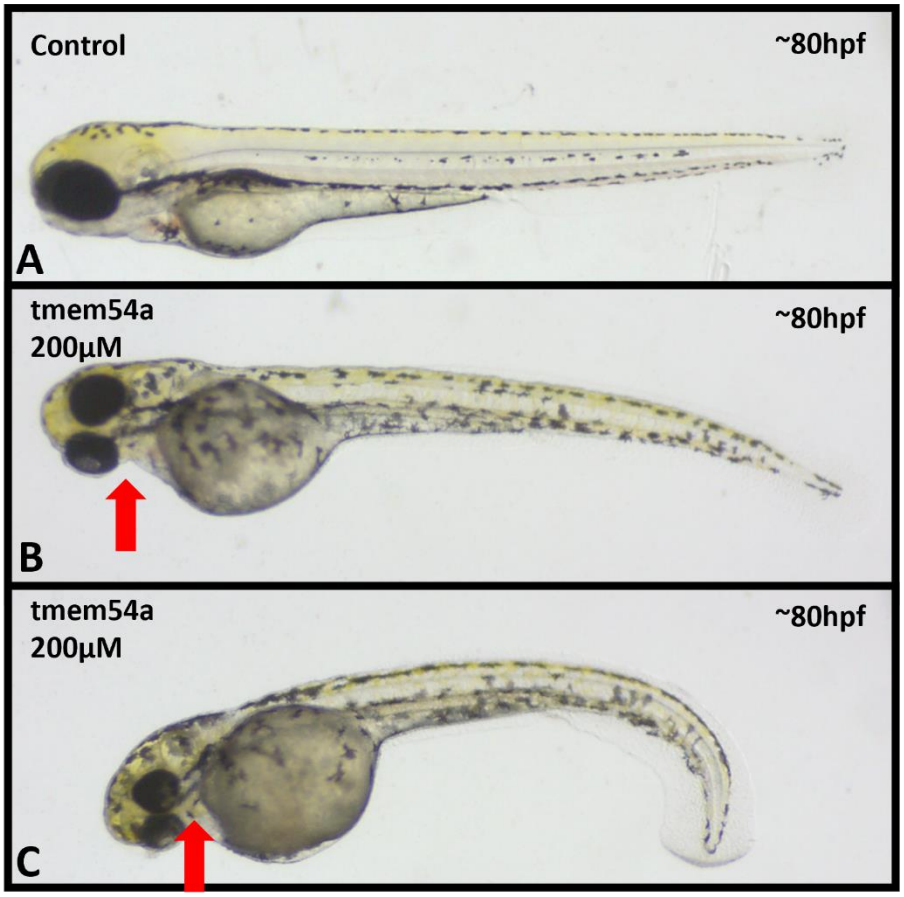

Figure 3.9: Axial and facial phenotypes in zebrafish embryos injected with *tmem54a* blocking morpholinos. Zebrafish embryos at ~80 hpf display loss of the Meckel's cartilage (lower jaw) among other craniofacial structures. Tail defects in *tmem54a* morphant larvae were characterised by a consistent downward curvature of varying severity. (A) Lateral view of control morpholino injected zebrafish larvae at 80hpf. (B) Lateral view of a *tmem54a* morpholino injected zebrafish larvae exhibiting loss of the lower jaw (red arrow) and mild axial defects. (C) lateral view of a *tmem54a* morpholino injected zebrafish larvae at 80hpf exhibiting loss of the lower jaw (red arrow) as well as a more severe axial defect (n=61).

The survival rates of zebrafish embryos were monitored over the course of 4 days, to establish whether morpholino injection was causing toxicity, or the presence of severe defects that may be reflected in embryo death. Of the 61 MO:*tmem54a* morpholinos monitored over 96hpf, the survival rate was 72.13% +/-6.65%, which was significantly different to the survival rate seen in

73 MO:control embryos (84.93% +/- 3.51%; Fig. 3.10, A). These data indicate that morpholino mediated inhibition of *tmem54a* leads to embryonic lethality at 4dpf.

The incidence of defects among the surviving embryos was also monitored over 4dpf. Incidence of overall defects was 64.10% +/- 6.21% in MO:*tmem54a* embryos, and 7.03% +/- 3.10% in MO:control embryos. Thus, Tmem54a morphants display a significant 57.07% increase in relative to control morpholino injected embryos, in overall defects (both craniofacial and axial defects) (Fig 3.10 B).

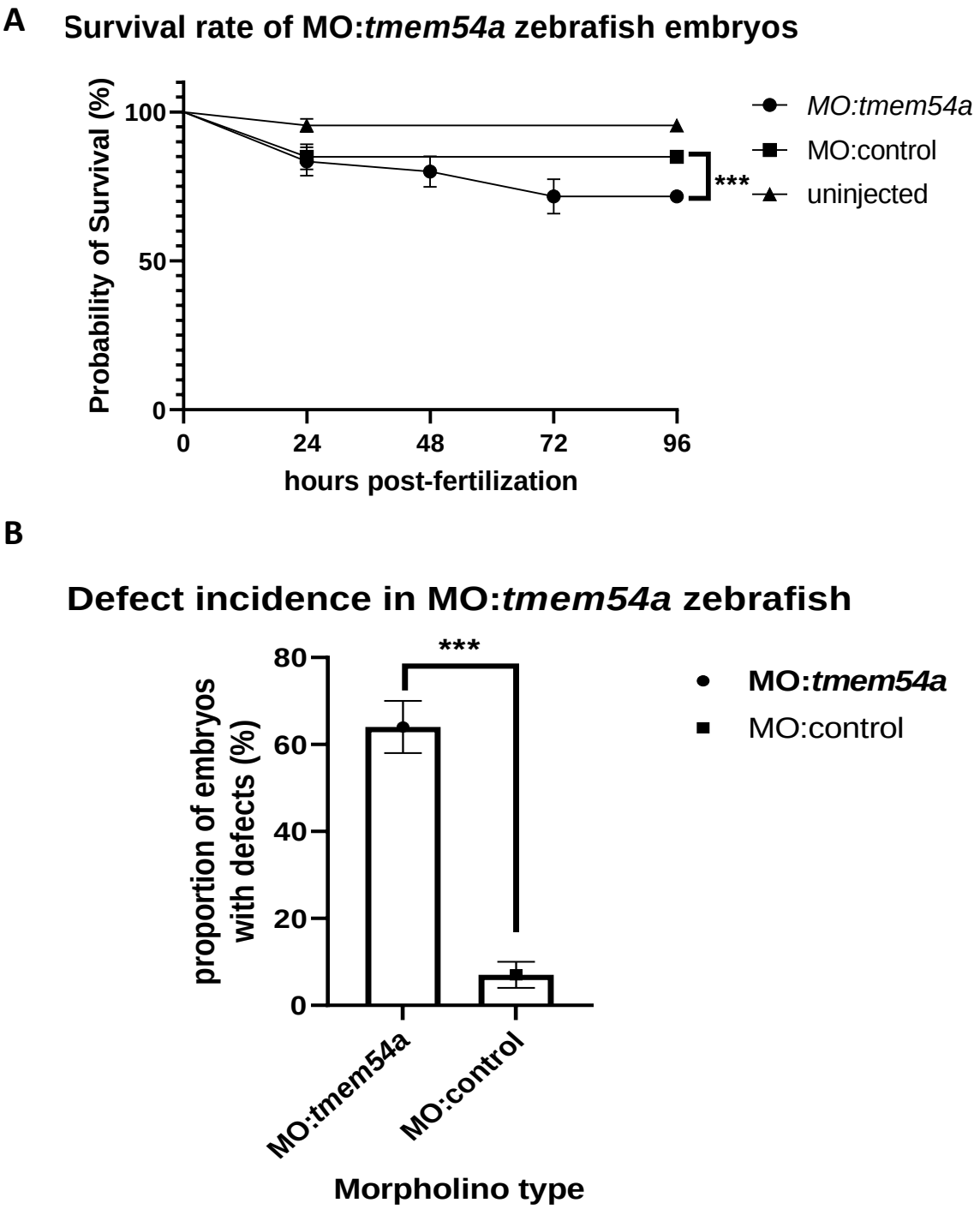

Figure 3.10: Injection of *tmem54a* translation (ATG)-blocking morpholinos results in a decrease in zebrafish embryo viability and an increase in the incidence of defects.A) MO:*tmem54a* zebrafish displayed a survival rate of 72.13% +/-6.65%, while the survival rate of MO:control embryos was 84.93% +/- 3.51%. Thus, a 12.80% decrease in viability over the course of 96 hours compared to control injected embryos was identified in *MO:tmem54a* embryos. Control morpholino injected zebrafish exhibited 11% lower viability compared to uninjected controls. B) The incidence of defects increased by 57% in *tmem54a* morphants at 96 hours post fertilization.

Error bars represent SEM. MO:*tmem54a* n = 61, MO:control n=73, uninjected n=88. P=0.0003 by Log-rank (Mantel-Cox) test.

Given the gross morphological defects observed in standard imaging of *tmem54a* morphants, alcian blue staining was used to visualise the cartilaginous facial skeleton of the zebrafish larvae. Compared to control injected embryos, *tmem54a* morphants displayed loss of all but two structures of the facial skeleton (fig 3.11: B, D). The only remaining structures were paired structures close to the midline and behind the eyes of the zebrafish, presumed to be aberrantly formed ceratohyal cartilages (ch), as well as another pair of structures lateral to those, which may represent similarly malformed parachordial cartilages (pch). The loss of various structures in the *tmem54a* morphant facial skeleton affected both viscerocranial structures – such as the Meckel's cartilage and palatoquadrate as well as neurocranial structures including the ethmoid plate and parachordial cartilage.

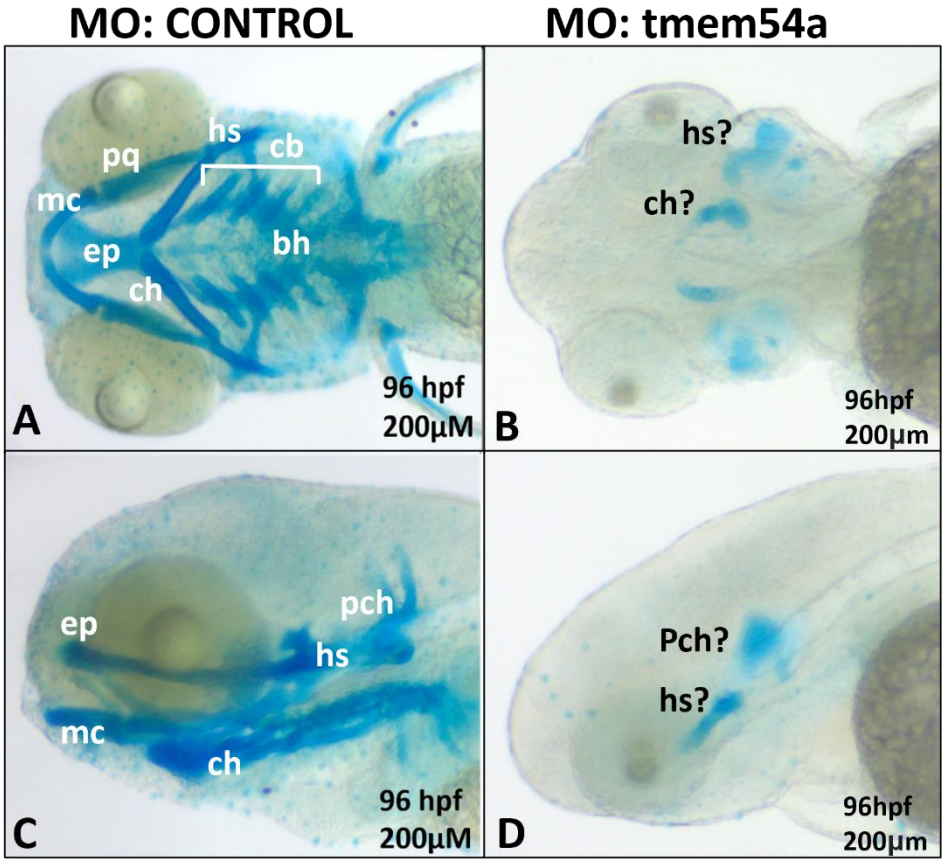

Figure 3.11: *tmem54a* morpholino injected zebrafish display loss of craniofacial structures of the neuro and viscerocranium. Zebrafish morphants display loss of Meckel's cartilage (mc), ethmoid plate (ep) palatoquadrate (pq) ceratohyal (ch) and ceratobrachial (cb) cartilages. The only remaining cartilages in *tmem54a* morphants appear to be hypomorphic parachordial (pch) and

hyosymplectic (hs) cartilages. (A) ventral view of 200µm control morpholino injected zebrafish embryo at 96hpf. (B ventral view of 200µm *tmem54a* morpholino-injected zebrafish at 96hpf. (C) Lateral view of a 200µm control-morpholino injected zebrafish at 96hpf. (D) Lateral view of a 200µm *tmem54a*-morpholino injected zebrafish at 96hpf (n=10-12).

3.2.5 Midbrain and hindbrain markers are unaffected by *tmem54a* inhibition

When MO:*tmem54a* zebrafish were congregated at the centre of their petri dishes for counting at 72hpf, it was observed that 46% +/-1.93% did not display any movement over the following 24 hours, while 6.25% +/-0.45% of control embryos remained at the centre and this change was found to be statistically significant ($p<0.005$) (fig 3.12). To investigate whether this observation was due to defects in motor signals or neuronal development, WISH was utilised. MO:*tmem54a* and MO:control embryos were probed for expression of *tfap2a* and *pax2a* at 24 hpf (fig 3.13 A-D). *tfap2a* is expressed by hindbrain and spinal cord neurons which are necessary for transmitting motor commands from the brain, whilst also exhibiting expression in the neural crest and tube. *Pax2a* exhibits strong staining in the midbrain-hindbrain boundary, optic stalk, as well as the otic vesicles which function similarly to the middle ear and thus influence balance. Expression of *tfap2a* in the hindbrain neurons and spinal cord was unchanged in MO:*tmem54a* zebrafish (3.13 A,C). Similarly, *pax2a* expression in the midbrain hindbrain boundary, otic vesicles and optic stalk of *tmem54a* was unchanged relative to control embryos (fig 3.14).

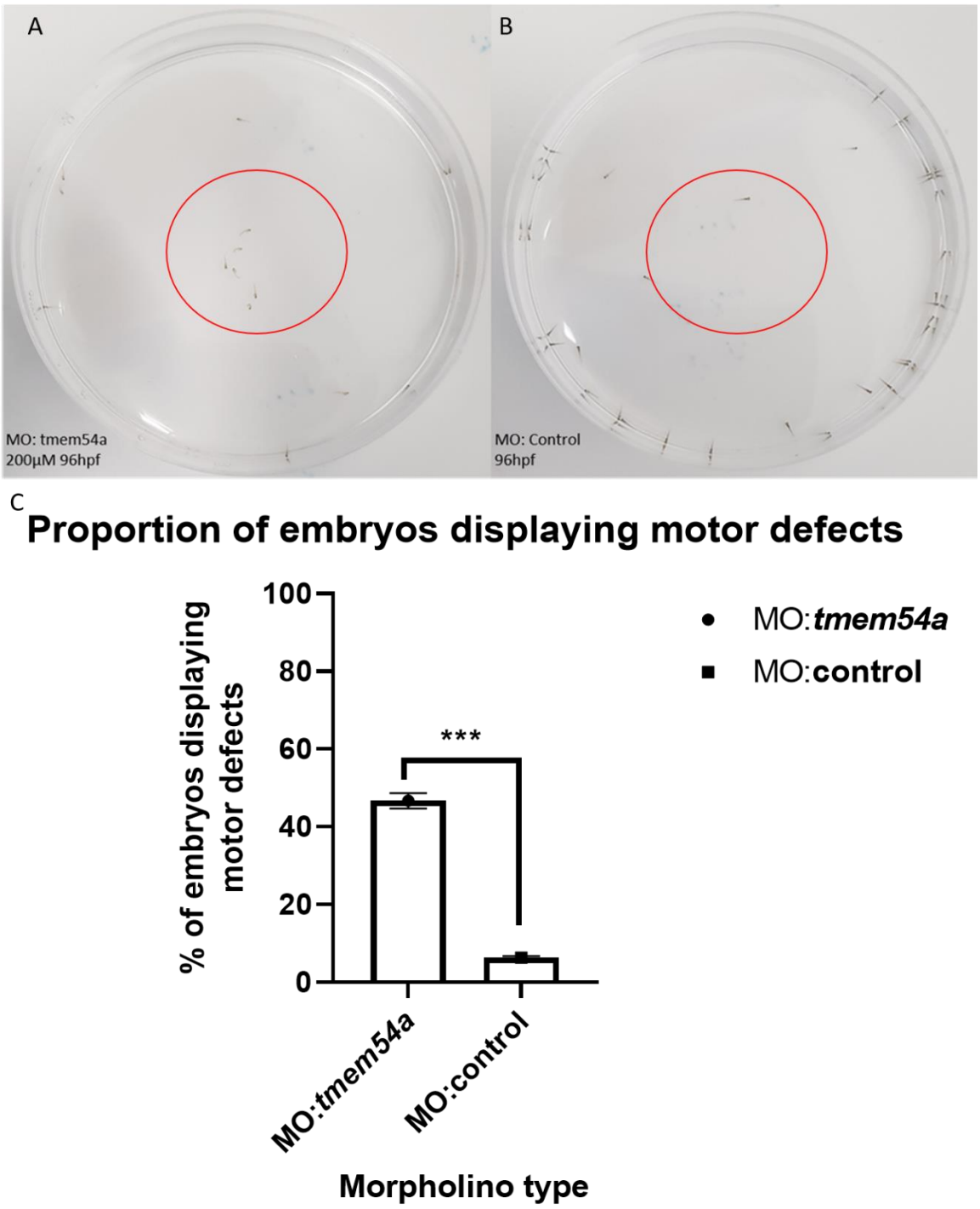

Figure 3.12: Decreased swimming activity in *tmem54a* morpholino injected zebrafish. When grouped at the centre of a petri dish in E3 embryo water, 46% +/- 1.93% (7/15) of MO:*tmem54a* zebrafish larvae remained at the centre of the dish from 72-96 hpf. 6.25% +/-0.45% of control morpholino injected zebrafish remained at the centre of the dish between 72 and 96hpf. A) petri dish containing MO:*tmem54a* zebrafish embryos at 96hpf. B) MO:control zebrafish embryos at 96hpf. C) proportion of MO:*tmem54a* and MO:control zebrafish embryos displaying motor defects (at centre of plate). MO:tmem54a n=15, MO:control n=32. P= <0.005 by Welch's t-test, error bars represent SEM.

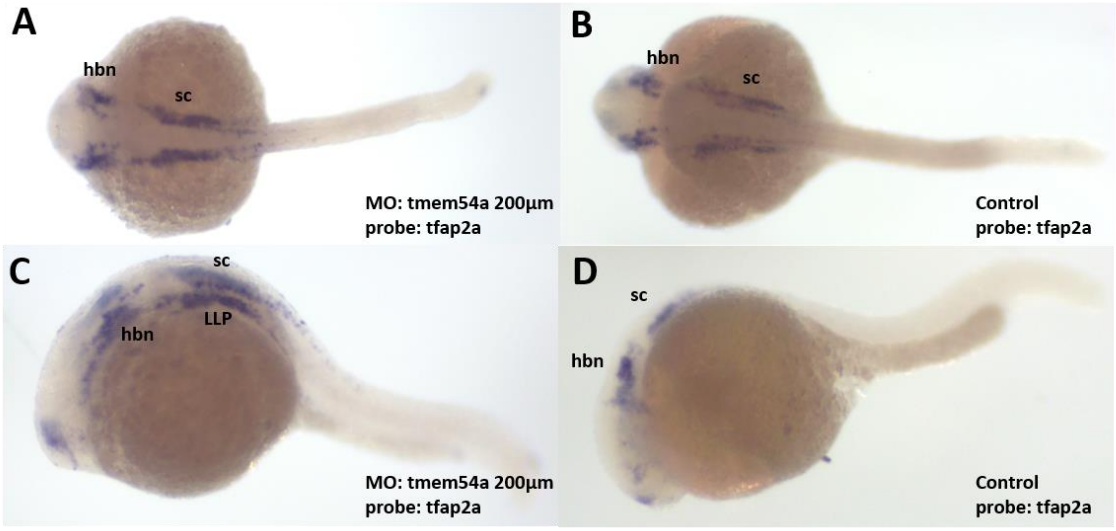

Figure 3.13: tfap2a ISH expression in MO:*tmem54a*-injected embryos. tfap2a is expressed in the developing neural crest, neural tube and their derivatives. These structures include hindbrain and spinal cord neurons which are integral for motor activity. *tmem54a* injected zebrafish displayed no differences in cell populations expressing the marker tfap2a, including the hindbrain (hbn) and spinal cord (sc) neurons and primordial lateral line (LLP) at 24hpf.

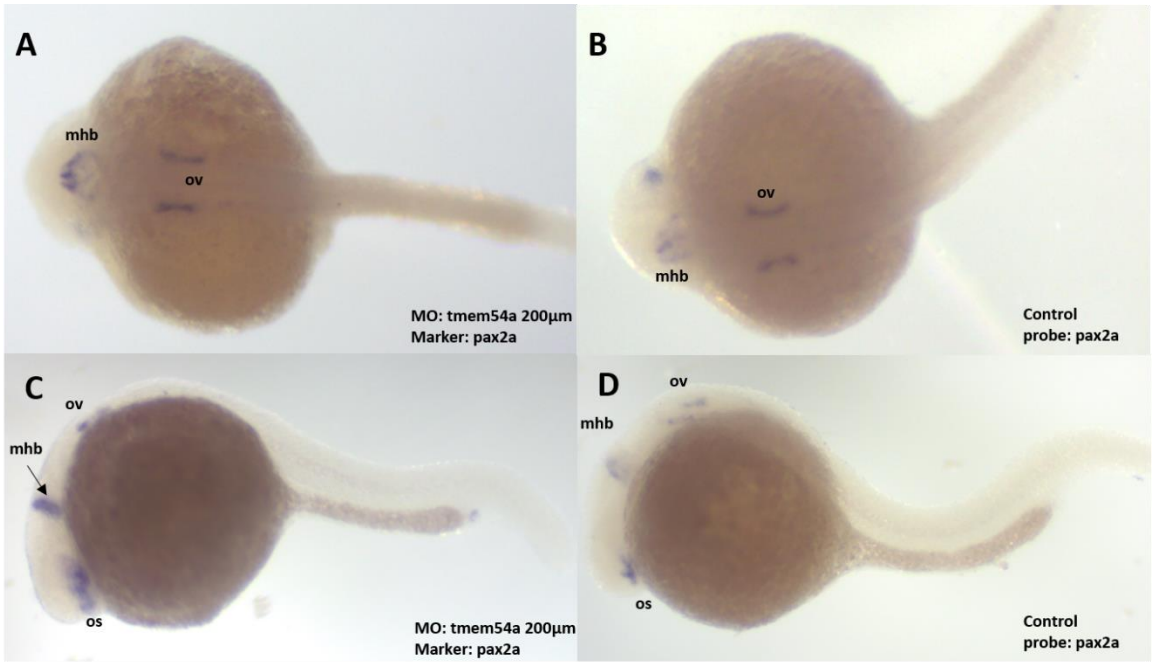

Figure 3.14: In-situ hybridisation of *tmem54a* morpholino injected zebrafish probed for pax2a expression. Pax2a is marks cell populations in the midbrain hindbrain boundary and otic vesicles, defects in which may result in aberrant swimming activity due to loss of motor movement or balance. MO:*tmem54a* injected zebrafish displayed no differences in cell populations expressing

the marker pax2a, including the midbrain-hindbrain boundary (mhb) optic stalk (os) and primordial otic vesicles (ov) at 24hpf.

3.2.6 *tmem54a* inhibition leads to aberrant development of rhombomeres 3 and 5

Given that development of the pharyngeal arches and craniofacial region rely on NCC migration from the rhombomeres, the rhombomeres were investigated for potential defects. To investigate potential abnormalities in rhombomeres 3 and 5, riboprobes for krox20 were generated and used on MO:*tmem54a* embryos at 24 hpf. MO:*tmem54a* embryos displayed loss of krox20 expression in the ventral-most portion of rhombomeres 3 and 5 in 12 out of 16 embryos, whereas all (n=7) control embryos displayed expression in the ventral rhombomeres. (R3, R5) (figure 3.15).

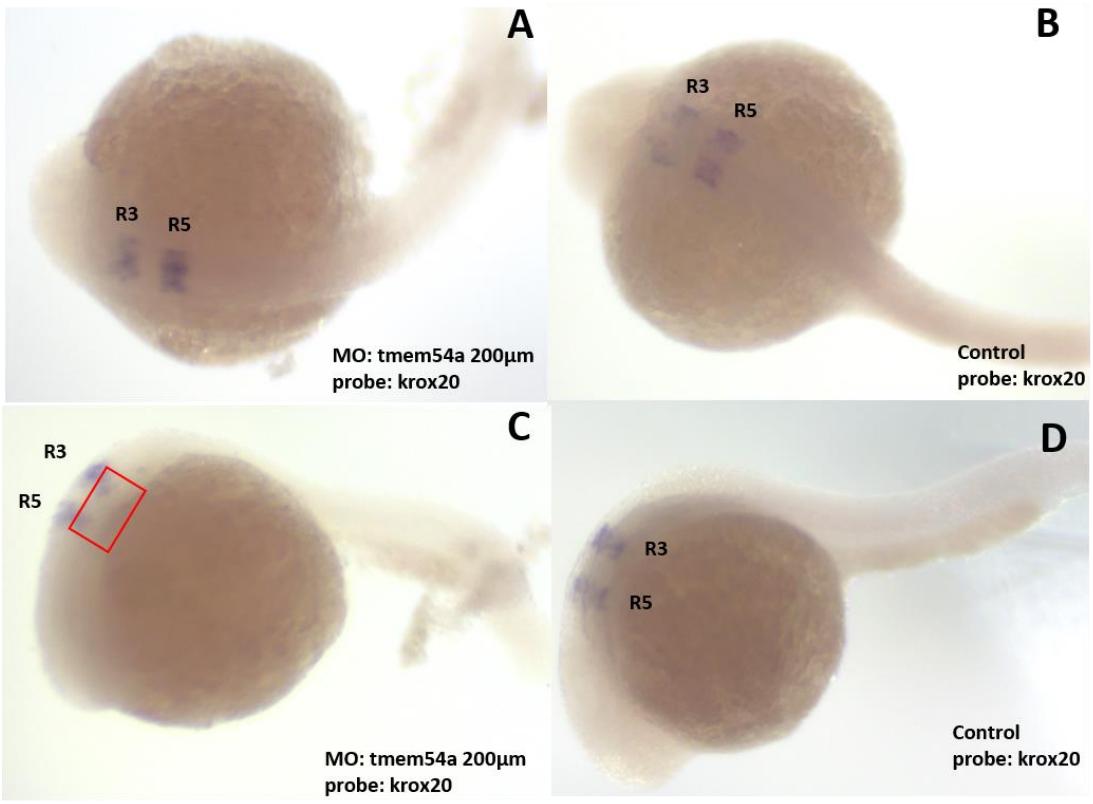

Figure 3.15: Rhombomere marker expression is reduced in *tmem54a* morpholino injected zebrafish at 24hpf. Krox20 is expressed in cells in the 3rd and 5th rhombomeres during embryonic development. In 12/16 MO:*tmem54a* injected zebrafish embryos, ventral areas of rhombomeres 3 (R3) and 5 (R5) show reduced expression of krox20 relative to control morpholino injected zebrafish embryos which displayed krox20 expression in all embryos. MO:*tmem54a* n=16, MO:control n=7.

3.2.7 Loss of *tmem54b* does not induce defects in zebrafish embryos

Zebrafish morpholino knockdown experiments were also performed on the second *tmem54* orthologue – *tmem54b* – to ascertain what role it performs in zebrafish craniofacial development. In an identical fashion to *tmem54a*, morpholinos were injected to inhibit the translation of *tmem54b* embryos and monitored over 96 hours post fertilisation.

Of the 124 MO:*tmem54b* morpholinos monitored over 96hpf, the survival rate was 85.58% +/- 4.5%, which was not significantly different to the survival rate seen in 112 MO:control embryos of 85.80% +/- 1.2% (Fig. 3.17). These data indicate that morpholino mediated inhibition of *tmem54b* did not lead to embryonic lethality. MO:*tmem54b* embryos also did not present with any observable defects relative to MO:control embryos (fig 3.16).

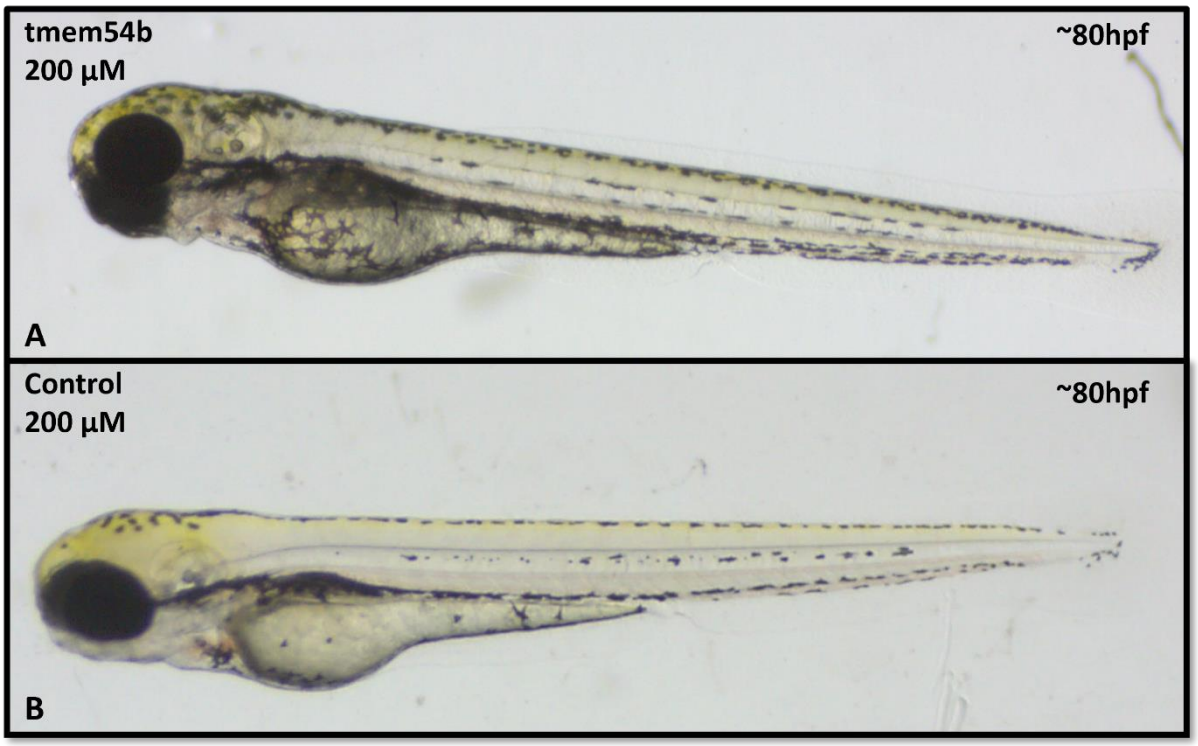

Figure 3.16: Injection of *tmem54b* morpholinos does not induce defects in zebrafish embryos. (A) lateral view of *tmem54b* morpholino injected zebrafish embryos at 80hpf. (B) lateral view of a control-morpholino injected zebrafish embryo at 80hpf (n=97).

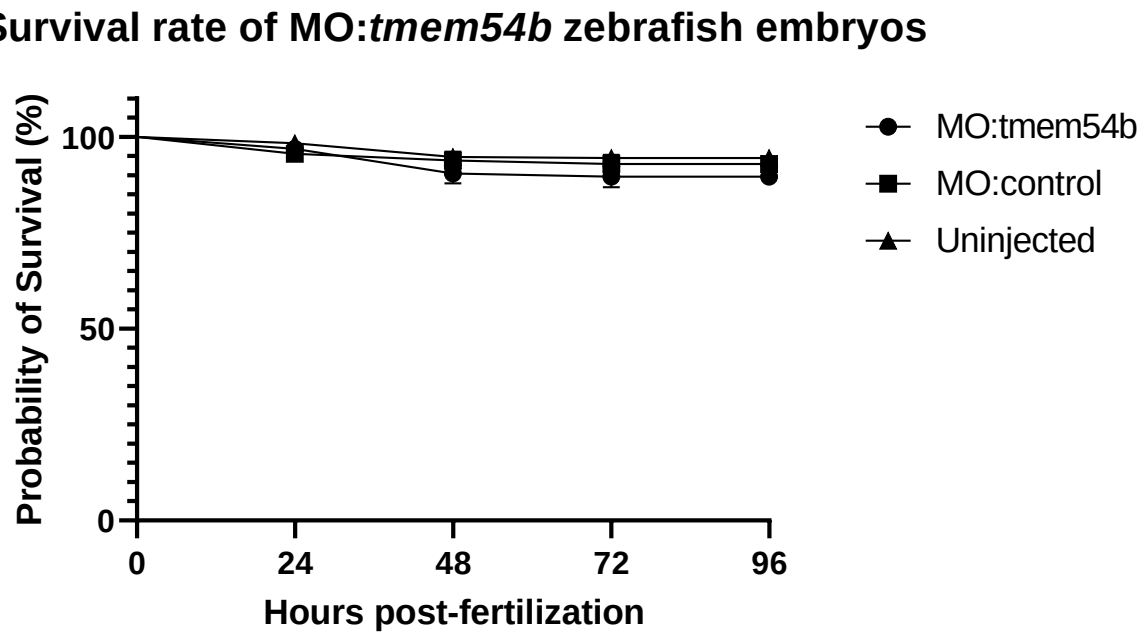

Figure 3.17: Injection of *tmem54b* morpholinos do not affect zebrafish embryo viability. MO:*tmem54b* morpholinos displayed a survival rate of 85.58% +/-4.5%, which was not significantly different to the survival rate seen in 112 MO:control embryos of 85.80% +/- 1.2% over 96 hours of monitoring. Error bars represent SEM, MO:*tmem54b* n= 97.MO:control n=97 Uninjected n=349.

To confirm that MO:*tmem54b* zebrafish presented with normal craniofacial morphology, an alcian blue cartilage stain was performed to visualise the cartilaginous facial skeleton of *tmem54b* morphant zebrafish. Alcian blue staining confirmed that there were no changes in the morphology, placement or composition of the facial cartilages of the *tmem54b* morphants in either the viscerocranium or the neurocranium (fig 3.18: B, D).

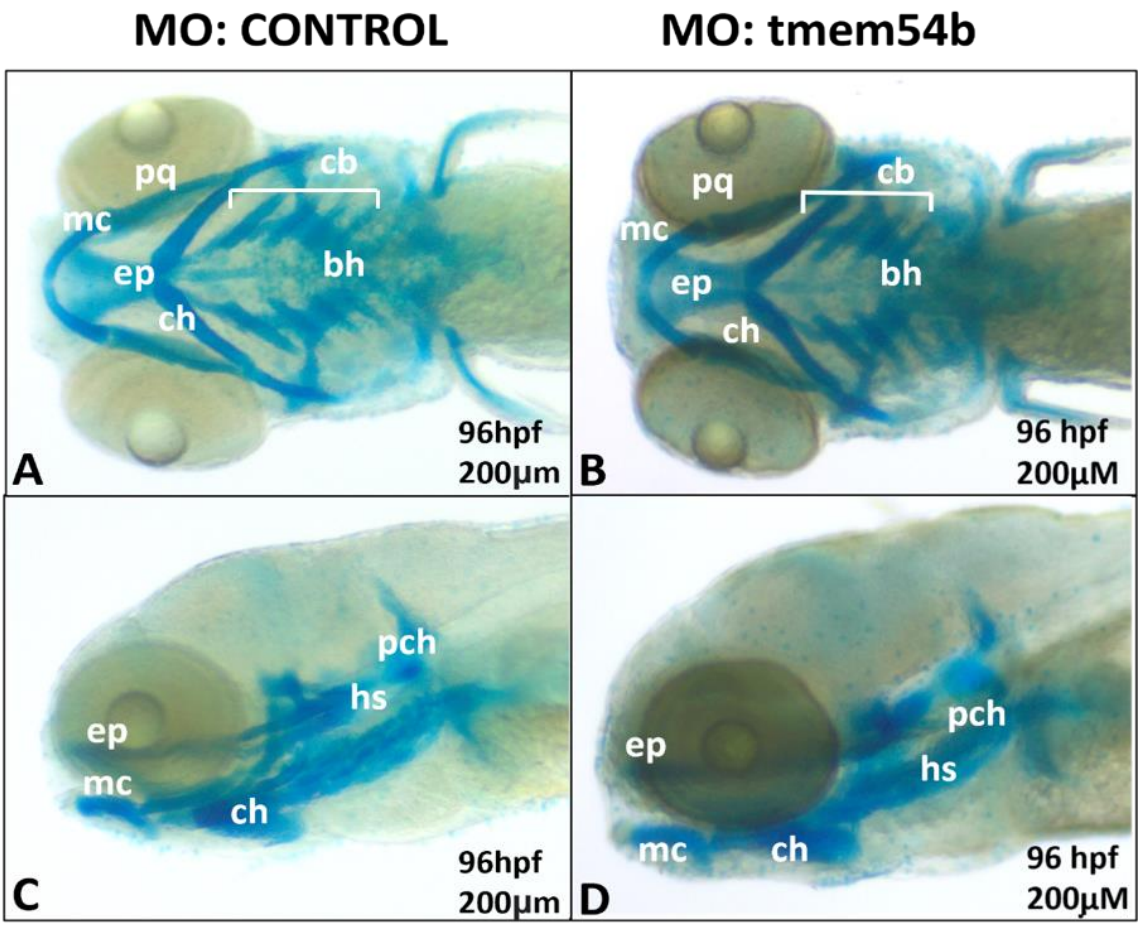

Figure 3.18: Craniofacial structures were unaffected by *tmem54b* blocking morpholinos in zebrafish embryos. Unlike *tmem54a* injections, *tmem54b* morpholino injection did not result in any defects to the craniofacial structures of zebrafish embryos relative to controls following alcian blue cartilage staining. (A) ventral view of 200µm MO:control zebrafish embryo at 96hpf. B) ventral view of 200µm MO:*tmem54b* zebrafish at 96hpf. (C) Lateral view of a 200µm MO:*tmem54b* zebrafish at 96hpf. (D) Lateral view of a 200µm MO:*tmem54b* zebrafish at 96hpf. (mc) Meckel's cartilage, (pq) palatoquadrate, (cb) ceratobranchials, (ep) ethmoid plate, (ch) ceratohyal cartilage, (bh) basihyal cartilage, (hs) hyosymplectic, (pch) parachordial cartilage.

3.2.8 *pvrl4* inhibition produces mild axial and craniofacial defects in zebrafish embryos.

MO:*pvrl4* zebrafish displayed more subtle defects than those observed in *tmem54a*. *pvrl4* morphant embryos displayed an axial defect wherein the spine of the embryo was curved downward more rostrally than was observed in the axial defects of *tmem54a* morphant embryos (Fig3.19 B). In 77 MO:*pvrl4* embryos, the survival rate at 4dpf was 53% +/- 12% while in 44 MO:control embryos, the survival rate was 64% +/- 6%. Thus, viability of *pvrl4* morphant embryos was not significantly affected by inhibition of *pvrl4*, as viability over 96 hours was not

significantly different to morpholino injected controls (fig. 3.20 A). The incidence of defects in MO:*pvrl4* embryos was 36% +/- 8.04% while MO:control defect incidence was 7.14% +/-5.14% (fig 3.20: B).

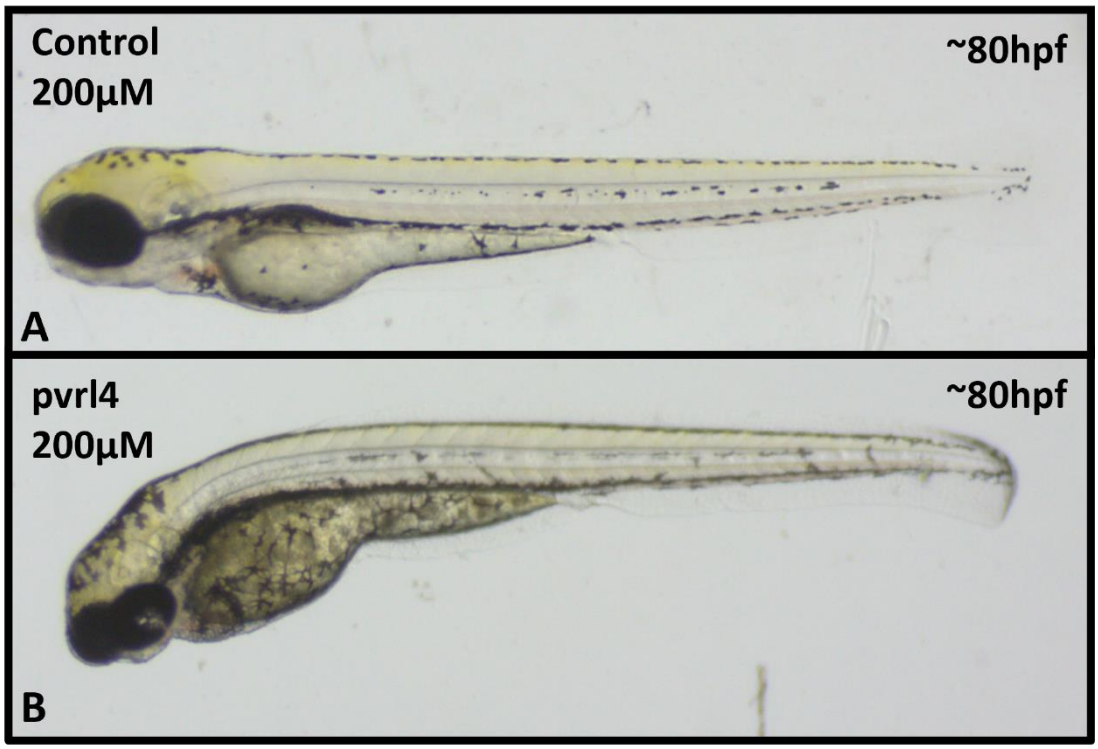

Figure 3.19: Axial phenotypes in zebrafish embryos injected with *pvrl4* blocking morpholinos. Embryos injected with *pvrl4* morpholinos displayed mild axial defects. (A) lateral view of control-morpholino injected embryos at 80hpf. (B) lateral view of *pvrl4* morpholino injected zebrafish at 80hpf (n=77).

A

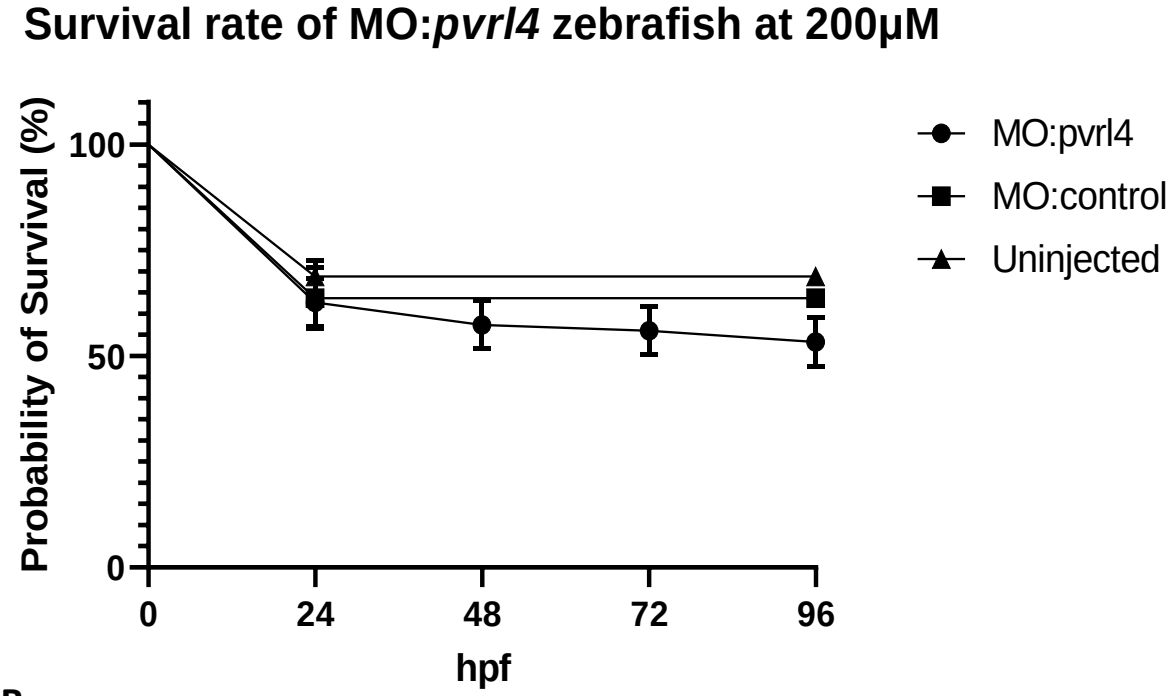

B

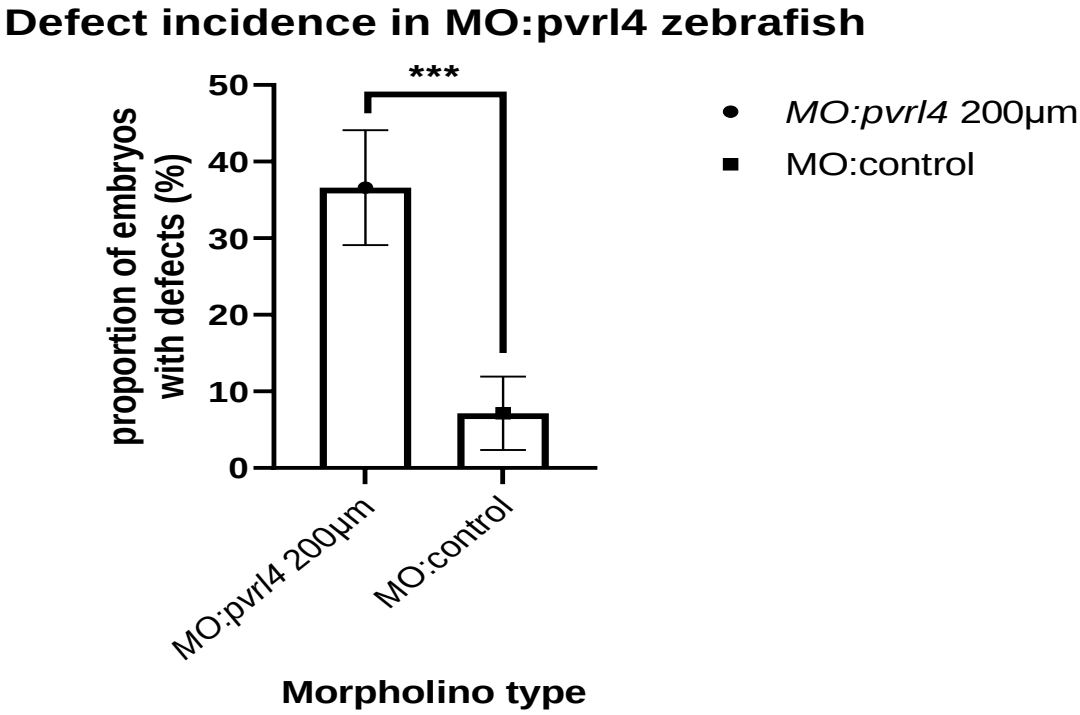

Figure 3.20: Injection of *pvrl4* morpholinos produces no differences in zebrafish embryo survival rates but an increase in defect incidence compared to controls. (A) Changes in survival rates for *pvrl4* injected zebrafish embryos were not statistically significant relative to control-morpholino injected zebrafish over 96 hours of monitoring post fertilization. (B) MO:*pvrl4* embryos displayed a defect incidence rate of 36.59%+/- 7.50 compared to 7.14+/-4.80 in MO:control embryos,

representing a 29% increase in the proportion of embryos with defects. Error bars represent SEM. MO:*pvrl4* n=77, MO:control n=44, Uninjected n=144. P=<0.0001 (Welch's t-test).

Alcian blue cartilage stains of zebrafish facial skeletons revealed hypoplasia of the ceratobranchial cartilages in *pvrl4* morphant embryos. Relative to controls, alcian blue staining of the ceratobranchial cartilages was significantly decreased, and other structures displayed subtle decreases in staining intensity including the ethmoid plate and the anterior portion of Meckel's cartilage (fig. 3.21: B, D) The basihyal cartilage appears to be entirely absent in *pvrl4* morphant embryos.

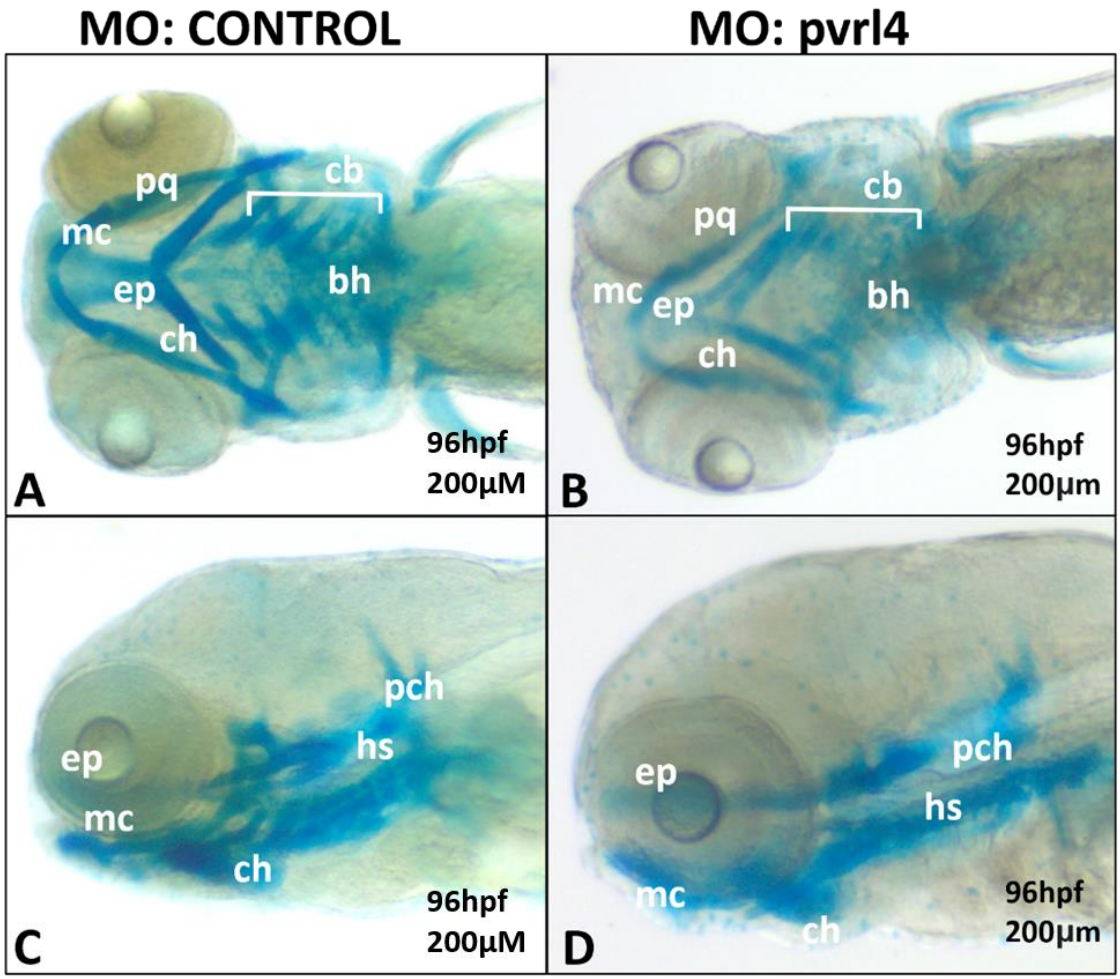

Figure 3.21: *pvrl4* morpholino injected zebrafish embryos display mild defects in facial cartilages. Embryos injected with *pvrl4* blocking morpholinos displayed hypomorphism of the ceratobranchials, Meckel's cartilage, basihyal and ethmoid plate relative to controls. (A) ventral view of 200µM control morpholino injected zebrafish embryo at 96hpf. (B ventral view of 200µM *pvrl4* morpholino-injected zebrafish at 96hpf. (C) Lateral view of a 200µm control-morpholino injected zebrafish at 96hpf. (D) Lateral view of a 200µm *pvrl4*-morpholino injected zebrafish at 96hpf. (mc) Meckel's cartilage, (pq) palatoquadrate, (cb) ceratobranchials, (ep) ethmoid plate,

(ch) ceratohyal cartilage, (bh) basihyal cartilage, (hs) hyosymplectic, (pch) parachordial cartilage (n=15).

To investigate whether the mild defects evident in 200µM dosages of *pvrl4*-inhibiting morpholinos could be further amplified using higher concentrations, zebrafish embryos were injected with 500µM *pvrl4* morpholinos and monitored for 5 days. Survival rates of zebrafish injected with *pvrl4* morpholinos were not significantly affected relative to control morpholino injected zebrafish (Figure 3.18, A), however the significant embryo death at 24hpf evident in 200µM dosages was not evident in 500µM concentrations. Craniofacial defects in 500µM *pvrl4* zebrafish were still relatively mild and were generally characterised by loss of or ectopic development of the posterior ceratobranchials (cb) (3.22, B). In rarer instances however, the palatoquadrates presented more rounded than in control embryos.

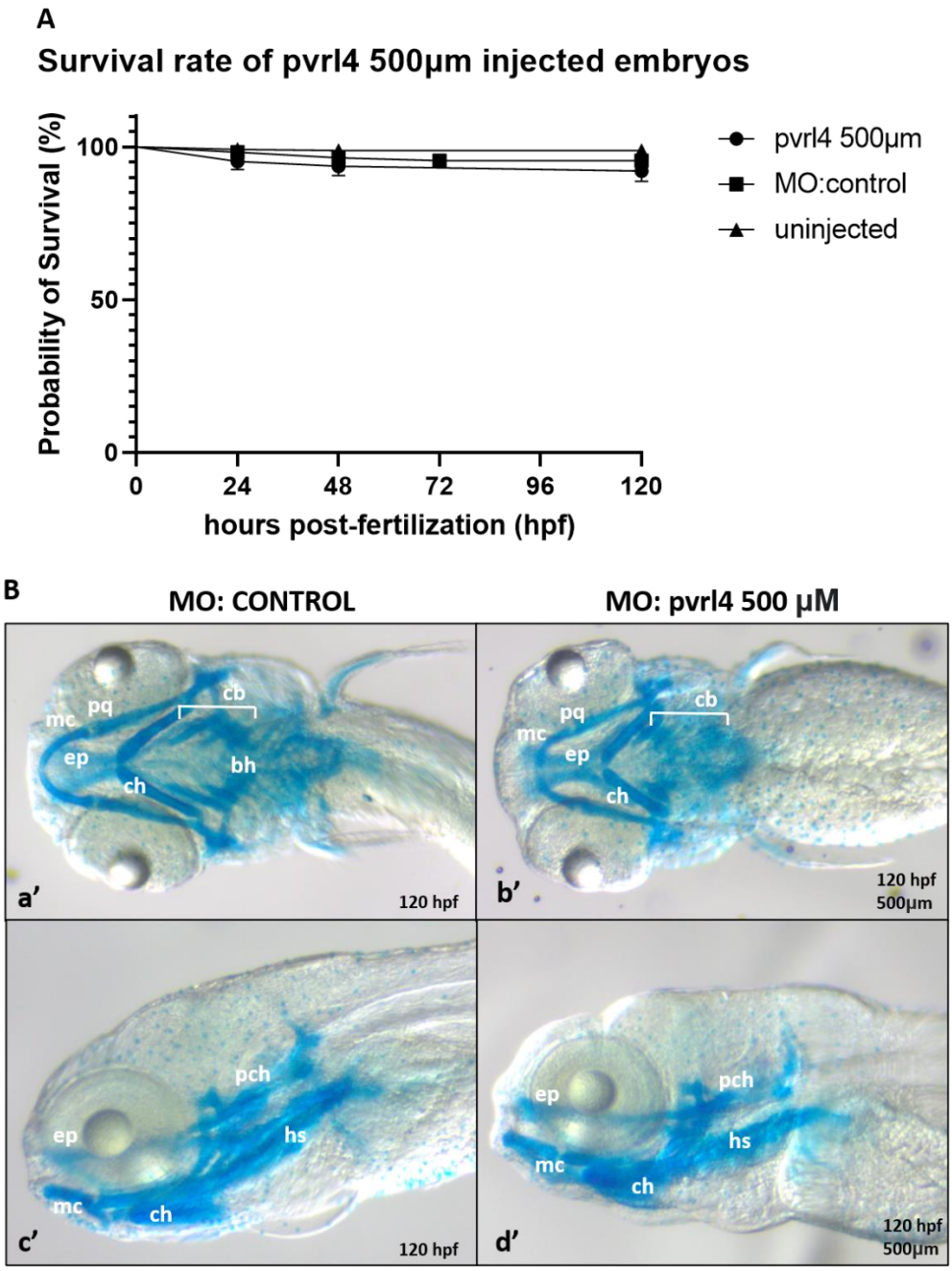

Figure 3.22: A) survival rate of zebrafish embryos injected with a 500µM dosage of *pvrl4* inhibiting morpholino. Increasing the dosage (500µM) of *pvrl4* morpholino did not have any significant effect on the survival rate of zebrafish embryos relative to control morpholino injected embryos. **B)** alcian blue staining of 500µM *pvrl4*-injected zebrafish embryos at 5 dpf. Minor defects affecting the ceratobranchials were common in MO:*pvrl4* embryos (MO:*pvrl4*: 77%, MO:control: 28.5%), as well as a less common rounded palatoquadrate phenotype (MO:*pvrl4*: 23.00%, MO:control: 11.40%). **a')** dorsal view of a zebrafish injected with a control morpholino, **b')** dorsal view of a zebrafish embryo injected with 500 µM of *pvrl4* inhibiting morpholino. **c')** lateral view of a zebrafish injected with a control morpholino, **d')** lateral view of a zebrafish embryo injected with 500 µM of *pvrl4* inhibiting morpholino. (mc) Meckel's cartilage,

(pq) palatoquadrate, (cb) ceratobranchials, (ep) ethmoid plate, (ch) ceratohyal cartilage, (bh) basihyal cartilage, (hs) hyosymplectic, (pch) parachordial cartilage (n=16).

3.2.9 *pvrl4* inhibition leads to reduced rhombomere marker expression

To identify potential mechanisms through which inhibition of *pvrl4* leads to craniofacial defects, the same methods as described for *tmem54a* above were utilised. MO:*pvrl4* embryos were probed for expression of *tfap2a*, *pax2a* and *krox20*. Whilst no significant changes in expression of *tfap2a* (figure3.23: A, C) or *pax2a* (fig 3.24, A, C) were evident, *krox20* expression in the rhombomeres was present in only 52.63% of MO:*tmem54a* embryos, vs 88.89% of MO:control embryos (figure 3.25 E, F).Given the absence of rhombomere expression, it was suggested that apoptosis may occur in the defective rhombomeres or during NCC migration to the pharyngeal arches. In order to investigate this, cell death was examined using acridine orange staining (for DNA damage). The transparent nature of these embryos meant that the pharyngeal arches were not clearly visible, so the area between the mhb and ov was used to approximate the pharyngeal arches and the migration route of NCC at approximately 24hpf (figure 3.21, A, B). Cells in this area were counted and a significant increase in the number of acridine orange positive cells was detected in MO:*pvrl4* embryos (32.00+/-8) compared to MO:control embryos (19.67+/-3.25)(p=0.019)(figure 3.26, C).

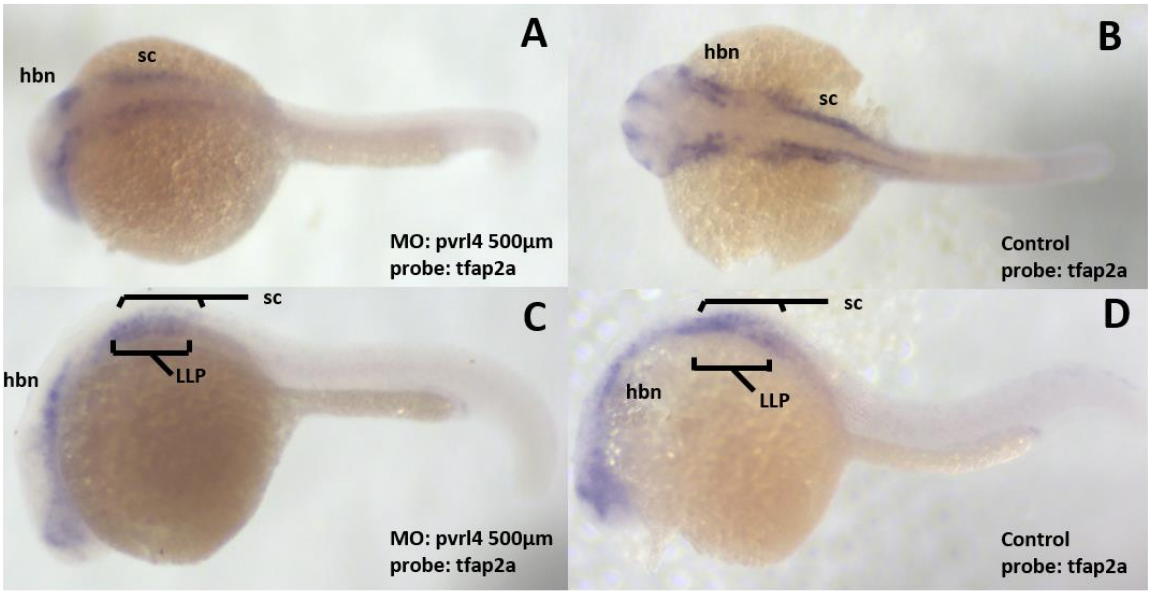

Figure 3.23: In situ hybridisation (ISH) of *pvrl4* morpholino injected zebrafish probed for tfap2a. *pvrl4* injected zebrafish displayed no differences in cell populations expressing the marker tfap2a, including the hindbrain (hbn) and spinal cord (sc) neurons and primordial lateral line (LLP) at 24hpf.

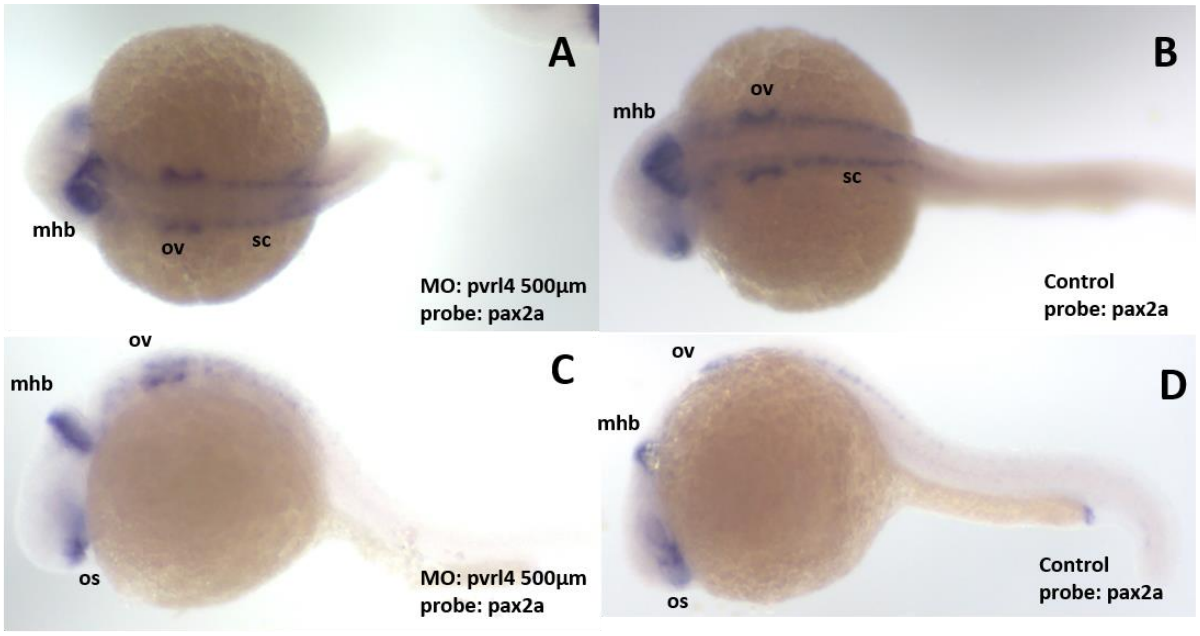

Figure 3.24: In-situ hybridisation of *pvrl4* morpholino injected zebrafish probed for pax2a expression. MO:*pvrl4* injected zebrafish displayed no differences in cell populations expressing the marker pax2a, including the midbrain-hindbrain boundary (mhb) optic stalk (os) and primordial otic vesicles (ov) at 24hpf.

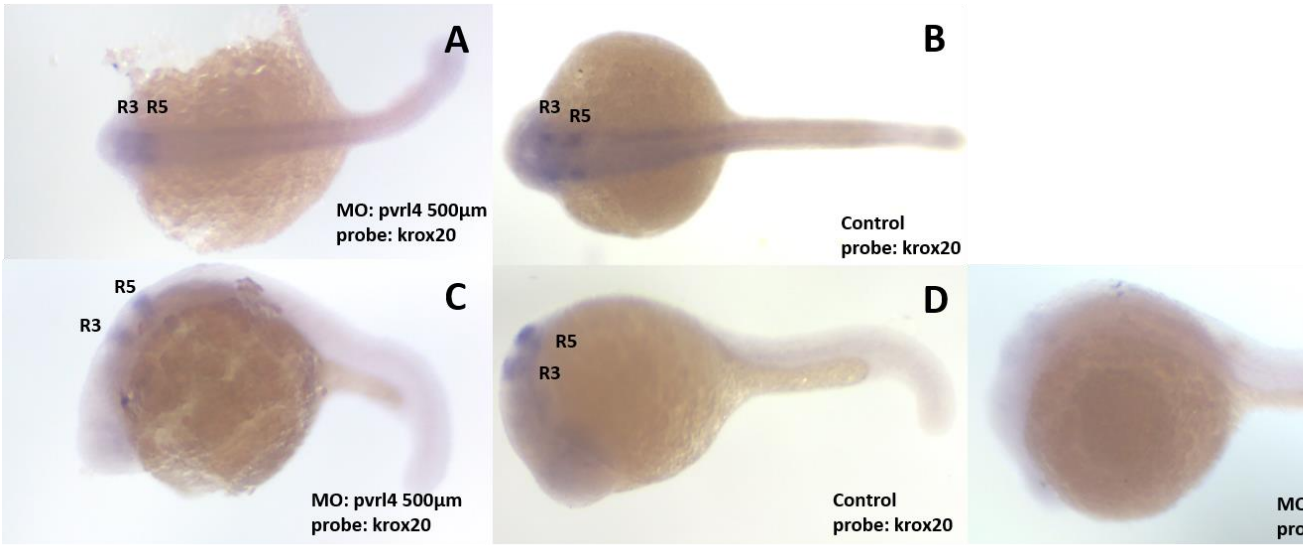

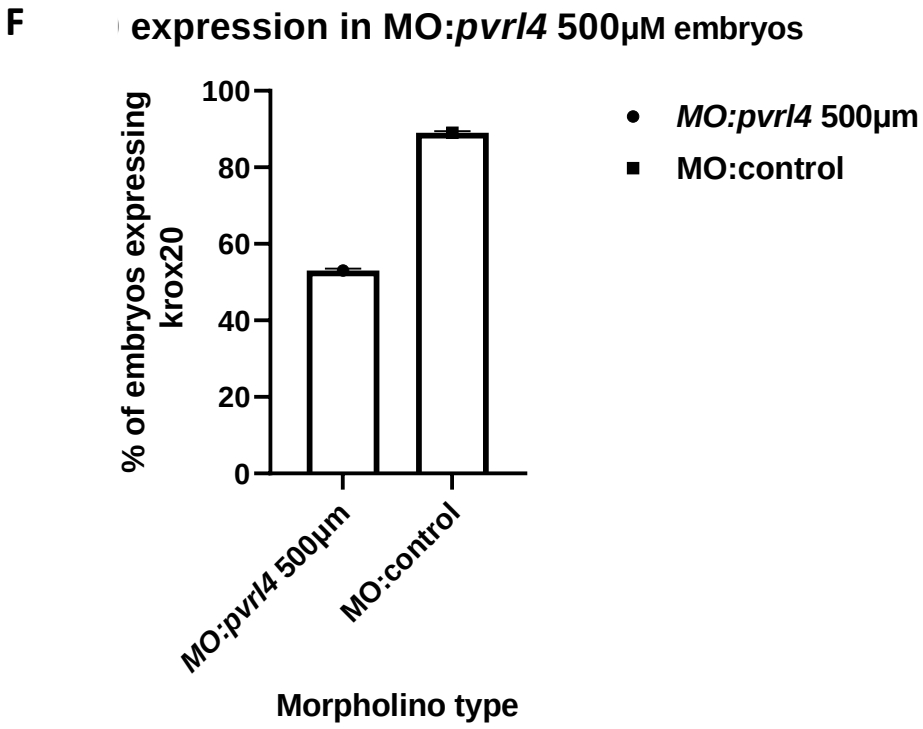

Figure 3.25: krox20 expression is absent in a proportion of *pvrl4* morpholino injected zebrafish. Krox20 expression is present in only 52.63%+/-0.51% of embryos (10/19) in MO:*pvrl4* embryos, compared to 88.89%+/-0.22% (16/18) of control morpholino treated embryos. A) dorsal view of a 24hpf *pvrl4* 500µM morpholino treated embryo probed with *krox20* riboprobes. B) dorsal view of a 24hpf control morpholino treated embryo probed with *krox20*. C) lateral view of a 24hpf 500µM *pvrl4* treated embryo probed with *krox20*. D) lateral view of a 24hpf Control MO treated embryo probed with *krox20,* E) lateral view of a 24hpf 500µM *pvrl4* treated embryo probed with *krox20* displaying no specific krox20 staining. F) percentage of *pvrl4* 500 µM injected embryos

displaying specific krox20 staining. R3) Rhombomere 3, R5) rhombomere 5. Error bars represent SEM, MO:*pvrl4* n=19, MO:control n=18 p<0.001 by welch's t-test.

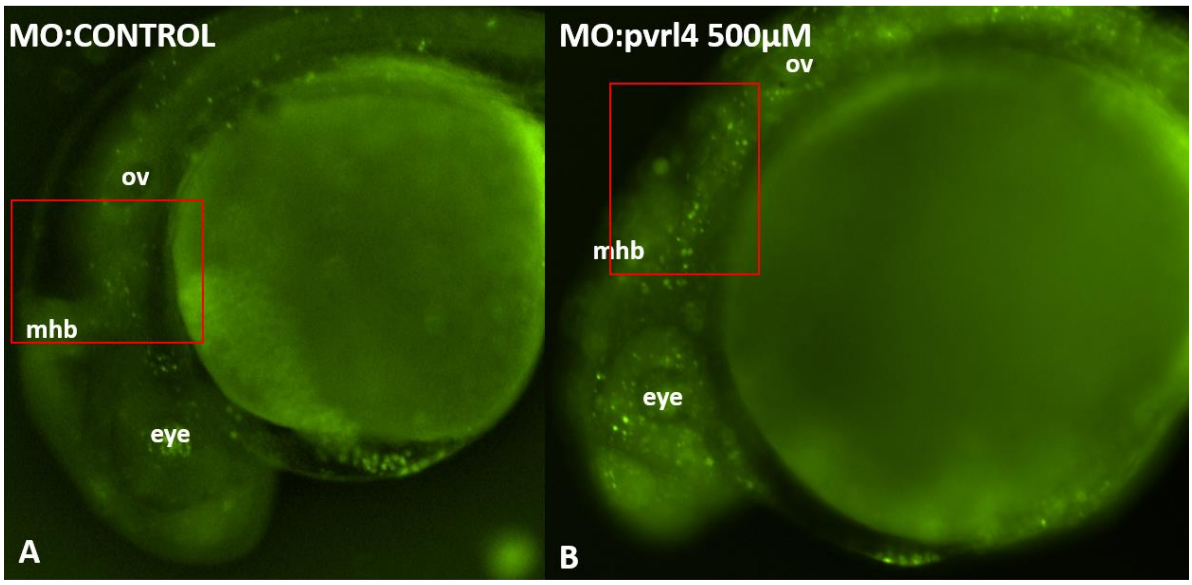

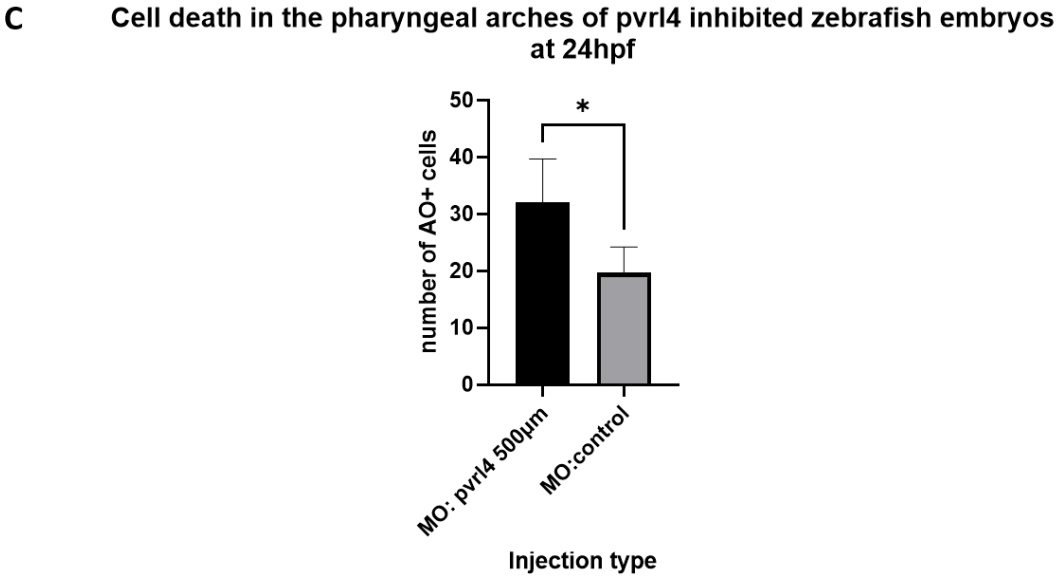

Figure 3.26: Cell death in the pharyngeal arches of 24hpf zebrafish embryos injected with a *pvrl4* inhibiting morpholino. Acridine orange staining was used to visualise DNA damage representing cells undergoing apoptosis in *pvrl4* morpholino injected embryos (A) and control morpholino injected embryos (B). Cells displaying fluorescence were assumed to be apoptotic or necrotic, and the number of these cells between the midbrain-hindbrain boundary (mhb) and the otic vesicles (ov) were counted (red box). MO:*pvrl4* embryos displayed a greater number of acridine orange positive cells (C) compared to control injected embryos, and this difference was found to be significant (p = 0.019 by students t-test).

3.3 Discussion

In this study, we establish a role for *grhl3* as a regulator of pathways involved in lower jaw development. Inhibition of *grhl3* in *Danio rerio* leads to a phenotype characterized by severe hypoplasia of jaw structures, but no significant effect on overall viability of embryos. The genetic pathways affected by *grhl3*-loss in the context of lower jaw development include the *edn1-dlx3-hand2* pathway in post-migratory NCCs within PA1, whilst excluding pre-migratory and migratory NCCs. further, outside PA1, e.g., in the otic vesicle (OV; *dlx3*) and heart (*hand2*) expression persists. These data show that *grhl3* expression regulates lower jaw development via regulation of NCC maintenance exclusively in the ventral pharyngeal arches.

3.3.1 *grhl3* inhibition leads to lower jaw defects in zebrafish

Knockdown of *grhl3* expression led to craniofacial defects mostly localised to the lower jaw. Of the structures affected, a number are considered analogues of skeletal structures in humans including Meckel's cartilage and the palatoquadrate. Meckel's cartilage functions as a lower jaw in zebrafish and is malformed in *grhl3* knockdown zebrafish embryos. In humans however, Meckel's cartilage is present only during embryological development, and the cells comprising Meckel's cartilage do not contribute to the mandible. Rather, Meckel's cartilage contributes to the development of the incus and malleus bones of the ear, and the mandible develops separately, although both structures are derived from the first pharyngeal arch. Thus, Meckel's cartilage does not necessarily fulfill the same role in humans as it does in zebrafish. However given the common origin of the lower jaw in zebrafish and humans (PA1), genetic mutations resulting in defects in the zebrafish Meckel's cartilage are still useful for modelling human lower jaw defects.

Genotyping studies of individuals with hearing loss have implicated mutations in another member of the grainyhead-like family – *Grhl2* as potentially associated with hearing loss (Van Laer et al., 2007), however our study of *grhl3* did not discover any changes in gene expression within the zebrafish otic vesicles at 24hpf. Moreover, previous studies have not shown aberrant *grhl3* expression in the OV of fish (Dworkin et al., 2014). Whilst this indicates that *grhl3* is not involved in zebrafish hearing loss, it is possible that given the importance of Meckel's cartilage-derived structures in mammalian ears, *Grhl3* may still have a function in mammalian hearing loss. While the roles of *grhl* genes in hearing loss is also not without precedent; defects in *grhl2b* expression would be more likely to cause hearing loss, given that it is the *grhl* orthologue present in the otic vesicles of the zebrafish (Han et al., 2011).

Despite the distinctly different role of Meckel's cartilage in humans, the role of *Edn1* and *Grhl* genes in the lower jaws of mice appear similar to MO:*grhl3* zebrafish. Studies that have disrupted *edn1* in mice have resulted in defects to analogous lower jaw structures (Kurihara et al., 1994). This suggests that the *grhl3* knockdown-induced lower jaw hypoplasia seen in our zebrafish model may be conserved across other species in the form of mandible hypoplasia. Knock-in of *Edn1* in mice has demonstrated that the presence of *Edn1* can lead to transformation of cells in the maxilla to a mandibular identity, further demonstrating a conserved role for *edn1* across species (Sato et al., 2008). Similarly, conditional deletion of *Grhl2* in mice using cre-lox models, reported micrognathia following loss of *Grhl2* in the epithelium specifically (de Vries *et al*, 2021). These results suggest that the roles of *grhl3* and *edn1* in zebrafish are mirrored by *Grhl2* and *Edn1* in mice, although interestingly, mice doubly heterozygous for Grhl2 and Edn1 (Grhl2+/-;Edn1+/-) did not present with lower jaw defects, suggesting either a functionally-distinct relationship between these genes in mice, or more likely, that the 50% functional gene dosage of both were sufficient to prevent craniofacial deformities (de Vries *et al,* 2021). Additionally, it supports the notion that *grhl*3 and edn1 interact in PA1 to contribute to the development of the lower jaw.

Our results also demonstrate a role for *grhl3* in the development of the zebrafish anterior neurocranium. As previously mentioned, the anterior structures of the neurocranium are derived from NCCs whilst the posterior structures are derived from mesoderm (Mongera et al., 2013). Our results show that the most anterior neurocranial structure, the ethmoid plate, is deformed following *grhl3* knockdown. Conversely, posterior neurocranial structures are unaffected by *grhl3* knockdown. The anterior neurocranium is functionally analogous to the mammalian hard palate; it separates the oral cavity from the cranial cavity above (Swartz, Sheehan-Rooney, Dixon, & Eberhart, 2011). Although the morphological development of the palate in humans and zebrafish differ somewhat, a growing body of evidence suggests that the genetic pathways involved are highly conserved between mammals and zebrafish (Ghassibe-Sabbagh et al., 2011; Swartz et al., 2011; Wada et al., 2005).

grhl3 itself has been identified as a risk factor for syndromic and non-syndromic CP. In zebrafish and mouse models, *grhl3* mutations associated with VWS resulted in aberrations of the oral periderm including cleft palate (Peyrard-Janvid et al., 2014a), whilst genome wide association studies have repeatedly linked *grhl3* with non-syndromic CP (Eshete et al., 2017; Elizabeth J. Leslie et al., 2016; Mangold et al., 2016; Y. Wang et al., 2016). Further, our results add to the evidence suggesting the zebrafish neurocranium is a suitable model for the mammalian palate, and that *grhl3* is a risk gene for syndromic cleft palate.

3.3.2 *grhl3* regulation of craniofacial development is restricted to pharyngeal endoderm-directed control of ventral NCCs

Within PA1, *grhl3* is expressed exclusively within the medial pharyngeal endoderm (Dworkin et al., 2014). The pharyngeal endoderm is vital for craniofacial development, particularly in sustaining NCC populations once they have migrated to the pharyngeal arches and supporting their differentiation into cartilage. Signals from the pharyngeal endoderm provide instructions for NCCs to pattern the skeletal structures in the face (Abu-Issa, Smyth, Smoak, Yamamura, & Meyers, 2002; Johnson et al., 2011). More specifically, it has been demonstrated that the most anterior portions of the pharyngeal endoderm will pattern NCCs to produce the skeleton of the jaw and face. NCCs will be receptive to regional cues from the endoderm in the pharyngeal arches, and these cues will subsequently alter the development of bones in the jaw.

However, both the paraxial mesoderm and the ectoderm in the pharyngeal arches contribute to craniofacial development, and many genes involved in facial skeleton development regulate cells in both germ layers. Aberration of the expression of the mesoderm and endoderm derived gene *gsc*, has yielded phenotypes similar to that of the *grhl3* phenotype (Rivera-Pérez, Mallo, Gendron-Maguire, Gridley, & Behringer, 1995). Given the role of *gsc* in mesoderm differentiation in embryo development, it would be expected that any interaction between *grhl3* and *gsc* would have manifested in the WISH experiments conducted in our study. Hence, these experiments indicate that *grhl3* does not influence genes in the developing mesoderm.

Although the cues derived from the pharyngeal microenvironment influence the behaviour of NCCs in craniofacial development, events prior to population of the pharyngeal arches can also influence NCC fate. Cell-intrinsic defects, such as mutations to the *Bbs* gene putatively responsible for Bardet-Biedl syndrome and Hirschsprung's disease, can disrupt migration patterns of cranial NCC, ultimately leading to hypoplasia in various craniofacial regions and an array of subtle facial anomalies as well as orofacial clefts (Tobin et al., 2008).
NCCs also communicate amongst each other during migration, with filopodia directly influencing the actions of neighbouring NCCs to ensure that the NCC continue migrating in the correct direction (Teddy & Kulesa, 2004). Our study determined no difference in NCC at premigratory or migratory stages of development following *grhl3* knockdown. This is consistent with the role of *grhl3*, given that it is not expressed within NCCs themselves and so should not affect NCC behaviour at migratory or pre-migratory stages. This also demonstrates that the regulation of craniofacial development by *grhl3* occurs after NCC population of the pharyngeal arches, further

highlighting the specificity of *grhl3* as a key transcription factor regulating lower jaw development through maintenance of the pharyngeal microenvironment.

Within the first pharyngeal arch, the ventral aspect will eventually contribute to the development of the Meckel's cartilage and lower jaw in vertebrates, whilst the dorsal aspect contributes to the development of the maxilla. Following *grhl3* knockdown, our WISH experiments showed decreased expression of *dlx3*, an important homeobox gene in the ventral area of the pharyngeal arch, but not the dorsally expressed *dlx2*. Studies of the craniofacial features of VWS patients have consistently showed maxillary hypoplasia as a common feature (Heliövaara, Karhulahti, & Rautio, 2015) (Oberoi & Vargervik, 2005). Our results suggest that this feature is unlikely to be associated with *grhl3* given that *dlx2* remained unaffected in the dorsal portion of the first PA. Given the influential role of *IRF6* mutations in VWS syndrome, maxillary hypoplasia may be attributed to a craniofacial pathway that is regulated by *irf* genes and is independent of *dlx2*. Regardless, our results demonstrate that even within the pharyngeal arches, *grhl3* regulation of craniofacial development is specific to NCCs of the ventral pharyngeal arch.

3.3.3 *grhl3* regulates genetic pathways within the first pharyngeal arch that are known to regulate craniofacial development.

Given *grhl3* is a transcription factor, it has the ability to regulate a vast array of genes and consequently, gene pathways. The knockdown of *grhl3* and its subsequent effects on the *edn1*-dlx-*hand2* pathway display similarities to previous studies investigating aberrant expression of this gene network. The *sucker* (Suc) mutant line is characterised by a lack of endothelin expression in zebrafish (C. T. Miller et al., 2000). Analysis of *edn1*-deficient zebrafish noted severe jaw hypoplasia as well as decreased expression of *dlx3* and *hand2* genes in the pharyngeal arches. However, sucker mutants displayed entirely absent lower jaws, as opposed to *grhl3* morphants which still retained some lower jaw structure. Additionally, *edn1* loss in mice was also shown to lead to an absent lower jaw, suggesting that overall loss of *edn1* is associated with a complete deletion of the lower jaw across various species (Kurihara et al., 1994). *Edn1* however, is expressed throughout the pharyngeal ectoderm, paraxial mesoderm as well as the endoderm, where it functions through activation of the receptors Ednra and Ednrb. The expression of *edn1* in the ectoderm and mesoderm of the pharyngeal arches may account for the respective differences in severity between *grhl3* knockdown and sucker mutant zebrafish. If *grhl3* knockdown only limits expression of endodermal *edn1*, the presence of a hypoplastic jaw (as opposed to the absence of a mandible seen in sucker mutants) may be due to partial compensation by ectoderm derived *edn1*.

Analysis of the Endothelin receptor Ednra in mutant mice, demonstrated a similar mandible phenotype to our morpholino knockdown, as Ednra$^{-/-}$ mice were found to possess hypoplastic but not absent lower jaws (Clouthier et al., 1998; Kurihara et al., 1994). Ednra$^{-/-}$ mice also displayed limited expression of *gsc* (Clouthier et al., 1998), which contrasts with our data which showed no difference in expression in gsc after *grhl3* knockdown. However, this does not contradict our results as it is likely due to the specific downregulation of endodermal *edn1* by *grhl3*, as Edn1/Ednra pathways in the paraxial mesoderm would be expected to function normally given the specificity of *grhl3* demonstrated in earlier experiments. Defects in the ethmoid palate observed in our *grhl3* knockdown study were also not described as a consequence of *edn1*-loss in sucker mutants (C. T. Miller et al., 2000). This indicates that it may be an endothelin-independent mechanism that leads to ethmoid defects in zebrafish following *grhl3* knockdown, and therefore, endothelin 1 is not necessarily a risk gene in orofacial cleft.

Our results display a significant loss of expression in *dlx3*, and widespread hypoplasia of lower jaw structures. The malformation of these structures bears some resemblance to existing knockdown and mutant strain studies of *dlx3* (Duverger et al., 2013). Although the mandible is specifically affected by aberrant *dlx3* expression, these defects typically result in demineralisation of the bone and teeth, rather than misshaped jaw bones (Duverger et al., 2013). *Dlx3* is a putative negative regulator of osteoclast differentiation (Isaac et al., 2014; Zhao et al., 2016), thus playing an important role in ensuring bones are mineralised within the facial skeleton. This provides a clear link between *dlx3* expression and craniofacial defects in mice but it's implications for *grhl3* morphants are unclear. Zebrafish larvae at <5dpf have few ossifying bones in the facial skeleton (Mork & Crump, 2015), and so increased osteoclast differentiation due to *dlx3* downregulation may not result in hypoplasia of cartilaginous structures. Given that apoptosis and osteoclast function were not investigated in our MO:*grhl3* zebrafish, whether *dlx3* produces similar defects in zebrafish remains to be seen.

Hand2 is located downstream of *edn1* and plays a critical role in craniofacial development, particularly in the intermediate domains of the pharyngeal arches (Craig T. Miller et al., 2003). *Hand2* mutant zebrafish have demonstrated a phenotype similar to that of the *grhl3* knockdown phenotype, with distinctive defects in the ventral cartilages of zebrafish (Craig T. Miller et al., 2003). In *hand2* mutants, the structures of the lower jaw joint anterior to the hyosymplectic are hypoplastic, however Meckel's cartilage and many other ventral structures are absent, and other remaining structures such as the palatoquadrate were deformed or hypoplastic (Craig T. Miller et al., 2003). Overall, The Hand2 mutant phenotype is more severe than that of *grhl3*. However,

both the phenotype of Hand2 mutants in the literature and our results following downregulation of *hand2* via *grhl3* knockdown are consistent with the putative role of *hand2* as a determinant of mandible identity in zebrafish. The difference in severity when comparing our *grhl3* phenotype and that of *hand2* mutants, may be a result of the widespread distribution of *hand2* expression throughout the pharyngeal arches and the heart. *Hand2* is critical for the development of the heart, and so hypoxia or cardiovascular defects stemming from impaired heart development may contribute to more severe phenotypes observed in *Hand2* mutants. As with *edn1*, expression of *hand2* outside of the pharyngeal arches may partially rescue mandible development and is supported by the unaffected expression of *Hand2* in the zebrafish heart following *grhl3* knockdown.

3.3.4 *tmem54a* inhibition produces zebrafish with severe craniofacial abnormalities.

Our study also demonstrated that one orthologue of the zebrafish tmem54 gene, *tmem54a*, was required for the development of facial structures in zebrafish. Morpholino oligonucleotide inhibition of *tmem54a* mRNA expression, resulted in the absence of almost all zebrafish facial structures. WISH experiments demonstrated that the cell populations in the ventral portions of rhombomeres 3 and 5 appeared to be affected by loss of *tmem54a*. In addition to the gross morphological abnormalities visible in the zebrafish head, *tmem54a* deficient zebrafish also displayed loss of movement, and reduced survival rates.

Unlike the defects induced by *grhl*3 morpholinos, *tmem54a* defects do not result in hypoplasia, but rather the complete loss of most of the structures of the zebrafish face. Additionally, while the cartilages of the viscerocranium are almost always absent, some cartilages of the neurocranium are present. In particular, the most posterior cartilage, the parachordial cartilage, remains despite the loss of most other structures. Again, the significance of this lies in the cells from which these structures are derived, as posterior neurocranium structures are mesoderm-derived, unlike the rest of the cranium which is NCC derived (Mork & Crump, 2015). That the only remaining cartilaginous structures are those that are most posterior, suggests that *tmem54a* affects neural crest cell function.

Given the effect of *tmem54a* loss on a wide range of NCC derived structures, it is likely that the defective process responsible affects all neural crest cells, rather than a single pharyngeal arch as seen in MO:*grhl3* embryos. A patterning defect affecting all pharyngeal arches is one potential cause of the *tmem54a* morpholino phenotype, however loss of other genes involved in PA patterning generally yielded phenotypes that retained parts of the palatoquadrate and Meckel's cartilage (Nissen, Amsterdam, & Hopkins, 2006). Alternatively, Morpholino knockdown of genes involved in NCC migration such as Alx1, caused similar loss of craniofacial structures. Moreover,

Sox9 deficient zebrafish larvae lack NCC derived structures in the craniofacial region, and *sox9b* is a key gene involved in the survival of pre-migratory NCCs (Liu et al., 2013). While morphologically, NCC migration defects appear to fit the *tmem54a* deficient phenotype, specific NCC migration pathways affected by loss of *tmem54a* have not been identified.

Inhibition of *tmem54a* appeared to lead to abnormal development of the ventral 3rd and 5th rhombomeres. While rhombomeres 3 and 5 do not contribute NCC to the pharyngeal arches, if the cells in the ventral regions of all rhombomeres are disrupted, this may lead to abnormal migration of NCC. Alternatively, if the disruption evident in ventral areas of rhombomeres 3 and 5 extends to the mesenchyme which usually repels NCC migration, this may lead to significant craniofacial abnormalities. This avenue of research is promising, given that sox10:egfp lines allow for the visualisation of NCC movement over time, and would reveal any potential disruptions in NCC migration (Kwak et al., 2013). In this way, the disruption of NCC migration due to defects in ventral rhombomere formation provide a promising hypothesis for the morphological defects evident in MO:*tmem54a* embryos.

It is not clear, however, through which gene pathways *tmem54a* would act to influence rhombomere development. The most likely downstream effectors that would cause rhombomere defects are the Hox family of genes, which are responsible for their segmentation (Choe, Zhang, Hirsch, Straubhaar, & Sagerström, 2011). However, given that rhombomeres 3 and 5 still appeared well defined and thus well segmented, and that the spinal cord neurons appeared unaffected at these spinal levels, abrogated Hox gene expression does not appear a likely downstream cause of rhombomere defects in MO:*tmem54a* zebrafish. *Fgf* genes have been identified in mice as regulating the ventral rhombomeres, and thus present a more fitting downstream target through which loss of *tmem54a* expression could cause rhombomere defects specific to the ventral regions (Weisinger, Kayam, Missulawin-Drillman, & Sela-Donenfeld, 2010). Given the lack of literature surrounding *tmem54a*, a relationship between *fgf* and *tmem54* has not been established but remains a promising area of interest for further study.

An alternate pathway for *tmem54a* in craniofacial development is Estrogen Receptor α (ERα), a known target of *Tmem54* with many relevant functions in development (Légaré & Basik, 2016). *Tmem54* was identified as a negative regulator of erα in mouse models, wherein *erα* is implicated in processes such as bone development including in the craniofacial region (Cohen, LaChappelle, Walker, & Lassiter, 2014). Diaz-Martin *et al* (2021) showed that in zebrafish exposed to glyphosate, Erα expression is increased, motor activity is decreased, and craniofacial defects occur. These results are consistent with what is observed in *tmem54a* embryos with respect to craniofacial and movement defects. The craniofacial defects are not nearly as

widespread or severe however, as the craniofacial defects were largely related to subtle changes in morphology rather than absence of the cartilages altogether.

Among the various similarities between *tmem54a* and *ER*α, both are involved in the regulation of EMT. Given the role of other consequential craniofacial genes in EMT, *tmem54a* could influence ERα's role in EMT suppression. Additionally, considering *ERα's* role in pharyngeal cancers, pharyngeal arch defects in erα could involve *tmem54a* as an upstream regulator. These defects would affect the development of NCC by promoting EMT in tissues of the pharyngeal arches which are required for patterning prior to the development of the facial prominences. The overlap in functions and established regulation of *erα* by *Tmem54* genes in other animal models provides a novel candidate gene for further investigation into the mechanisms behind *tmem54a* gene defects.

3.3.5 *pvrl4* inhibition leads to craniofacial and rhombomere abnormalities and induces cell death.

Relative to defects observed following inhibition of *tmem54a* and *grhl*3, defects arising from inhibition of *pvrl4* affected were more subtle and specific - only the palatoquadrate and ceratobranchial cartilages in the developing zebrafish larvae were affected. It was also found that in almost half of all embryos where *pvrl4* expression was inhibited, the rhombomere 3 and 5 marker krox20 was not detectable. Yet despite the loss of krox20 expression throughout the rhombomeres, survival rate was not significantly affected in embryos treated with higher dosages of *pvrl4* morpholino. This suggests that any rhombomere malformations are likely to be mild and consequently have a minor affect on cells such as NCC, as more severe defects would likely lead to greater embryo death. Increases in cell death around the pharyngeal arches were also observed however, providing an alternate explanation for MO:*pvrl4* defects. Thus, it appears that the two primary contributing factors in the incidence of this phenotype are rhombomere defects and pharyngeal arch cell death.

Increases in cell death around the pharyngeal arches appears to support a mechanism involving NCC death during migration or in the pharyngeal arches. In the first instance, NCC death would need to be specific to those NCC which would ultimately have contributed to palatoquadrate and ceratobranchial development. This is complicated by the fact that the NCC from which these cartilages are derived originate from different pharyngeal arches, and any widespread death in migrating NCC would likely lead to equally widespread defects in craniofacial structures. Alternatively, cell death in the pharyngeal arches is a well evidenced cause of craniofacial structures. Acridine orange staining does not, however, provide data on the types of cells that are dying. As a consequence, it is unclear whether the stained cells are NCCs, part of the

pharyngeal arch, or any other cell type in the area such as the epithelium or mesenchyme. Nevertheless, cell death during NCC migration and pharyngeal arch defects represent plausible causes for craniofacial defects in *pvrl4* inhibited zebrafish.

The loss of *krox20* expression in some *pvrl4* inhibited embryos suggests that the mechanism responsible for the defects may involve the development of the rhombomeres. Many of *pvrl4*'s functions stem from its interactions with *nectin 1* which itself has been associated with numerous targets genes relevant to craniofacial development and disease (Lough et al., 2020; Mollo et al., 2015). One such target of *nectin* 1 is *Fgf*, which as discussed above, is important for the development of the ventral rhombomeres. Thus, a *pvrl4*-nectin-1-fgf rhombomere regulatory pathway could conceivably be responsible for the lack of *krox20* marker expression. This putative pathway would only account for ventral rhombomere function, not the lack of expression in dorsal regions. Further, defects in the rhombomeres would be expected to influence the development of numerous facial structures given that all of the NCC that contribute to craniofacial development must migrate from the rhombomeres. Alternatively, defects in the rhombomeres could be minor and relatively inconsequential, and instead, Fgf mediates these defects independently of the rhombomeres, as murine Fgf has been identified as playing a key role in palatal shelf outgrowth and could regulate the development of other craniofacial structures in zebrafish (Jin, Han, Taketo, & Yoon, 2012). Nectin 1 contributes to the maintenance of filopodia that are required in a number of settings during development of the facial region (Kawakatsu et al., 2002). Without filopodia, NCC death during migration is likely, providing a link between a target of *pvrl4* and NCC migration. Evidently, the various roles of nectin genes, including *pvrl4*, provide multiple potential mechanisms for defects in the zebrafish face, however few of them adequately explain the specific pattern of defect observed.

Pvrl4 shares interactions with many genes that are implicated in craniofacial development in zebrafish. Most of these genes, however, are involved in cleft lip or palate in other organisms. *Nectin 1* is linked to cleft palate both syndromically with regard to ectodermal dysplasia, and non-syndromically, while *IRF6* is a putative regulator of *pvrl4* expression (Mollo et al., 2015). Despite these links however, the craniofacial defects observed following inhibition of *pvrl4* are not those that bare resemblance cleft palate. The ethmoid plate, which separates the brain cavity from the viscerocranium, was unaffected, whilst the structures that displayed defects were derived from PA 3-7, not PA1. It has been proposed that members of the nectin gene family are able to compensate to some degree, following loss of one or more members (Son et al., 2016). It is possible that given the overlap in function and interactions between *pvrl4* and other nectin genes in the literature, *pvrl4* inhibited embryos are rescued from more severe defects by compensation from *nectin 1-3*. Inhibition of other nectin genes, with a focus on the

development of the ethmoid plate and the target genes proposed above, would yield valuable information regarding the influence of these genes on craniofacial defects.

3.3.6 Future Directions

An important limitation of this study is the reliance on morpholino oligonucleotides. Morpholinos are valuable for easily and efficiently knocking down gene activity in zebrafish, however they are known to suffer from a number of drawbacks which limit the degree to which we can associate morphant phenotypes with naturally occurring defects (Kok et al., 2015). The next step for investigating these genes is the generation of zebrafish lines with each of these genes deleted using CRISPR/Cas9 gene editing techniques. These lines would allow for the investigation of loss of gene expression over the lifespan of the zebrafish, as well as the complete loss of gene expression rather than "knockdown" of gene expression as produced in morpholino experiments.

Given the constraints relating to COVID-19, several avenues remain unexplored by this study. Firstly, whilst our results did indicate that the craniofacial phenotype was due to *grhl3* knockdown, NCC apoptosis at various points was not addressed; clearly, NCC death would also result in hypoplastic cartilage of the craniofacial skeleton. For this reason, testing for apoptosis following morpholino knockdown of *grhl3* is important for future research into this gene. Additionally, the effect of *grhl3* on the ectoderm and endoderm could be investigated using similar techniques to those described in this study, with the inclusion of markers such as *gcm2* and *sox 17*. The effect of *grhl3* knockdown on the *edn1*-dlx-*hand2* pathway may also be further investigated by exploring whether re-injection of *edn1* and downstream targets rescues the phenotype in later stages of development. Similarly, Morpholino experiments targeting *edn1*, *dlx3*, and *hand2* in *grhl3*-deficient zebrafish could potentially reveal the roles of each of the genes in this pathway more extensively. Our results reveal that palatogenesis may be disrupted following inhibition of *grhl3* expression in the pharyngeal endoderm, as evidenced by malformations of the ethmoid cartilage in zebrafish. Further experiments in this area are necessary to ascertain the mechanism through which *grhl3* loss .leads to palatal defects, as literature analyses indicate it is likely to be *edn1*-independent (C. T. Miller et al., 2000). Given the role of the first pharyngeal arch in patterning the malleus and incus in mammalian ears, investigating *grhl3* knockdown in mammals may also establish a link between *grhl3* knockdown and hearing loss.

The severe craniofacial defects evident in MO*:tmem54a* zebrafish larvae make it a model of considerable interest for further experiments. The use of sox10-gfp zebrafish lines combined

with the current morpholino oligonucleotide approach, will provide valuable insight into the function of neural crest cells at various timepoints of zebrafish development as fluorescence is expressed in neural crest cells expressing *sox10* (Betancur, Bronner-Fraser, & Sauka-Spengler, 2010). The optimisation of WISH forms a solid basis for continued investigation of defects in other developing structures, utilising riboprobes that weren't available to this project during experimentation with *tmem54a* and *pvrl4*. In particular, probing for pharyngeal arch genes such as *dlx2*, *dlx3*, *sox9b*, and *hand2* as used in *grhl*3 inhibited embryos, as well as rhombomere-specific probes such as hoxb2a would be useful. Longer term investigation may also attempt to relate the defects in zebrafish to mice by deriving *Tmem54* null mice.

Future studies regarding *pvrl4* in zebrafish will prioritise the identification of genes downstream of *pvrl4* that are affected by its' inhibition. Identifying changes in the expression of *fgf* at key timepoints in embryonic development, such segmentation of the rhombomeres, will support these genes as a contributing to *pvrl4*-inhibition induced defects. Similarly, analysing the expression of other members of the nectin family, specifically *nectin 1*, will provide further support for these genes in *pvrl4*-related defects. Ultimately, if these are found to be differentially expressed, the use of Chromatin Immunoprecipitation (ChIP) assays could provide insight into direct regulation of *pvrl4* with its' putative target genes, thus validating these pathways. Lastly, the use of TUNEL staining would be an invaluable technique to build upon the cell death identified using acridine orange staining. TUNEL staining would allow for the differentiation of cells undergoing DNA damage, from those specifically undergoing apoptosis, and thus more convincingly demonstrate the contribution of apoptosis to defects in these embryos.

Despite the severe abnormalities evident following *tmem54a* inhibition, the role of *tmem54b*, if any, remains unclear. The literature surrounding *tmem54b* provides no evidence of any function in any tissue. It thus appears most likely that *tmem54a* fulfills all the developmental roles of *Tmem54* in mammals, and that *tmem54b* is an artifact of the teleost genome duplication event and has simply become a redundant gene. However CRISPR *tmem54b*$^{-/-}$ zebrafish lines would allow the study of *tmem54b* deletion to be examined over the full lifespan of the zebrafish.

Overall, these findings are significant in that they demonstrate the role of *grhl3, tmem54a and pvrl4 in vivo* and begin to reveal potential mechanisms through which these genes regulate craniofacial development. Additionally, these data support the future investigation of these genes in craniofacial development in other animal models. In conclusion, these results provide a solid foundation for the further study of genetic factors in craniofacial development.

Chapter 4: *Grhl*2 downstream genes

4.1 Introduction

4.1.1 *Grhl*2 target genes

Given its' function as a transcription factor, *Grhl*2 regulates expression of various other genes and their associated pathways in order to fulfill its role in palatal and neural tube development. *Grhl*2 is able to regulate a vast array of pathways and as a result, regulates many cellular processes. *Grhl*2 can either repress or activate gene transcription depending on the promoter region involved, and is subject to alternative splicing which can modify its function (Miles, Dworkin, & Darido, 2017). An example of the complexity of inherent in *Grhl*2 regulation is exemplified by its' interaction with *ZEB1*. *ZEB1* is an upstream inhibitor of *Grhl*2, however together they mutually inhibit each other in the governance of epithelial and mesenchymal cell identity. The over-expression of *Grhl*2 can indirectly lead to *Zeb1* upregulation, as upregulation of downstream genes including *ESRP1* will in turn promote the transcription of *Zeb1*, which itself will decrease transcription of *Grhl*2 (Carpinelli et al., 2020)]. This feedback loop is critical to the maintenance of proper epithelial and mesenchymal cell identity throughout the body. Additionally, the presence of alternative splicing and start points can modify the function of *Grhl*2 regulation. The loss of the N-terminal transactivation domain is proposed to result in the loss of transcriptional activity leading to a dominant-negative proteins when compared to full length proteins, and examples of these truncated proteins have been identified in breast cancer cell lines (Britton et al., 2008). Additionally, phosphorylation of sites on *Grhl* genes has been demonstrated as being critical to their function, particularly in epidermal wound healing in mice and drosophila (Miles, Dworkin, et al., 2017). These examples display the diversity of both *Grhl*2's transcriptional pathways, as well as the different transcriptional methods through which *Grhl*2 may regulate its targets.

4.1.2 Putative gene pathways

Identifying the genes that rely on *Grhl* expression is a critical aspect in determining the mechanisms through which *Grhl*-induced craniofacial defects occur. The loss of *Grhl*2 in mice, and the subsequent severe NT and facial defects that result, undoubtedly involve perturbation of several gene pathways that are critical for the development of these regions. Identifying which of these critical pathways may be affected by *Grhl*2 knockdown is an important step in understanding how these severe defects occur.

The *sonic hedgehog* (*Shh*) pathway is a well described and critical regulator of embryological development and is evolutionarily well-conserved. *Shh* null mice present with broadly similar

phenotypes reminiscent of those seen in *Grhl*2, namely holoprosencephaly and cleft palate. Although the open neural tube and cleft face phenotypes are distinctly different forms of defect compared to those of *Shh*, both appear to stem from failures in NC and NCC function (Litingtung & Chiang, 2000). To this end, *Shh* is an important regulator of neural cells during and following neurulation and is expressed in the facial primordia during development of the facial prominence. Shh regulates cranial NCC via the fox family of genes, which themselves are important for NCC survival and differentiation of various cell types (Mukherjee et al., 2018). *Shh* function is generally mediated by a canonical pathway (fig. 4.1.1), consisting of the membrane receptors *patched* (*ptc*) and *Smoothened* (*smo*) as well as the *Gli* family of proteins intracellularly (Litingtung & Chiang, 2000). The phenotypic similarities, as well as the well-established mechanisms behind Shh signalling, establish it as an interesting target for investigation in *Grhl*2 null embryos.

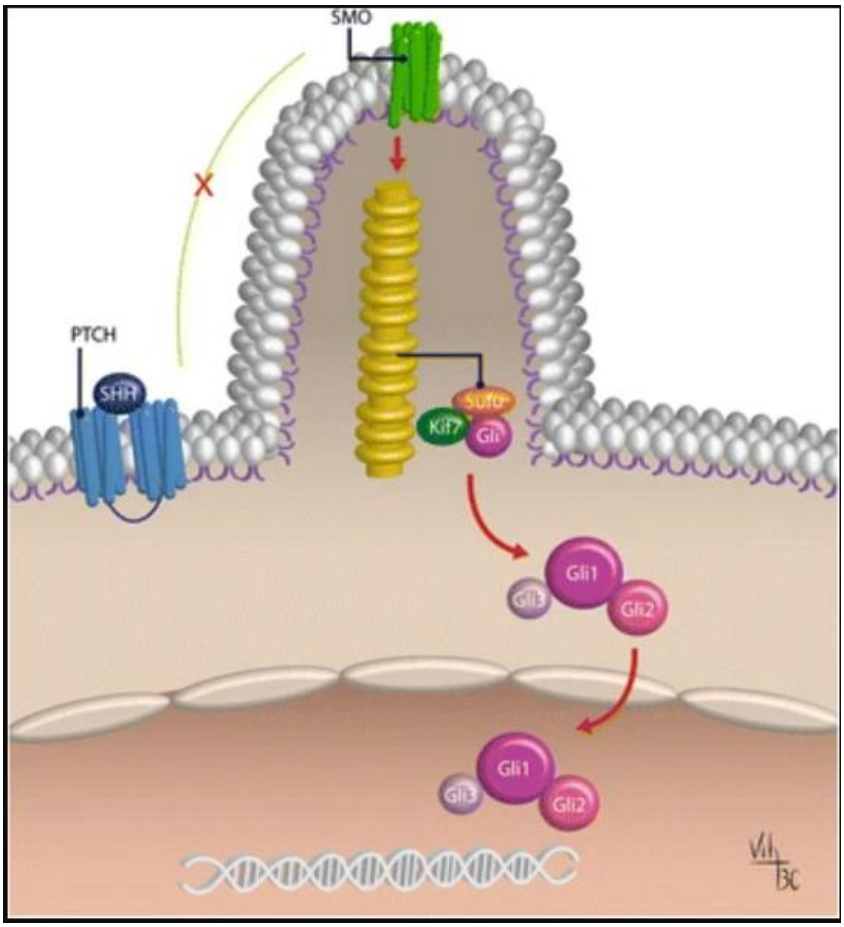

Figure 4.1.1: The *Sonic Hedgehog (Shh)* canonical pathway. Shh binds to the membrane receptor Patched, removing its inhibition of *Smoothened* (*Smo*). In the absence of *Shh*, *Patched* is able to prevent over-expression of *Smo*, however with its ligand attached, *Smo* accumulates at the primary cilium. *Smo* prevents cleavage of the Ci protein, which in turn is able to enter the nucleus and begin the translocation of the *Gli* family of proteins (Gli1, Gli2 and Gli3) into the nucleus. Adapted from Carballo, Honorato, de Lopes, and Spohr (2018).

The Fibroblast growth factor receptor (*FGFR*) family of genes is another family of genes with roles in neural tube and craniofacial development. The role of *Fgfr2* in regulating neural crest function is well characterized; *Fgfr2* is critical for the proliferation and survival of CNCC's and consequently, neural crest derived structures are disproportionately affected by loss of *Fgfr2* (Siismets & Hatch, 2020). Several studies have linked mutations in the *FGFR* gene with syndromic and non-syndromic cleft palate in humans. Additionally, *FGFR* is necessary for proper development of the neural tube (Deng et al., 1997). These characteristics, as in Shh, suggest that *FGFRs* may be one of many downstream targets that are implicated in disease in response to *Grhl*2 loss. Further, Fgfr and *Grhl*2 share activity with *Esrp1*. *Esrp1* was demonstrated to be a downstream target of *Grhl*2, and likely an important factor in the maintenance of epithelial phenotypes by *Grhl*2. *ESRP1* has a known role in alternative splicing in *FGFR* pre-mRNA and is thus implicated in mediating both *Grhl*2 and *FGFR* function in the epithelium (Warzecha, Shen, Xing, & Carstens, 2009). As a result of these similarities in phenotypes and common gene interactions, *FGFR* represents another putative target gene in *Grhl*2 null embryos.

The *Ovol* family of genes are a conserved family of genes which in mice comprise three orthologues (*Ovol1*, *Ovol2*, *Ovol3*). These genes are involved in epithelial differentiation and epidermal development as well as mesenchymal to epithelial transition (MET) (Roca et al., 2013). *Ovol2* in particular is critical to neural tube formation, as *Ovol2* null mice display an open cranial neural tube. Interestingly, the neural tube defects were proposed to be due to ectopic Shh expression and signalling, which was observed in the *ovol2* null embryos (Mackay, Hu, Li, Rhéaume, & Dai, 2006). Further, *Ovol2* null embryos also displayed a reduction in the size of the surface ectoderm, where *Grhl* signals are derived. While *Grhl* genes have to date not been associated with the neural tube defects attributed to *Ovol2*, these gene families evidently share many functions and interact with similar genes. Indeed, *Ovol2* has been identified as a downstream target of *Grhl*2 in the kidney, where it is responsible for epithelial barrier function (Aue et al., 2015). Given the significant overlap in phenotypes, function and genes with which they overlap, *Ovol2* is a worthwhile target for analysis in *Grhl*2 null craniofacial and NT defects.

This chapter will seek to identify novel genes and gene pathways that may be implicated in the severe craniofacial and neural tube morphology that follows from loss of *Grhl*2. The gene expression of *FGFR*, *Ovol2*, and the *Shh* pathway will be compared in tissue samples taken from facial prominences and the pharyngeal arches of *Grhl*2 null and wild type embryos, in order to establish a basis for further research into *Grhl*2 target genes in these regions.

4.2 Results

4.2.1 Quantitative RT-PCR reveals changes in target genes

Given that the facial prominences of *Grhl*2$^{-/-}$ mice show severe malformations, quantitative RT-PCR was used to examine the expression of a number of putative target genes with roles in CFD. *Shh* and it's intracellular effectors – *Gli1*, *Gli2* and *Gli3* – were assessed across each facial prominence, as well as *Ovol1* and *Fgfr2*. In MXP tissue, Shh pathway genes were unchanged, however both *Ovol1* and *Fgfr2* displayed minor changes, Ovol1 expression increasing 0.64 fold (p=0.039), and *Fgfr2* decreasing 0.84 fold (p=0.03) (fig 4.2). These changes were partially reflected in MDP tissue, as Shh pathway expression levels were similarly unaffected; however both *Ovol1* and *Fgfr2* were not affected by loss of *Grhl*2 in the MDP additionally (Fig 4.3). In FNP tissue, *Gli1* and *Gli3* were not affected, however there was a 1.4 fold decrease in Gli2 expression (p=0.0125) and a 0.88 fold decrease in Shh relative to wild type embryos (p=0.0371) (fig 4.4). *Fgfr2* expression in the FNP, and unlike in MXP tissue; was not affected by *Grhl*2 loss, whilst *Ovol1* expression appeared to be negatively regulated 0.74 fold (p=0.0124) (fig. 4.4). These data indicate that the relationship between *Grhl*2 and these putative target genes is complex with respect to each facial prominence.

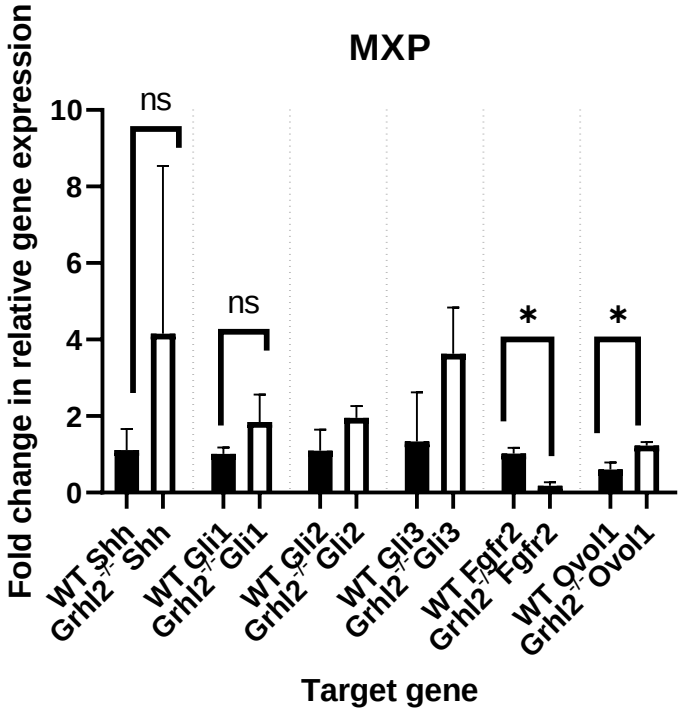

Figure 4.2: Q-RT PCR of target genes in the maxillary prominences of *Grhl*2$^{-/-}$ Mice. Shh pathway genes (*Shh-Gli1-Gli2-Gli3*) showed no significant difference in expression relative to a HPRT housekeeping gene in *Grhl*2$^{-/-}$ compared to *Grhl*2$^{+/+}$ (wild type) controls. Relative expression of *Fgfr2* in *Grhl*2$^{-/-}$ embryos dropped by 0.84 fold, whilst expression of Ovol1 increased 0.64 fold. Analysis was conducted via

the ΔCT method and significance was analysed with a students t test. *Fgfr2* p = 0.030, Ovol1 p=0.039. N= 2-3 for each condition.

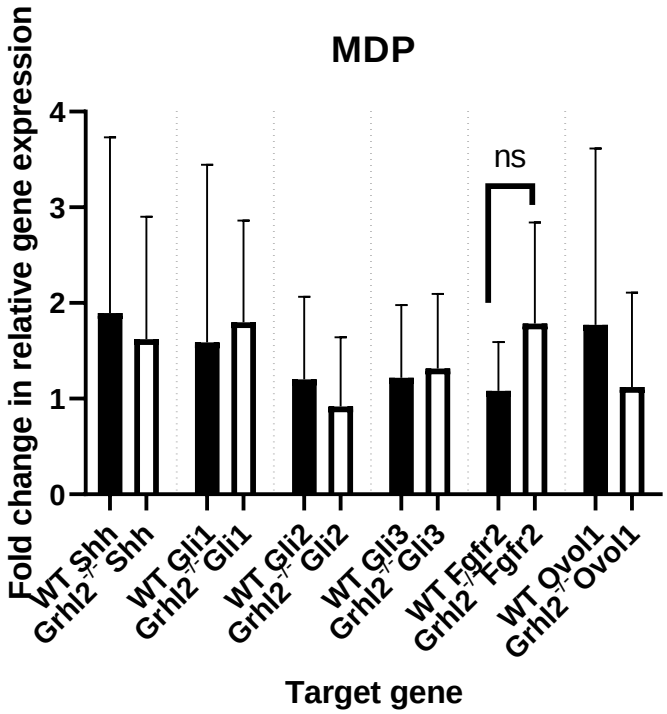

Figure 4.3: Q-RT PCR of target genes in the mandibular prominences of *Grhl2*$^{-/-}$ Mice. None of the target genes analysed showed significant differences relative to the housekeeping gene (*Hprt*). Analysis was conducted via the ΔCT method. N=3 for each condition.

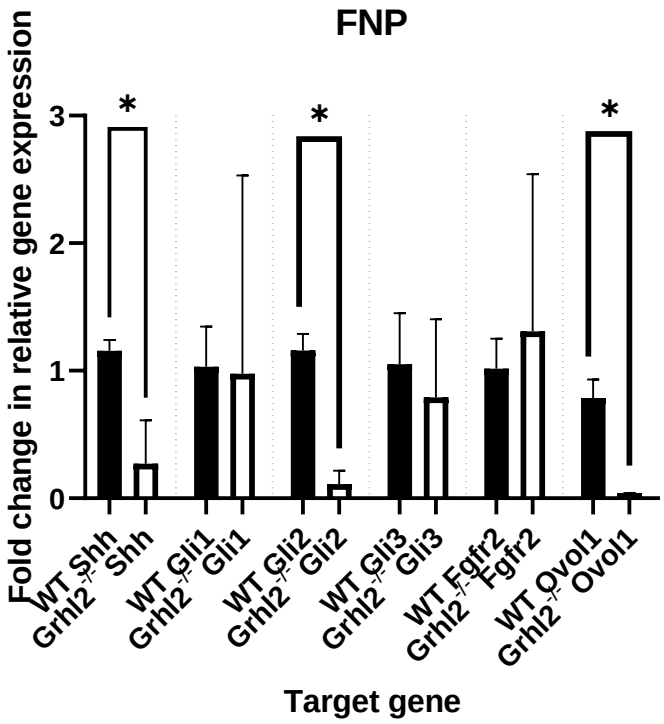

Figure 4.4: Q-RT PCR of target genes in the fronto-nasal prominences of *Grhl2*$^{-/-}$ Mice. *Shh, Ovol1* and *Gli2* were significantly downregulated in *Grhl2*$^{-/-}$ embryos relative to the housekeeping gene (Hprt). *Ovol1* expression decreased 0.74 fold, while *Gli2* exhibited a 1.4 fold decrease and Shh a 0.88 fold decrease relative to housekeeper. Analysis was conducted via the ΔCT method and significance was determined via students t-test. *Shh* p = 0.0371 Gli2 p =0.0125 *Ovol1* p = 0.0124 . N=3 for each condition.

In addition to monitoring expression of these putative target genes in the facial prominences, the same Q-RT-PCR approach was used to identify potential target genes that may be implicated in severe neural tube defects observed in *Grhl2*$^{-/-}$ mice. Epithelium and mesenchyme were extracted from the 1st pharyngeal arches of *Grhl2*$^{-/-}$ and *Grhl2*$^{+/+}$ embryos and analysed for differences in Shh pathway genes, *Fgfr2* and *Ovol1*. PA1 epithelial and mesenchymal tissue displayed no differences in Shh pathway genes relative to wild type controls, and the changes in *Fgfr2* gene expression that were evident in MXP and FNP tissue were not evident in the pharyngeal arches. Expression of Ovol1 was, however, significantly decreased in the epithelium of the first pharyngeal arch of *Grhl2*$^{-/-}$ mice (Fig. 4.4), but not in the mesenchyme (fig.4.5). Evidently, loss of *Grhl*2 in the epithelium of PA1 has the opposite effect when compared to changes in Ovol1 in the facial prominences, and the regulatory role of *Grhl*2 between tissues not only differs but can have entirely inverse effects on the expression of downstream genes.

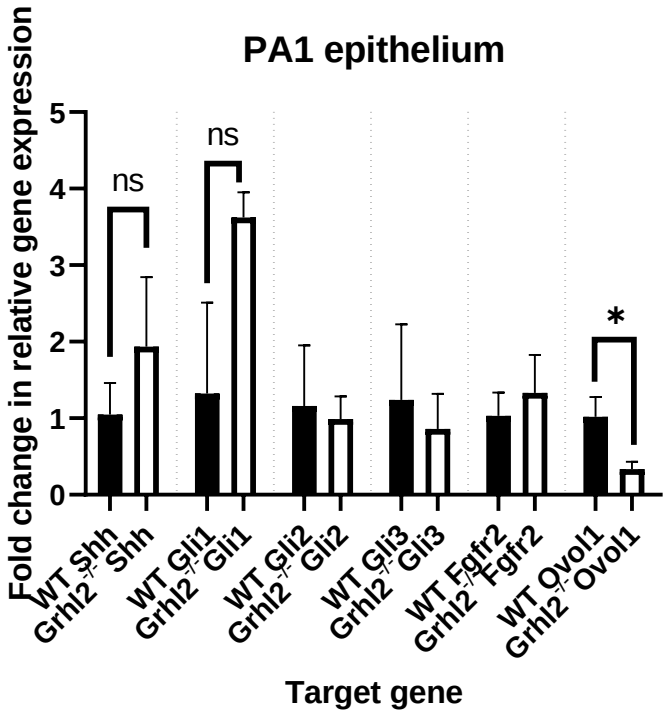

Figure 4.4: Q-RT PCR of target genes in the epithelium of the first pharyngeal arch in *Grhl2*$^{-/-}$ Mice. *Shh* and *Gli1* expression showed a 0.68 fold change relative to the housekeeping gene (HPRT). Expression of *Ovol1* was significantly increased in *Grhl2*$^{-/-}$ compared to control embryos. Analysis was conducted via the ΔCT method. Ovol1 p = 0.0123 N=3 for each condition.

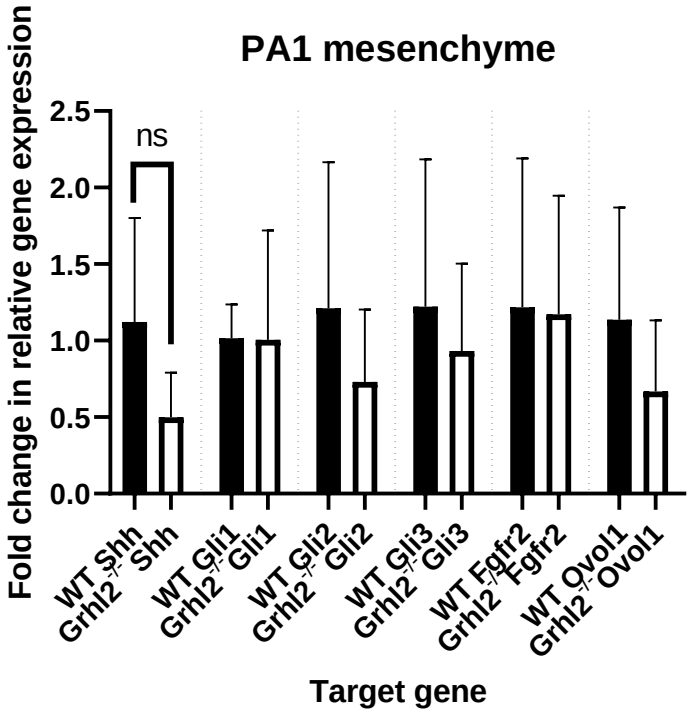

Figure 4.5: Q-RT PCR of target genes in the mesenchyme of the first pharyngeal arch in *Grhl*2$^{-/-}$ Mice. No significant differences were detected in any of the putative target genes tested when their expression was compared to a hprt housekeeping gene. N=3 for each condition.

4.3 Discussion

This study aimed to identify novel target genes downstream of *Grhl*2 through the analysis of mRNA expression in *Grhl*2$^{-/-}$ mice. More specifically, genes previously linked to craniofacial abnormalities similar to that of *Grhl*2 null mice were investigated for abnormal expression in the first pharyngeal arch and facial prominences of *Grhl*2$^{-/-}$ mice. Members of the Sonic hedgehog pathway, a pathway with known roles in craniofacial development, were analysed for changes in expression via qPCR. Changes in *Shh* and *Gli2* were detected in some tissues, but not other members of the pathway. Additionally, *Ovol1* and *Fgfr2* mRNA expression was analysed owing to their associations with craniofacial defects in the literature. Ovol1 was differentially expressed in the mxp, fnp and PA1 epithelium, while *Fgfr2* was only differentially expressed in the maxillary prominence of *Grhl*2$^{-/-}$ embryos.

Many defects evident in *Grhl*2 null embryos share similarities with *Fgfr2* null phenotypes and syndromes with which *Fgfr2* has been associated. *Fgfr2* was downregulated specifically in the maxillary prominence of *Grhl*2$^{-/-}$ embryos, suggesting that *Fgfr2* relies on *Grhl*2 expression in the MXP, but not in other tissues of the developing embryo. The incidence of cleft palate in embryos with mutant *Fgfr2* alleles suggests that regardless of the influence of *Grhl*2, *Fgfr2* is required for

proper palatal development (Snyder-Warwick et al., 2010). The changes in *Fgfr2* expression are not indicative of direct regulation of *Fgfr2* by *Grhl*2, however both *Fgfr2* and *Grhl*2 have common upstream regulators which may influence the incidence of cleft palate in clinical cases associated with either gene. Esrp1 for example, was identified downstream of *Grhl*2, but upstream of *Fgfr2*, particularly in the context of EMT. Given the importance of maintaining epithelial integrity in tissue fusion events, ectopic expression of both *Grhl*2 and *Fgfr2* in the maxillary prominence could conceivably result in defects at the MES during palatal development. Conversely however, loss of *Fgfr2* was not evident in other structures, including the pharyngeal arches where both *Grhl*2 and *Fgfr2* are expressed. This indicates that the contribution of *fgfr2* to syndromes affecting prominences other than the mxp are unlikely to involve *Grhl*2 regulation. Clearly, any potential link between *Grhl*2 and Fgfr2 in terms of craniofacial development, is restricted to the development of the maxillary prominence and its derivatives.

While abnormal expression of *fgfr2* itself contributes to the incidence of defects, the binding activity of *fgfr2* with respect to its ligands presents an additional mechanism for the development of defects. Many defects, particularly de novo mutations producing syndromic craniofacial abnormalities, are owed to increased binding affinity of *fgfr2* to its' ligands as a result of constitutive activation of *Fgfr2* (Azoury, Reddy, Shukla, & Deng, 2017). *Branchless* represents the homolog of *fgf* in Drosophila and regulates epithelial organisation in the developing tracheal tube via regulation of drosophila Grainyhead (Grh) (Hemphälä, Uv, Cantera, Bray, & Samakovlis, 2003). This relationship appears to be conserved across species, as *Fgf10* and *Grhl*2 are both involved in lung morphogenesis, and *Grhl*2 has been identified as a putative downstream target of Fgf10 (Jones et al., 2019). If *Fgfr2* exists downstream of *Grhl*2, downregulation of *Fgfr2* in *Grhl*2 null embryos may lead to a loss of function of *Fgf* ligands and, given the roles of *Fgf* and *Fgfr2* in EMT, exacerbate EMT dysregulation in the epithelia of tissues such as the MES, which require normal EMT regulation for tissue fusion. Further, *Fgf8* mutations have been shown to result in lower jaw defects and exists upstream of *Edn1* in mice, similarly to the findings outlined in chapter 3. This provides further evidence that both *Fgfr2* as well as its' ligands share phenotypes, pathways, and regulation with *Grhl* family genes.

The lack of change in *Fgfr2* expression in the pharyngeal arches of *Grhl*2$^{-/-}$ mice does not support the established role of *Fgfr2* in the neural crest and neural crest cells. Therefore, if *Fgfr2* loss is responsible for defects in *Grhl*2$^{-/-}$ mice, it should affect the epithelial tissues of the facial prominences and pharyngeal arches, as opposed to the maxillary prominence. It is possible however, that other isoforms of *Fgfr2* are able to compensate if only one form of *Fgfr2* is downregulated by loss of *Grhl*2. *Fgfr2b* is the isoform of *Fgfr2* that is specific to epithelial tissues, and it has been demonstrated that expression of the mesenchymal isoform – *Fgfr2c* – in

epithelial tissues is associated with defects (Nanni, Ranieri, Persechino, Torrisi, & Belleudi, 2019; Ranieri et al., 2016). Additionally, in other organs, *Fgfr2b* can compensate for loss of *Fgfr2c* (Filant, DeMayo, Pru, Lydon, & Spencer, 2014). If the reverse is true, and this occurs in the pharyngeal arches or facial prominences, defects in receptor expression and tissue organisation could still occur when overall *Fgfr2* mRNA expression appears normal. Compensation by the mesenchymal isoform of *Fgfr2* may be particularly relevant to tissue fusion, as loss of *Fgfr2b* and higher expression of *Fgfr2c* are associated with a shift towards EMT, and could potentially contribute to the disorganized epithelial *Grhl*2 phenotypes detailed in chapter 5 (Ranieri et al., 2016). The intricacies of *Fgfr2* expression require further investigation to characterize the relationship, if any, between *Grhl*2 and *Fgfr2* in craniofacial disease.

In addition to *Fgfr2*, *Ovol1* was also differentially regulated in *Grhl*2$^{-/-}$ embryos, specifically in the FNP, MXP and PA1 where it was downregulated. Given the functional similarities between *Grhl*2 and *Ovol1* in terms of EMT regulation and epidermal differentiation, the loss of *Ovol1* in *Grhl*2 tissues has the potential to contribute to many of the defects evident in *Grhl*2 mice. Loss of *Ovol1* can contribute to the epithelial disorganisation and mesenchymal cell traits that are generally attributed to loss of *Grhl*2 in the epithelium of the developing MXP. Additionally, while *Ovol2*, not *Ovol1*, is generally responsible for neural tube fusion, Teng *et al* (2007) provided evidence that *Ovol2* is a functional target for *Ovol1*, at least in the epidermis. If *Ovol1* is able to target *Ovol2* expression in the neural tube or surrounding tissues, its' absence could contribute to dysregulation and neural tube defects additionally. Evidently, *Ovol1's* function mirrors *Grhl*2 in a number of key areas relevant to craniofacial development.

The structures displaying low Ovol1 expression coincide with the severe morphological and epithelial defects described in chapter 5. Additionally, *Ovol1* and *Grhl*2 also share many downstream target genes, further implicating *Ovol1* in the aforementioned defects. These shared targets could be either the result of their parallel functions in regulating EMT, or alternatively, that they are members of the same pathway. While some of these shared targets are common among EMT regulators – for example E-cadherin and vimentin – some more specific targets suggest a co-operative role between *Grhl*2 and *Ovol1*. In particular, *Zeb1/2* form negative feedback loops with both *Grhl*2 and *Ovol1* (Roca et al., 2013). This has a number of implications, firstly, members of the *fgfr* family typically promote high *ZEB1*/2 expression however *Fgfr2* itself is not necessarily one such member. More importantly though, loss of *Grhl*2 and the consequential loss of *ZEB1*/2 inhibition may lead to higher *Zeb1*/2 levels and in turn, higher *Zeb1*/2 levels would lead to additional downregulation of *Ovol1*. Regardless of its' relationship with *Grhl*2, the loss of *Ovol1* has the potential to contribute to epithelial defects owing to its role and shared target genes in EMT.

Interestingly, *Ovol1* expression in PA1 epithelium was significantly downregulated and yet not all structures derived from PA1 were subsequently affected. The results were largely consistent with RNA-seq experiments conducted by Carpinelli *et al* (2020) who found a 14 fold decrease in Ovol1 expression in PA1 epithelial tissue at E9.5. Thus while these data are consistent with the literature and defects observed in *Grhl*2$^{-/-}$ embryos, it remains unclear why only some facial prominences are affected by loss of *Grhl*2, as well as the significance of *Ovol1* in the occurrence of these defects.

While *Shh* and *Gli2* were downregulated in the fnp, other members of the *Shh* pathway were not, and this did not occur in any other tissues analysed. The downregulation of Shh in *Grhl*2$^{-/-}$ fnp tissue is unusual given that only one of its' downstream intracellular targets is also downregulated, and its expression in other tissues is not significantly abrogated. Non-canonical Shh pathways have been identified in the context of other pathologies such as cancer. For example, the activation of *Gli* proteins without activation of human SMO or PTC1 was reported via ERK pathway genes, however this pathway did not result in Shh activation and would be expected to influence *Gli1* and *Gli3* if active in mice (Riobo, Haines, & Emerson, 2006). Beyond its role in the Shh pathway, *Gli2* is known to contribute to epidermal hyperplasia when constitutively activated, a similar function to that of *Grhl* genes. Additionally, *Gli2* has been identified as an EMT inducing gene, through co-operative interactions with *Zeb1* in repressing E-cadherin and is also a putative downstream target of *Irf6*, and by extension *Grhl*3 (Dai, Yu, Si, Fang, & Shen, 2015). Despite these similarities, it is unclear if *Shh* or *Gli2* are causative agents in the craniofacial evident in *Grhl*2$^{-/-}$ embryos.

These data provide the basis for future research into the nature of *Grhl*2 regulation of these target genes, as well as differential regulation of these in other affected organs in *Grhl*2$^{-/-}$ mice. Further research in this area would benefit from additional qPCR experiments utilising greater sample sizes to provide greater validity for the data gathered, and the use of ChIP assays would reveal if *Ovol1*, *Fgfr2* or *Gli2* are directly regulated by *Grhl*2, or whether their ectopic expression in these embryos is the result of an indirect pathway. While a number of Shh pathway genes were analysed in this study, some important members of the pathway were omitted due to covid-based time and primer availability constraints, including *Smo* and *Ptc1* which ideally would also have been included in this analysis if possible. Given the relationship between the epithelial and mesenchymal isoforms of *Fgfr2* in defects, investigation of the expression patterns of these receptors in defective tissue via Immunohistochemistry/immunofluorescence may yield another potential mechanism behind *Grhl*2$^{-/-}$ epithelial defects. Lastly, using techniques such as primordial palate explant cultures would allow for the circumvention of embryonic lethality, and subsequently allow for the application of target gene mRNA which could be used to test for

rescue of palatal fusion defects by increasing levels of *Ovol1* and *Gli2*. Overall, these data provide novel putative target genes for further research into *Grhl2*$^{-/-}$ induced defects.

Chapter 5: The role of *Noggin* in *Grhl*2 defects

5.1 Introduction

5.1.1 Noggin

Investigations into the effects of *Grhl*2 regulation on the mRNA transcription of various candidate genes revealed substantial downregulation of the BMP antagonist *Noggin* (Michael de Vries, 2020). This is significant as *BMP* genes are a major gene family with a multitude of functions and which have previously been implicated in tissue fusion failure in various instances (McMahon et al., 1998).

Noggin is an evolutionarily conserved antagonist of the BMP family that plays key roles in head and craniofacial development (Stottmann, Berrong, Matta, Choi, & Klingensmith, 2006). Unlike *Grhl* genes, Noggin is not a transcription factor, rather, it is secreted into the extracellular space where it binds and inactivates specific members of the BMP family, namely BMP 2, 4, 5, and 7. Noggin affinity for each BMP subtype varies, with the highest affinity interaction occurring with BMP-4 (Glaser et al., 2003). Noggin is produced as a 26 kda monomer, however it is modified post translation into a disulphide linked homodimer of approximately 68 kDa prior to secretion (Costamagna, Mommaerts, Sampaolesi, & Tylzanowski, 2016; Tang et al., 2009). BMP proteins bind to a receptor on the cell membrane, namely BMP-receptor II (BMPR2) which in turn phosphorylates BMP-receptor I (Sieber, Kopf, Hiepen, & Knaus, 2009). From there, intracellular signals are mediated by the SMAD pathway. Noggin binds tightly to the BMP ligand, preventing its' activation of the BMP receptors and thus preventing intracellular signalling.

5.1.2 Noggin expression in palate, mesenchymal/EMT

Given its wide ranging influence on craniofacial development, *noggin* is expressed in an array of embryological structures and tissues including the maxilla, Meckel's cartilage and tongue. In the palate it is expressed initially across the entirety of the palatal epithelium at E11.5, but at E12.5 expression in the anterior palatal shelf at the nasal and medial edge epithelium ceases (F. He et al., 2010). By E13.5, *noggin* expression is limited to the oral aspect of the palatal shelves. Noggin is a soluble morphogen which sets concentrations gradients in tissues that surround it, and so can occur at varying concentrations across a given tissue (Smith, 1999).

The development of the palate, like many other tissues, requires the appropriate expression of *BMP* genes in order to avoid defects. It is therefore little surprise that ectopic expression of a BMP antagonist such as Noggin has also been documented to produce defects. He (*et al*) amongst other studies, reported cleft palate defects in Noggin$^{-/-}$ embryos accompanied with the

expected increases in BMP activity in the epithelium. The increase in BMP activity and related cleft palate phenotype observed in mouse models is coherent with preliminary data (Michael de Vries, 2020) which observed defects in Noggin-/- mutants, however the cleft was far more severe, encompassing the entirety of the maxillary prominence (Michael de Vries, 2020). Additionally, it was shown that that over-expression of Noggin also led to palatal defects. The mechanism through which BMP deficiency leads to cleft palate, has more recently been attributed to osteogenesis. Complicating matters however, is that in models which knockout *Msx*, a downstream mediator of BMP function, cleft palate phenotypes also occur (Alappat, Zhang, & Chen, 2003). This is contrary to other studies which have suggested that it is over-expression of BMP which is responsible for cleft palate (Bonilla-Claudio et al., 2012). The BMP-deficient cleft palate phenotype may be due to a separate role for BMP in cellular proliferation, rather than in tissue fusion. An alternative mechanism for Noggin-BMP contribution to cleft palate is a defect in epithelial and mesenchymal cell identity. *BMP* genes have been implicated in instances of physiological MET, as well as EMT in cancer (Huang et al., 2017). In cases of renal damage, BMP has been shown to arrest and reverse the effects of other Tgf-β proteins which drive EMT (Zeisberg et al., 2003). This would, however, be at odds with existing data in the palatal epithelium which demonstrates mesenchymal traits when Noggin is not present and, presumably, BMP activity is higher (F. He et al., 2010). Nonetheless, it is clear that any change in Noggin and consequently BMP activity could have significant implications for the organisation of the epithelium in the developing face and neural tube.

5.1.3 Noggin Expression in Neural tube

Noggin and BMP function are similarly critical to neural tube development. Noggin is expressed in the notochord as well as the dorsal midline of the neural tube following mouse neural tube fusion at E9 (McMahon et al., 1998). Loss-of-function Noggin mutants display open neural tubes, body axis defects and limb defects, which ultimately lead to embryonic lethality. Despite the localized expression of Noggin around the dorsal NT midline, severe NT fusion defects in Noggin$^{-/-}$ embryos, and decreases in cell proliferation in these areas, downstream genes including BMP 6 and 7, and Msx genes are unaffected. Ectopic expression of BMP 4 in the notochord and ventral midline in caudal regions of the embryo was observed (McMahon et al., 1998; Sela-Donenfeld & Kalcheim, 1999), which is consistent with Noggins' antagonism of BMP, given that Noggin is able to inhibit BMP4 more effectively than other members of the BMP family. Signals from the notochord, in particular *Shh* and *Noggin*, are known to influence structures local to the dorsal neural tube after fusion, notably the roof plate and the migration of NCC (Nguyen et al., 2000; Selleck, Garcia-Castro, Artinger, & Bronner-Fraser, 1998). Considering the contribution of NCC to

craniofacial development, a lack of *noggin* secretion in the NT or notochord may also affect the development of the external face via improper patterning of NCC function.

Recent unpublished data indicate novel details regarding the function of *Grhl*2/Noggin interaction in neural tube and palatal fusion (Michael de Vries, 2020). Firstly, *Grhl*2$^{+/-}$ ex vivo MXP cultures as well as immunohistochemistry have identified disruption in epithelium in the absence of *Grhl*2, as the normally discrete epithelium takes on more mesenchymal cell types. It has been proposed that increases in *Noggin* expression are responsible for the shift towards mesenchymal cell identities in the palatal epithelium. Additionally, preliminary data suggests that Noggin produces an atypical concentration gradient in wild type MXP tissue. In the NT, isolated cases of neural tube fusion amongst *Grhl*2$^{-/-}$ Nog$^{-/+}$ suggest that normalising Nogging protein expression can partially rescue the effects of *Grhl*2 deficiency.

This chapter investigates whether the genetic relationship between *Grhl*2 and *Noggin* extends to protein expression. The effects of *Grhl*2 inhibition of *noggin* on craniofacial and neural tube defects will be examined, as well as the specific pattern of Noggin secretion in the palate and its contribution to palatal fusion. Lastly, the potential for *Grhl*2 defect rescue by Noggin expression normalisation will be determined.

5.2 Results

5.2.1 *Noggin* and β-*actin* expression were not detected by western blot

Mice were genotyped for *Grhl*2 and *Noggin* alleles separately prior to western blotting and immunohistochemistry.

In order for accurate comparison of 1st pharyngeal arch samples across different samples on the subsequent western blot experiments, total protein needed to be estimated. To achieve this, a biotin chromatin assay (BCA) was preferred as the RIPA buffer in which each sample was suspended can react with other protein estimation reagents (for example, Bradford reagent).

Western blotting was utilised to detect *noggin* expression in *Grhl*2$^{-/-}$ mouse 1st pharyngeal arch samples. 1st pharyngeal arches of *Grhl*2$^{-/-}$ and *Grhl*2$^{+/+}$ mice were run in triplicate and probed for both *noggin* and beta-actin. No bands presented for either *noggin* or beta-actin.

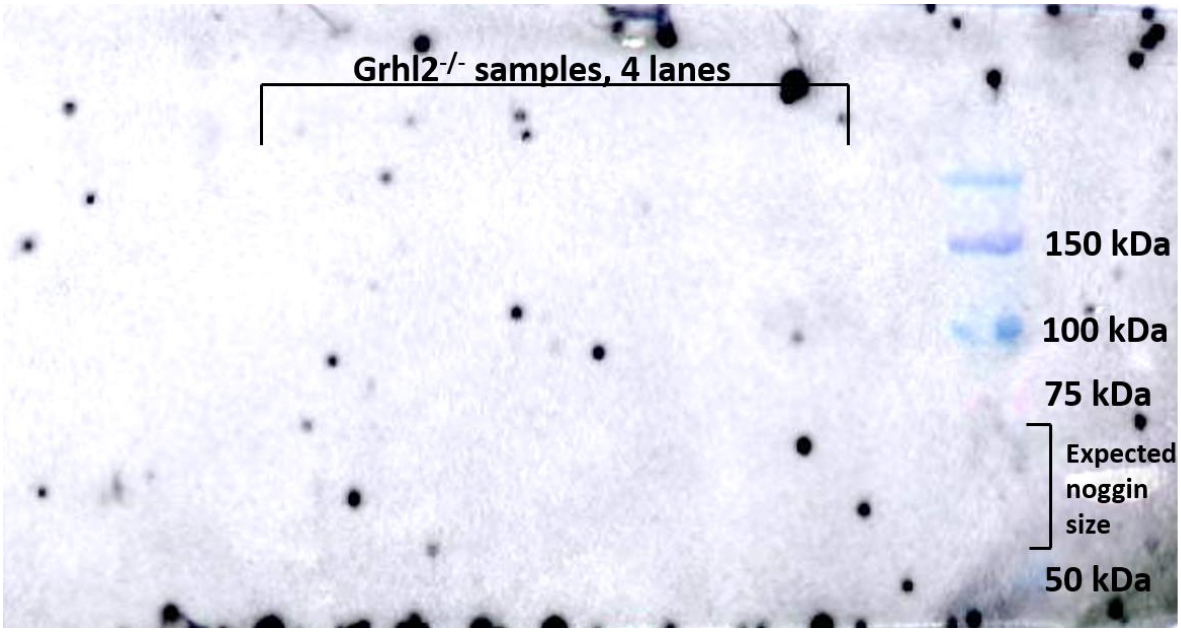

Figure 5.1: Western Blot using an anti-*noggin* antibody. Anti-Noggin and anti-**β**-Actin antibodies were used in order to detect *noggin* and β-actin protein expression in *Grhl*2$^{-/-}$ 1st pharyngeal arch samples. Neither *noggin* nor the β-actin control band was detected.

It was thus necessary to validate the western blotting technique and control antibodies so as to ensure that the above detection issues were not a consequence of ineffective antibodies or defective reagents. HeLa cells were used as the use of the primary anti-β-actin antibody and anti-goat secondary antibodies on these cells had been well validated previously. 1mg/ml samples of total protein yielded strong bands in each of the four wells to which they were added (fig. 5.2). Detection of these bands occurred within 5 seconds using the same western detection reagents used on previous western runs.

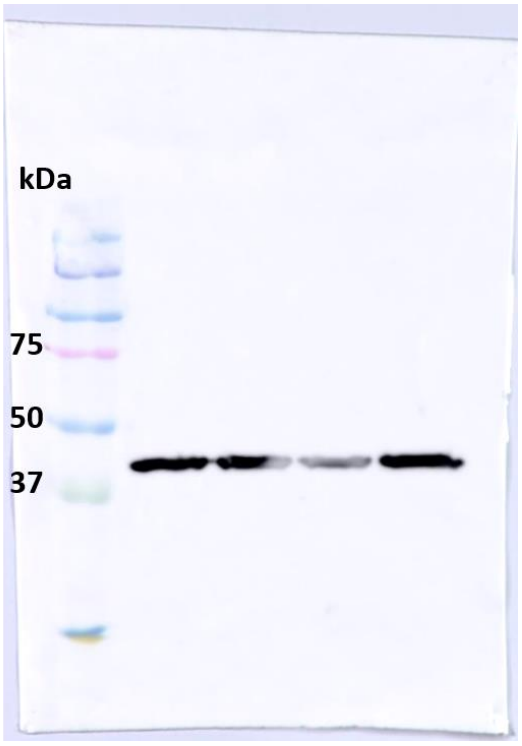

Figure 5.2: Beta-actin control antibody validation. Anti-**β**-actin primary and anti-rabbit secondary antibodies were validated using HeLa cells. In all four lanes **β**-actin was detected at approximately its' expected size. Exposure time: 5s

To address the possibility that insufficient total protein was responsible for lack of beta actin and *noggin* detection, pieces of the upper and lower jaws of E14 mice were probed for expression of *noggin* and beta-actin. Feint bands were detected consistent with the expected size of beta-actin, however no bands were present indicating *noggin* expression (fig. 5.3).

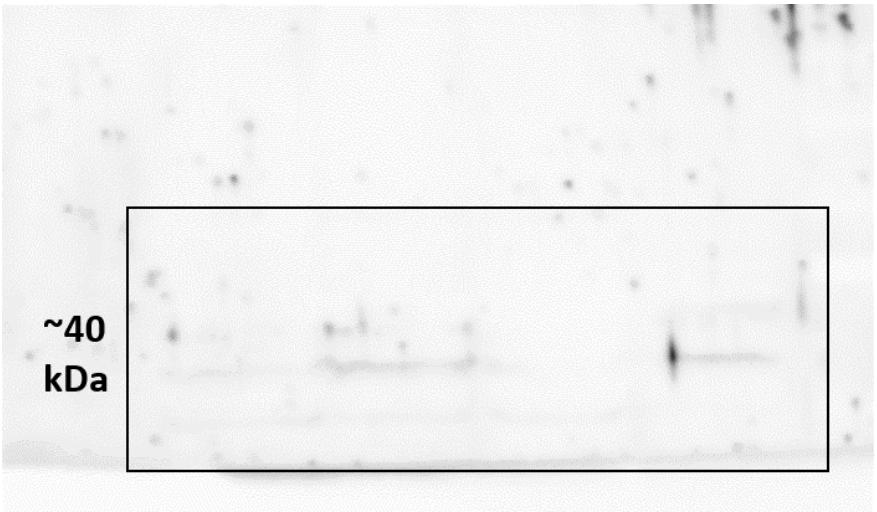

Figure 5.3: Faint beta actin detection on *Grhl2*$^{-/-}$ E14.5 nose samples. Faint bands were detected at approximately 40kDa, the expected size of beta actin bands in 3 out of 4 lanes.

5.2.2 Immunohistochemistry using *noggin* antibodies produces high background

Sections of *Grhl2*$^{-/-}$ and *Grhl2*$^{+/+}$ E9.5 embryos were obtained from the Australian centre for blood disease in lieu of the La trobe-housed *Grhl2* line embryos which were not available due to import delays. Application of a *noggin* antibody (Bioss 2975R) and anti-rabbit secondary antibody yielded non-specific background staining of the NT, mxp and mandibular prominence mdp (figure 5.4).

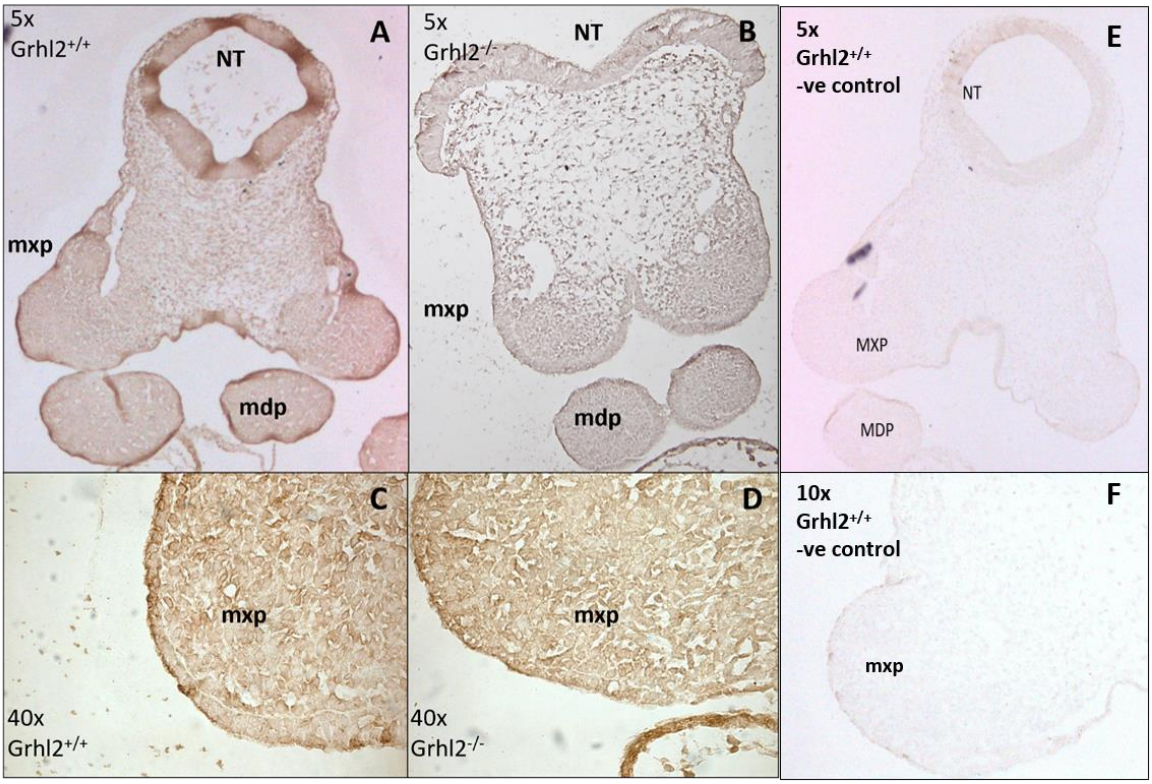

Figure 5.4: Detection of *noggin* using immunohistochemistry produced non-specific staining. E9.5 *Grhl2*$^{-/-}$ and *Grhl2*$^{+/+}$ sections prepared by the Australian centre for blood diseases were obtained and probed with an anti-*noggin* antibody. The resulting staining was not specific to *noggin* expression, as high background was evident in both *Grhl2*$^{-/-}$ and *Grhl2*$^{+/+}$ sections and in all structures. The unfused neural tube (NT) is evident in *Grhl2*$^{-/-}$ embryos. Negative control sections treated without primary antibody display substantially reduced background staining. Mxp) maxillary prominence, mdp) mandibular prominence. A) Grhl2$^{+/+}$ coronal section, 5x magnification; B) Grhl2$^{-/-}$ coronal section, 5x magnification. C) Grhl2$^{+/+}$ coronal section, 40x magnification, D) Grhl2$^{-/-}$ coronal section 40x magnification. E) Grhl2$^{+/+}$ coronal section negative control (no primary antibody) 5x magnification, F) Grhl2$^{+/+}$ coronal section negative control, 10x magnification.

5.3 Discussion

Efforts to detect Noggin expression in 1st pharyngeal arch and maxillary prominence samples were not successful. Due to a number of factors including COVID-19 related delays, ideal samples were not able to be obtained in time for these experiments. As a result, the samples utilised were in most cases, older than would have otherwise been used and consequently the quality and quantity of protein was degraded.

It is unclear whether the inability to detect *noggin* and beta actin in western blot experiments and the unsuccessful staining of *noggin* in IHC are due to poor sample quality or an ineffective antibody. Western blot analysis using HeLa cells validated the control primary and secondary antibodies as being effective in detecting beta actin (fig 5.2), however when tested on recently harvested E14 nose samples (fig 5.3), only feint staining was detected. This suggests that although poor sample quality was a factor in the poor detection of *noggin* in western blot trials, either the primary anti-*noggin* or secondary anti-rabbit antibodies were not effective. Similarly, IHC experiments suffered issues with specific detection of *noggin*, in this instance, through excessive background staining. Negative control samples also displayed background staining (fig 5.4 E,F), however it was significantly reduced in intensity compared to those wherein the primary-anti-*noggin* antibody was applied. This suggests that poor sample quality produced some background, however the non-specific primary antibody amplified the severity of non-specific staining. Therefore, it is evident that in both IHC and western blotting applications, a combination of poor quality sample and an ineffective primary antibody contributed to poor *noggin* detection.

A priority for this project going forward is to optimise the western blot techniques which have been unsuccessful thus far. One approach to rectifying the low protein concentrations hindered the western blot approach is to pool samples of the same genotype. This is not an ideal solution, given that the number of samples at present is limited and pooling samples would require more samples to generate to technical replicates. The use of more sensitive detection reagents would also be useful, especially given that little background signal was detected until unusually long exposure times were used. A combination of greater total protein concentration, shorter storage times following embryo extraction and dissection, and more specific detection reagents and antibodies, are likely to drastically increase the quality of data.

Similarly, improvements in the quality of immunohistochemistry data also rely on better sample quality and more effective reagents. While the high background in IHC experiments supports the notion that the primary antibody used was not effective in binding to *noggin* as demonstrated in western blotting the long-term storage of the sections likely had a significant effect on the

availability of antigens. While tissue samples suspended in paraffin blocks will generally retain their antigens after several years, once sectioned, the slides are vulnerable to degradation from oxidation and temperature (Ramos-Vara, Webster, DuSold, & Miller, 2013). Additionally, membrane receptors were shown to be particularly vulnerable to light and temperature changes, and whilst *noggin* is not a membrane receptor, it is still secreted outside the cell membrane and may be subject to breakdown from these factors. An alternate approach to gaining higher quality samples is to utilise cryosectioning in place of paraffin embedding. Cryosectioning often allows for greater preservation of antigens, particularly membrane receptors (Fischer, Jacobson, Rose, & Zeller, 2008). However smaller proteins are capable of being damaged by certain common cryosectioning fixatives such as acetone or ethanol (van der Loos, 2007). Furthermore, cryosectioning generally does not preserve tissue morphology as effectively as paraffin processing, and consequently may result in difficulties when examining E9.5 embryos, given that they already produce small and fragile sections. Nevertheless, given the issues that were evident following paraffin embedding, cryosectioning is still a viable alternative.

5.3.2 Future Directions

Beyond the optimisation of IHC and western blotting to determine changes in *noggin* protein expression in *Grhl2*$^{-/-}$ mice, future directions include the investigation of downstream targets, the effects of *noggin* normalisation on *Grhl2*$^{-/-}$ defects and the use of palatal explant cultures.

Translating the gene network established through IHC and western blot experiments into a model for cleft palate in *Grhl2*$^{-/-}$ mice requires that *noggin*'s downstream effectors be well characterized and their own functions in the palate investigated. Understanding the specific cellular role of these downstream proteins, including BMP's and phosphor-smad, in the fusion event (or lack thereof) in palatal development is critical. To address this, the additional western blotting and IHC experiments to analyse phospho-smad expression is critical. It is also necessary to establish the mechanism through which *Grhl2*, expressed in the epithelium, is able to affect the fusion of mesenchymal tissues in palatal fusion. Further, it would also be useful to explore potential changes in apical projections which could impact the fusion of leading edge tissues in the development of the palate.

Many of these aspects regarding palatal fusion are difficult to achieve in *Grhl2*$^{-/-}$embryos, given their embryonic lethality prior to the event. However the development of explant cultures using palatal tissue, can recreate the formation of the palate whilst circumventing embryonic lethality (Aoyama et al., 2019). In addition to embryonic lethality, such tissue culture techniques also allow for parts of the surrounding maxillary tissue to remain, an important aspect given the influence of signals from the environment around the given tissue (Dixon, Marazita, Beaty, & Murray, 2011). Recent advances in free floating maxillary prominence explant cultures allow for

the presumptive palatal shelves to grow out from the maxillary tissue, as the tissue being cultured is not fixed to any supporting apparatus which could restrict growth (Michael de Vries, 2020). Based on this, it is clear that tissue culture studies have much to offer in terms of studying morphological events pertaining to tissue fusion.

Overall, whilst the investigation of *noggin*'s role in *Grhl2*$^{-/-}$ defects was not successful, it remains a promising avenue for *Grhl* research. Despite the setbacks imposed during this project, the outline for the study of Noggin expression in *Grhl2*$^{-/-}$ remains sound for future investigation.

Concluding remarks

Given the relatively common incidence of craniofacial defects, as well as the difficulty of corrective surgeries, identifying the genetic causes that contribute to these conditions is of paramount importance (Hsieh et al., 2010; Parker et al., 2010). This thesis details the steps that are necessary to identify genes that could potentially be implicated in craniofacial defects. This includes investigating their effects in animal models and characterising the mechanisms through which they govern craniofacial development.

Chapter 3 explores *grhl3* function in zebrafish as well as putative target genes *pvrl4* and *tmem54* in craniofacial development. *grhl3* inhibition was found to produce defects which mirror, to some extent, defects observed in *Grhl* orthologues in mice. Additionally, WISH techniques allowed for the identification of perturbed PA1 development to be identified as the likely cause of grhl3 defects. The same approach was used to examine the role of *pvrl4* and *tmem54a*, which yielded different phenotypes in the craniofacial region and identified rhombomere defects as the likely cause. These findings validated the zebrafish as a model for identifying influential genes in craniofacial development and lay the groundwork for future study of these genes in mammalian models.

Chapter 4 highlights one approach to identifying differentially regulated genes that may act downstream of Grhl2 in craniofacial development. Using quantitative RT-PCR, the tissue-specific requirements of various genes were demonstrated, as genes differentially regulated in one facial prominence were often not affected in other tissues. Additionally, genes of significant importance to craniofacial development, including members of the *Shh* pathway, *Fgfr2* and *Ovol1,* were identified as differentially regulated in some tissues when *Grhl2* expression was lost. In this way, the data generated in chapter 4 provide genes for further investigation in animal models, using methods demonstrated in chapter 3 and 5.

Whilst unsuccessful in generating data pertaining to the role of *Noggin* in *Grhl2*$^{-/-}$ embryos, chapter 5 demonstrates the approach that may be taken toward characterising morphological defects in mouse models. The use of IHC and western blotting on PA samples, can be improved through the use of higher quality samples to produce the desired results. In addition, these techniques form the basis for the use of tissue cultures which can provide clear evidence of the effect of Grhl2 and Noggin expression on primordial palate tissue fusion. These methods represent the process through which identified target genes can be effectively characterised in a mammalian model.

Overall, the process for identifying Grhl target genes and characterising their role in craniofacial development are described in this thesis, and additionally, novel downstream genes of Grhl

transcription factors were identified and their functions characterised. Thus, these data provide the basis for further research and contribute to the understanding of the genetic basis of craniofacial defects.

References

Abu-Issa, R., Smyth, G., Smoak, I., Yamamura, K.-i., & Meyers, E. N. (2002). Fgf is required for pharyngeal arch and cardiovascular development in the mouse. *Development, 129*(19), 4613. Retrieved from http://dev.biologists.org/content/129/19/4613.abstract

Ahmed, I., & Afzal, A. (2009). Diagnosis and evaluation of Crouzon syndrome. *J Coll Physicians Surg Pak, 19*(5), 318-320.

Alappat, S., Zhang, Z. Y., & Chen, Y. P. (2003). Msx homeobox gene family and craniofacial development. *Cell Research, 13*(6), 429-442. doi:10.1038/sj.cr.7290185

Angelo, S., Lohr, J., Lee, K. H., Ticho, B. S., Breitbart, R. E., Hill, S., . . . Srivastava, D. (2000). Conservation of sequence and expression of Xenopus and zebrafish dHAND during cardiac, branchial arch and lateral mesoderm development. *Mech Dev, 95*(1-2), 231-237. doi:10.1016/s0925-4773(00)00334-8

Aoyama, G., Kurosaka, H., Oka, A., Nakatsugawa, K., Yamamoto, S., Sarper, S. E., . . . Yamashiro, T. (2019). Observation of Dynamic Cellular Migration of the Medial Edge Epithelium of the Palatal Shelf in vitro. *Frontiers in Physiology, 10*(698). doi:10.3389/fphys.2019.00698

Arth, A. C., Tinker, S. C., Simeone, R. M., Ailes, E. C., Cragan, J. D., & Grosse, S. D. (2017). Inpatient Hospitalization Costs Associated with Birth Defects Among Persons of All Ages - United States, 2013. *MMWR Morb Mortal Wkly Rep, 66*(2), 41-46. doi:10.15585/mmwr.mm6602a1

Atta, C. A. M., Fiest, K. M., Frolkis, A. D., Jette, N., Pringsheim, T., St Germaine-Smith, C., . . . Metcalfe, A. (2015). Global Birth Prevalence of Spina Bifida by Folic Acid Fortification Status: A Systematic Review and Meta-Analysis. *American Journal of Public Health, 106*(1), e24-e34. doi:10.2105/AJPH.2015.302902

Auden, A., Caddy, J., Wilanowski, T., Ting, S. B., Cunningham, J. M., & Jane, S. M. (2006a). Spatial and temporal expression of the Grainyhead-like transcription factor family during murine development. *Gene Expr Patterns, 6*(8), 964-970. doi:10.1016/j.modgep.2006.03.011

Auden, A., Caddy, J., Wilanowski, T., Ting, S. B., Cunningham, J. M., & Jane, S. M. (2006b). Spatial and temporal expression of the Grainyhead-like transcription factor family during murine development. *Gene Expression Patterns, 6*(8), 964-970. doi:https://doi.org/10.1016/j.modgep.2006.03.011

Aue, A., Hinze, C., Walentin, K., Ruffert, J., Yurtdas, Y., Werth, M., . . . Schmidt-Ott, K. M. (2015). A Grainyhead-Like 2/Ovo-Like 2 Pathway Regulates Renal Epithelial Barrier Function and Lumen Expansion. *Journal of the American Society of Nephrology, 26*(11), 2704. doi:10.1681/ASN.2014080759

Azevedo, C. d. M. S., Machado, R. A., Martelli-Júnior, H., Reis, S. R. d. A., Persuhn, D. C., Coletta, R. D., & Rangel, A. L. C. A. (2020). Exploring GRHL3 polymorphisms and SNP-SNP interactions in the risk of non-syndromic oral clefts in the Brazilian population. *Oral Diseases, 26*(1), 145-151. doi:https://doi.org/10.1111/odi.13204

Azoury, S. C., Reddy, S., Shukla, V., & Deng, C.-X. (2017). Fibroblast Growth Factor Receptor 2 (FGFR2) Mutation Related Syndromic Craniosynostosis. *International journal of biological sciences, 13*(12), 1479-1488. doi:10.7150/ijbs.22373

Basch, M. L., Bronner-Fraser, M., & García-Castro, M. I. (2006). Specification of the neural crest occurs during gastrulation and requires Pax7. *Nature, 441*(7090), 218-222. doi:10.1038/nature04684

Basnet, S., Gauchan, E., Shrestha, J., & Jha, J. (2021). Patterns of Clinically Identifiable Congenital Defects in Neonates. *J Nepal Health Res Counc, 19*(1), 62-65. doi:10.33314/jnhrc.v19i1.3125

Bender, P. L. (2000). Genetics of cleft lip and palate. *Journal of Pediatric Nursing, 15*(4), 242-249. doi:https://doi.org/10.1053/jpdn.2000.8148

Bessenyei, B., Nagy, A., Szakszon, K., Mokánszki, A., Balogh, E., Ujfalusi, A., . . . Oláh, É. (2015). Clinical and genetic characteristics of craniosynostosis in Hungary. *167*(12), 2985-2991. doi:10.1002/ajmg.a.37298

Betancur, P., Bronner-Fraser, M., & Sauka-Spengler, T. (2010). Genomic code for Sox10 activation reveals a key regulatory enhancer for cranial neural crest. *Proceedings of the National Academy of Sciences, 107*(8), 3570. doi:10.1073/pnas.0906596107

Bonilla-Claudio, M., Wang, J., Bai, Y., Klysik, E., Selever, J., & Martin, J. F. (2012). Bmp signaling regulates a dose-dependent transcriptional program to control facial skeletal development. *Development, 139*(4), 709-719. doi:10.1242/dev.073197

Botto, L. D. (2015). *Epidemiology and Prevention of Congenital Heart Defects*: Karger.

Bowling, E. L., & Burstein, F. D. (2006). Crouzon syndrome. *Optometry - Journal of the American Optometric Association, 77*(5), 217-222. doi:https://doi.org/10.1016/j.optm.2006.03.005

Boyadjiev, S. A. (2007). Genetic analysis of non-syndromic craniosynostosis. *Orthodontics & Craniofacial Research, 10*(3), 129-137. doi:https://doi.org/10.1111/j.1601-6343.2007.00393.x

Brancati, F., Fortugno, P., Bottillo, I., Lopez, M., Josselin, E., Boudghene-Stambouli, O., . . . Dallapiccola, B. (2010). Mutations in PVRL4, Encoding Cell Adhesion Molecule Nectin-4, Cause Ectodermal Dysplasia-Syndactyly Syndrome. *The American Journal of Human Genetics, 87*(2), 265-273. doi:https://doi.org/10.1016/j.ajhg.2010.07.003

Britton, D. J., Scott, G. K., Schilling, B., Atsriku, C., Held, J. M., Gibson, B. W., . . . Baldwin, M. A. (2008). A novel serine phosphorylation site detected in the n-terminal domain of estrogen receptor isolated from human breast cancer cells. *Journal of the American Society for Mass Spectrometry, 19*(5), 729-740. doi:10.1016/j.jasms.2008.02.008

Brouns, M. R., De Castro, S. C. P., Terwindt-Rouwenhorst, E. A., Massa, V., Hekking, J. W., Hirst, C. S., . . . Greene, N. D. E. (2011). Over-expression of Grhl2 causes spina bifida in the Axial defects mutant mouse. *Human Molecular Genetics, 20*(8), 1536-1546. doi:10.1093/hmg/ddr031

Brunskill, E. W., Potter, A. S., Distasio, A., Dexheimer, P., Plassard, A., Aronow, B. J., & Potter, S. S. (2014). A gene expression atlas of early craniofacial development. *Developmental Biology, 391*(2), 133-146. doi:https://doi.org/10.1016/j.ydbio.2014.04.016

Burg, M. L., Chai, Y., Yao, C. A., Magee, W., & Figueiredo, J. C. (2016). Epidemiology, Etiology, and Treatment of Isolated Cleft Palate. *Frontiers in Physiology, 7*(67). doi:10.3389/fphys.2016.00067

Bush, J. O., & Jiang, R. (2012). Palatogenesis: morphogenetic and molecular mechanisms of secondary palate development. *Development, 139*(2), 231-243. doi:10.1242/dev.067082

Carballo, G. B., Honorato, J. R., de Lopes, G. P. F., & Spohr, T. C. L. d. S. e. (2018). A highlight on Sonic hedgehog pathway. *Cell Communication and Signaling, 16*(1), 11. doi:10.1186/s12964-018-0220-7

Carey, M. F., Peterson, C. L., & Smale, S. T. (2009). Chromatin immunoprecipitation (ChIP). *Cold Spring Harb Protoc, 2009*(9), pdb.prot5279. doi:10.1101/pdb.prot5279

Carpinelli, M. R., de Vries, M., Auden, A., Butt, T., Deng, Z., Partridge, D. D., . . . Jane, S. M. (2020). Inactivation of Zeb1 in GRHL2-deficient mouse embryos rescues mid-gestation viability and secondary palate closure. *Disease Models & Mechanisms, 13*(3). doi:10.1242/dmm.042218

Carpinelli, M. R., de Vries, M., Jane, S. M., & Dworkin, S. (2017). Grainyhead-like Transcription Factors in Craniofacial Development. *Journal of Dental Research, 96*(11), 1200-1209. doi:10.1177/0022034517719264

Chen, W., Xiao Liu, Z., Oh, J. E., Shin, K. H., Kim, R. H., Jiang, M., . . . Kang, M. K. (2012). Grainyhead-like 2 (GRHL2) inhibits keratinocyte differentiation through epigenetic mechanism. *Cell Death & Disease, 3*(12), e450-e450. doi:10.1038/cddis.2012.190

Cheung, M., Chaboissier, M.-C., Mynett, A., Hirst, E., Schedl, A., & Briscoe, J. (2005). The Transcriptional Control of Trunk Neural Crest Induction, Survival, and Delamination. *Developmental Cell, 8*(2), 179-192. doi:https://doi.org/10.1016/j.devcel.2004.12.010

Choe, S.-K., Zhang, X., Hirsch, N., Straubhaar, J., & Sagerström, C. G. (2011). A screen for hoxb1-regulated genes identifies ppp1r14al as a regulator of the rhombomere 4 Fgf-signaling center. *Developmental Biology, 358*(2), 356-367. doi:https://doi.org/10.1016/j.ydbio.2011.05.676

Christensen, K., Juel, K., Herskind, A. M., & Murray, J. C. (2004). Long term follow up study of survival associated with cleft lip and palate at birth. *BMJ, 328*(7453), 1405. doi:10.1136/bmj.38106.559120.7C

Chung, V. Y., Tan, T. Z., Ye, J., Huang, R.-L., Lai, H.-C., Kappei, D., . . . Huang, R. Y.-J. (2019). The role of GRHL2 and epigenetic remodeling in epithelial–mesenchymal plasticity in ovarian cancer cells. *Communications Biology, 2*(1), 272. doi:10.1038/s42003-019-0506-3

Ciruna, B., Jenny, A., Lee, D., Mlodzik, M., & Schier, A. F. (2006). Planar cell polarity signalling couples cell division and morphogenesis during neurulation. *Nature, 439*(7073), 220-224. doi:10.1038/nature04375

Clouthier, D. E., Hosoda, K., Richardson, J. A., Williams, S. C., Yanagisawa, H., Kuwaki, T., . . . Yanagisawa, M. (1998). Cranial and cardiac neural crest defects in endothelin-A receptor-deficient mice. *Development, 125*(5), 813. Retrieved from http://dev.biologists.org/content/125/5/813.abstract

Cohen, S. P., LaChappelle, A. R., Walker, B. S., & Lassiter, C. S. (2014). Modulation of estrogen causes disruption of craniofacial chondrogenesis in Danio rerio. *Aquatic Toxicology, 152*, 113-120. doi:https://doi.org/10.1016/j.aquatox.2014.03.028

Colas, J.-F., & Schoenwolf, G. C. (2001). Towards a cellular and molecular understanding of neurulation. *Developmental Dynamics, 221*(2), 117-145. doi:https://doi.org/10.1002/dvdy.1144

Copp, A. J., & Greene, N. D. E. (2010). Genetics and development of neural tube defects. *The Journal of Pathology, 220*(2), 217-230. doi:https://doi.org/10.1002/path.2643

Copp, A. J., Greene, N. D. E., & Murdoch, J. N. (2003). The genetic basis of mammalian neurulation. *Nature Reviews Genetics, 4*(10), 784-793. doi:10.1038/nrg1181

Cordero, D. R., Brugmann, S., Chu, Y., Bajpai, R., Jame, M., & Helms, J. A. (2011). Cranial neural crest cells on the move: Their roles in craniofacial development. *American Journal of Medical Genetics Part A, 155*(2), 270-279. doi:https://doi.org/10.1002/ajmg.a.33702

Costamagna, D., Mommaerts, H., Sampaolesi, M., & Tylzanowski, P. (2016). Noggin inactivation affects the number and differentiation potential of muscle progenitor cells in vivo. *Scientific Reports, 6*, 31949-31949. doi:10.1038/srep31949

Cubitt, J. J., Hodges, A. M., Van Lierde, K. M., & Swan, M. C. (2014). Global Variation in Cleft Palate Repairs: An Analysis of 352,191 Primary Cleft Repairs in Low- to Higher-Middle-Income Countries. *The Cleft Palate-Craniofacial Journal, 51*(5), 553-556. doi:10.1597/12-270

Dai, J., Yu, H., Si, J., Fang, B., & Shen, S. G. (2015). Irf6-Related Gene Regulatory Network Involved in Palate and Lip Development. *Journal of Craniofacial Surgery, 26*(5). Retrieved from https://journals.lww.com/jcraniofacialsurgery/Fulltext/2015/07000/Irf6_Related_Gene_Regulatory_Network_Involved_in.35.aspx

Darido, C., Georgy, Smitha R., Wilanowski, T., Dworkin, S., Auden, A., Zhao, Q., . . . Jane, Stephen M. (2011). Targeting of the Tumor Suppressor GRHL3 by a miR-21-Dependent Proto-Oncogenic Network Results in PTEN Loss and Tumorigenesis. *Cancer Cell, 20*(5), 635-648. doi:https://doi.org/10.1016/j.ccr.2011.10.014

De Castro, S. C. P., Leung, K.-y., Savery, D., Burren, K., Rozen, R., Copp, A. J., & Greene, N. D. E. (2010). Neural tube defects induced by folate deficiency in mutant curly tail (Grhl3) embryos are associated with alteration in folate one-carbon metabolism but are unlikely to result from diminished methylation. *Birth Defects Research Part A: Clinical and Molecular Teratology, 88*(8), 612-618. doi:https://doi.org/10.1002/bdra.20690

de la Garza, G., Schleiffarth, J. R., Dunnwald, M., Mankad, A., Weirather, J. L., Bonde, G., . . . Cornell, R. A. (2013). Interferon Regulatory Factor 6 Promotes Differentiation of the Periderm by Activating Expression of Grainyhead-Like 3. *Journal of Investigative Dermatology, 133*(1), 68-77. doi:https://doi.org/10.1038/jid.2012.269

de Vries, M. (2020). The Role of Grainyhead-like 2 (Grhl2) Transcription Factor in Embryonic Development. *Monash University*. doi:https://doi.org/10.26180/5e60376864784

de Vries, M., Owens, H. G., Carpinelli, M. R., Partridge, D., Kersbergen, A., Sutherland, K. D., . . . Dworkin, S. (2021). Delineating the roles of Grhl2 in craniofacial development through tissue-specific conditional deletion and epistasis approaches in mouse. *Developmental Dynamics, 250*(8), 1191-1209. doi:https://doi.org/10.1002/dvdy.322

de Wilde, J. A., van Buuren, S., & Middelkoop, B. J. C. (2013). Trends in birth weight and the prevalence of low birth weight and small-for-gestational-age in Surinamese South Asian babies since 1974: cross-sectional study of three birth cohorts. *BMC Public Health, 13*(1), 931. doi:10.1186/1471-2458-13-931

Deng, C., Bedford, M., Li, C., Xu, X., Yang, X., Dunmore, J., & Leder, P. (1997). Fibroblast Growth Factor Receptor-1 (FGFR-1) Is Essential for Normal Neural Tube and Limb Development. *Developmental Biology, 185*(1), 42-54. doi:https://doi.org/10.1006/dbio.1997.8553

Díaz-Martín, R. D., Carvajal-Peraza, A., Yáñez-Rivera, B., & Betancourt-Lozano, M. (2021). Short exposure to glyphosate induces locomotor, craniofacial, and bone disorders in zebrafish (Danio rerio) embryos. *Environ Toxicol Pharmacol, 87*, 103700. doi:10.1016/j.etap.2021.103700

Dixon, M. J., Marazita, M. L., Beaty, T. H., & Murray, J. C. (2011). Cleft lip and palate: understanding genetic and environmental influences. *Nat Rev Genet, 12*(3), 167-178. doi:10.1038/nrg2933

Dudas, M., Li, W.-Y., Kim, J., Yang, A., & Kaartinen, V. (2007). Palatal fusion – Where do the midline cells go?: A review on cleft palate, a major human birth defect. *Acta Histochemica, 109*(1), 1-14. doi:https://doi.org/10.1016/j.acthis.2006.05.009

Dunkel, H., Chaverra, M., Bradley, R., & Lefcort, F. (2020). FGF signaling is required for chemokinesis and ventral migration of trunk neural crest cells. *Developmental Dynamics, 249*(9), 1077-1097. doi:https://doi.org/10.1002/dvdy.190

Duverger, O., Isaac, J., Zah, A., Hwang, J., Berdal, A., Lian, J. B., & Morasso, M. I. (2013). In vivo impact of Dlx3 conditional inactivation in neural crest-derived craniofacial bones. *Journal of Cellular Physiology, 228*(3), 654-664. doi:10.1002/jcp.24175

Dworkin, S., Auden, A., Partridge, D. D., Daglas, M., Medcalf, R. L., Mantamadiotis, T., . . . Ting, S. B. (2017). Grainyhead-like 3 (Grhl3) deficiency in brain leads to altered locomotor activity and decreased anxiety-like behaviors in aged mice. *Dev Neurobiol, 77*(6), 775-788. doi:10.1002/dneu.22469

Dworkin, S., Darido, C., Georgy, S. R., Wilanowski, T., Srivastava, S., Ellett, F., . . . Jane, S. M. (2012). Midbrain-hindbrain boundary patterning and morphogenesis are regulated by diverse grainy head-like 2-dependent pathways. *Development, 139*(3), 525-536. doi:10.1242/dev.066522

Dworkin, S., Heath, J. K., deJong-Curtain, T. A., Hogan, B. M., Lieschke, G. J., Malaterre, J., . . . Mantamadiotis, T. (2007). CREB activity modulates neural cell proliferation, midbrain–hindbrain organization and patterning in zebrafish. *Developmental Biology, 307*(1), 127-141. doi:https://doi.org/10.1016/j.ydbio.2007.04.026

Dworkin, S., Simkin, J., Darido, C., Partridge, D. D., Georgy, S. R., Caddy, J., . . . Jane, S. M. (2014). Grainyhead-like 3 regulation of endothelin-1 in the pharyngeal endoderm is critical for growth and development of the craniofacial skeleton. *Mechanisms of Development, 133*, 77-90. doi:https://doi.org/10.1016/j.mod.2014.05.005

Eshete, M. A., Liu, H., Li, M., Adeyemo, W. L., Gowans, L. J. J., Mossey, P. A., . . . Butali, A. (2017). Loss-of-Function GRHL3 Variants Detected in African Patients with Isolated Cleft Palate. *Journal of Dental Research, 97*(1), 41-48. doi:10.1177/0022034517729819

Eshete, M. A., Liu, H., Li, M., Adeyemo, W. L., Gowans, L. J. J., Mossey, P. A., . . . Butali, A. (2018). Loss-of-Function GRHL3 Variants Detected in African Patients with Isolated Cleft Palate. *J Dent Res, 97*(1), 41-48. doi:10.1177/0022034517729819

Eswarakumar, V. P., Ozcan, F., Lew, E. D., Bae, J. H., Tomé, F., Booth, C. J., . . . Schlessinger, J. (2006). Attenuation of signaling pathways stimulated by pathologically activated FGF-

receptor 2 mutants prevents craniosynostosis. *Proc Natl Acad Sci U S A, 103*(49), 18603-18608. doi:10.1073/pnas.0609157103

Farlie, P. G., Kerr, R., Thomas, P., Symes, T., Minichiello, J., Hearn, C. J., & Newgreen, D. (1999). A Paraxial Exclusion Zone Creates Patterned Cranial Neural Crest Cell Outgrowth Adjacent to Rhombomeres 3 and 5. *Developmental Biology, 213*(1), 70-84. doi:https://doi.org/10.1006/dbio.1999.9332

Feldkamp, M. L., Carey, J. C., Byrne, J. L. B., Krikov, S., & Botto, L. D. (2017). Etiology and clinical presentation of birth defects: population based study. *BMJ, 357*, j2249. doi:10.1136/bmj.j2249

Ferrero, G. B., Baldassarre, G., Panza, E., Valenzise, M., Pippucci, T., Mussa, A., . . . Silengo, M. C. (2009). A heritable cause of cleft lip and palate—Van der Woude syndrome caused by a novel IRF6 mutation. Review of the literature and of the differential diagnosis. *European Journal of Pediatrics, 169*(2), 223. doi:10.1007/s00431-009-1011-3

Filant, J., DeMayo, F. J., Pru, J. K., Lydon, J. P., & Spencer, T. E. (2014). Fibroblast Growth Factor Receptor Two (FGFR2) Regulates Uterine Epithelial Integrity and Fertility in Mice. *Biology of Reproduction, 90*(1). doi:10.1095/biolreprod.113.114496

Fischer, A. H., Jacobson, K. A., Rose, J., & Zeller, R. (2008). Cryosectioning tissues. *CSH Protoc, 2008*, pdb.prot4991. doi:10.1101/pdb.prot4991

Ghassibe-Sabbagh, M., Desmyter, L., Langenberg, T., Claes, F., Boute, O., Bayet, B., . . . Vikkula, M. (2011). FAF1, a gene that is disrupted in cleft palate and has conserved function in zebrafish. *Am J Hum Genet, 88*(2), 150-161. doi:10.1016/j.ajhg.2011.01.003

Glasauer, S. M., & Neuhauss, S. C. (2014). Whole-genome duplication in teleost fishes and its evolutionary consequences. *Mol Genet Genomics, 289*(6), 1045-1060. doi:10.1007/s00438-014-0889-2

Glaser, D. L., Economides, A. N., Wang, L., Liu, X., Kimble, R. D., Fandl, J. P., . . . Shore, E. M. (2003). In Vivo Somatic Cell Gene Transfer of an Engineered Noggin Mutein Prevents BMP4-Induced Heterotopic Ossification. *JBJS, 85*(12). Retrieved from https://journals.lww.com/jbjsjournal/Fulltext/2003/12000/In_Vivo_Somatic_Cell_Gene_Transfer_of_an.10.aspx

Goldie, S. J., Arhatari, B. D., Anderson, P., Auden, A., Partridge, D. D., Jane, S. M., & Dworkin, S. (2016). Mice lacking the conserved transcription factor Grainyhead-like 3 (Grhl3) display increased apposition of the frontal and parietal bones during embryonic development. *BMC Developmental Biology, 16*(1), 37. doi:10.1186/s12861-016-0136-7

Graham, A., & Richardson, J. (2012). Developmental and evolutionary origins of the pharyngeal apparatus. *EvoDevo, 3*, 24. doi:10.1186/2041-9139-3-24

Greene, N. D. E., & Copp, A. J. (2014). Neural Tube Defects. *Annual Review of Neuroscience, 37*(1), 221-242. doi:10.1146/annurev-neuro-062012-170354

Greene, N. D. E., Stanier, P., & Copp, A. J. (2009). Genetics of human neural tube defects. *Human Molecular Genetics, 18*(R2), R113-R129. doi:10.1093/hmg/ddp347

Hall, J. G., & Solehdin, F. (1998). Genetics of neural tube defects. *4*(4), 269-281. doi:10.1002/(sici)1098-2779(1998)4:4<269::Aid-mrdd6>3.0.Co;2-8

Han, Y., Mu, Y., Li, X., Xu, P., Tong, J., Liu, Z., . . . Meng, A. (2011). Grhl2 deficiency impairs otic development and hearing ability in a zebrafish model of the progressive dominant hearing loss DFNA28. *Human Molecular Genetics, 20*(16), 3213-3226. doi:10.1093/hmg/ddr234

Hannah, P., Emily, C., Jessica, G., Shandra, J., Emily, P., & Julia Thom, O. (2014). Genetic and molecular aspects of DiGeorge syndrome. *BIOS, 86*(2), 109-117. doi:10.1893/0005-3155-86.2.109

Harding, A., & Grunwell, P. (1996). Characteristics of cleft palate speech. *International Journal of Language & Communication Disorders, 31*(4), 331-357. doi:https://doi.org/10.3109/13682829609031326

He, F., Xiong, W., Wang, Y., Matsui, M., Yu, X., Chai, Y., . . . Chen, Y. (2010). Modulation of BMP signaling by Noggin is required for the maintenance of palatal epithelial integrity during palatogenesis. *Developmental Biology, 347*(1), 109-121. doi:10.1016/j.ydbio.2010.08.014

He, J., Feng, C., Zhu, H., Wu, S., Jin, P., & Xu, T. (2020). Grainyhead-like 2 as a double-edged sword in development and cancer. *American journal of translational research, 12*(2), 310-331. Retrieved from https://pubmed.ncbi.nlm.nih.gov/32194886

https://www.ncbi.nlm.nih.gov/pmc/articles/PMC7061838/

Heliövaara, A., Karhulahti, R., & Rautio, J. (2015). Craniofacial morphology in children with van der Woude syndrome and isolated cleft palate. *Journal of Plastic Surgery and Hand Surgery, 49*(4), 209-213. doi:10.3109/2000656X.2014.992904

Hemphälä, J., Uv, A., Cantera, R., Bray, S., & Samakovlis, C. (2003). Grainy head controls apical membrane growth and tube elongation in response to Branchless/FGF signalling. *Development, 130*(2), 249-258. doi:10.1242/dev.00218

Hernández-Díaz, S., Werler, M. M., Walker, A. M., & Mitchell, A. A. (2000). Folic Acid Antagonists during Pregnancy and the Risk of Birth Defects. *New England Journal of Medicine, 343*(22), 1608-1614. doi:10.1056/NEJM200011303432204

Hislop, N. R., Caddy, J., Ting, S. B., Auden, A., Vasudevan, S., King, S. L., . . . Jane, S. M. (2008). Grhl3 and Lmo4 play coordinate roles in epidermal migration. *Developmental Biology, 321*(1), 263-272. doi:https://doi.org/10.1016/j.ydbio.2008.06.026

Honein, M. A., Paulozzi, L. J., Mathews, T. J., Erickson, J. D., & Wong, L.-Y. C. (2001). Impact of Folic Acid Fortification of the US Food Supply on the Occurrence of Neural Tube Defects. *JAMA, 285*(23), 2981-2986. doi:10.1001/jama.285.23.2981

Hsieh, C., Ko, E., Chen, P., & Huang, C.-S. (2010). The Effect of Gingivoperiosteoplasty on Facial Growth in Patients With Complete Unilateral Cleft Lip and Palate. *The Cleft palate-craniofacial journal : official publication of the American Cleft Palate-Craniofacial Association, 47*, 439-446. doi:10.1597/08-207

Hu, F., He, Z., Sun, C., & Rong, D. (2019). Knockdown of GRHL2 inhibited proliferation and induced apoptosis of colorectal cancer by suppressing the PI3K/Akt pathway. *Gene, 700*, 96-104. doi:https://doi.org/10.1016/j.gene.2019.03.051

Huang, P., Chen, A., He, W., Li, Z., Zhang, G., Liu, Z., . . . Wang, J. (2017). BMP-2 induces EMT and breast cancer stemness through Rb and CD44. *Cell Death Discovery, 3*(1), 17039. doi:10.1038/cddiscovery.2017.39

Hunt, O., Burden, D., Hepper, P., Stevenson, M., & Johnston, C. (2006). Self-Reports of Psychosocial Functioning among Children and Young Adults with Cleft Lip and Palate. *The Cleft Palate-Craniofacial Journal, 43*(5), 598-605. doi:10.1597/05-080

Isaac, J., Erthal, J., Gordon, J., Duverger, O., Sun, H. W., Lichtler, A. C., . . . Morasso, M. I. (2014). DLX3 regulates bone mass by targeting genes supporting osteoblast differentiation and mineral homeostasis in vivo. *Cell Death & Differentiation, 21*(9), 1365-1376. doi:10.1038/cdd.2014.82

Jackson, O., Basta, M., Sonnad, S., Stricker, P., Larossa, D., & Fiadjoe, J. (2013). Perioperative risk factors for adverse airway events in patients undergoing cleft palate repair. *Cleft Palate Craniofac J, 50*(3), 330-336. doi:10.1597/12-134

Jaffe, E., & Niswander, L. (2021). Loss of Grhl3 is correlated with altered cellular protrusions in the non-neural ectoderm during neural tube closure. *Developmental Dynamics, 250*(5), 732-744. doi:https://doi.org/10.1002/dvdy.292

Jeong, J., Cesario, J., Zhao, Y., Burns, L., Westphal, H., & Rubenstein, J. L. R. (2012). Cleft palate defect of Dlx1/2−/− mutant mice is caused by lack of vertical outgrowth in the posterior palate. *Developmental Dynamics, 241*(11), 1757-1769. doi:https://doi.org/10.1002/dvdy.23867

Jin, Y.-R., Han, X. H., Taketo, M. M., & Yoon, J. K. (2012). Wnt9b-dependent FGF signaling is crucial for outgrowth of the nasal and maxillary processes during upper jaw and lip development. *Development, 139*(10), 1821-1830. doi:10.1242/dev.075796

Johnson, C. W., Hernandez-Lagunas, L., Feng, W., Melvin, V. S., Williams, T., & Artinger, K. B. (2011). Vgll2a is required for neural crest cell survival during zebrafish craniofacial development. *Developmental Biology, 357*(1), 269-281. doi:https://doi.org/10.1016/j.ydbio.2011.06.034

Jones, M. R., Dilai, S., Lingampally, A., Chao, C.-M., Danopoulos, S., Carraro, G., . . . Bellusci, S. (2019). A Comprehensive Analysis of Fibroblast Growth Factor Receptor 2b Signaling on Epithelial Tip Progenitor Cells During Early Mouse Lung Branching Morphogenesis. *Frontiers in Genetics, 9*(746). doi:10.3389/fgene.2018.00746

Jung, J., Choi, I., Ro, H., Huh, T. L., Choe, J., & Rhee, M. (2020). march5 Governs the Convergence and Extension Movement for Organization of the Telencephalon and Diencephalon in Zebrafish Embryos. *Mol Cells, 43*(1), 76-85. doi:10.14348/molcells.2019.0210

Juriloff, D. M., & Harris, M. J. (2018). Insights into the Etiology of Mammalian Neural Tube Closure Defects from Developmental, Genetic and Evolutionary Studies. *Journal of Developmental Biology, 6*(3). doi:10.3390/jdb6030022

Kawakatsu, T., Shimizu, K., Honda, T., Fukuhara, T., Hoshino, T., & Takai, Y. (2002). Trans-interactions of nectins induce formation of filopodia and Lamellipodia through the respective activation of Cdc42 and Rac small G proteins. *J Biol Chem, 277*(52), 50749-50755. doi:10.1074/jbc.M209846200

Ketwaroo, P. D., Robson, C. D., & Estroff, J. A. (2015). Prenatal Imaging of Craniosynostosis Syndromes. *Seminars in Ultrasound, CT and MRI, 36*(6), 453-464. doi:https://doi.org/10.1053/j.sult.2015.06.002

Kikulska, A., Rausch, T., Krzywinska, E., Pawlak, M., Wilczynski, B., Benes, V., . . . Wilanowski, T. (2018). Coordinated expression and genetic polymorphisms in Grainyhead-like genes in human non-melanoma skin cancers. *BMC Cancer, 18*. doi:10.1186/s12885-017-3943-8

Kim, Y.-R., Kim, M.-A., Sagong, B., Bae, S.-H., Lee, H.-J., Kim, H.-J., . . . Kim, U.-K. (2015). Evaluation of the contribution of the EYA4 and GRHL2 genes in Korean patients with autosomal dominant non-syndromic hearing loss. *PLoS One, 10*(3), e0119443-e0119443. doi:10.1371/journal.pone.0119443

Kimmel, C. B., Warga, R. M., & Kane, D. A. (1994). Cell cycles and clonal strings during formation of the zebrafish central nervous system. *Development, 120*(2), 265-276.

Kirby, R. S. (2017). The prevalence of selected major birth defects in the United States. *Seminars in Perinatology, 41*(6), 338-344. doi:https://doi.org/10.1053/j.semperi.2017.07.004

Knobloch, J., & Rüther, U. (2008). Shedding light on an old mystery: Thalidomide suppresses survival pathways to induce limb defects. *Cell Cycle, 7*(9), 1121-1127. doi:10.4161/cc.7.9.5793

Knopik, V. S., Maccani, M. A., Francazio, S., & McGeary, J. E. (2012). The epigenetics of maternal cigarette smoking during pregnancy and effects on child development. *Development and psychopathology, 24*(4), 1377-1390. doi:10.1017/S0954579412000776

Kok, F. O., Shin, M., Ni, C. W., Gupta, A., Grosse, A. S., van Impel, A., . . . Lawson, N. D. (2015). Reverse genetic screening reveals poor correlation between morpholino-induced and mutant phenotypes in zebrafish. *Dev Cell, 32*(1), 97-108. doi:10.1016/j.devcel.2014.11.018

Kousa, Y. A., Zhu, H., Fakhouri, W. D., Lei, Y., Kinoshita, A., Roushangar, R. R., . . . Schutte, B. C. (2019). The TFAP2A–IRF6–GRHL3 genetic pathway is conserved in neurulation. *Human Molecular Genetics, 28*(10), 1726-1737. doi:10.1093/hmg/ddz010

Kuo, B., & Erickson, C. (2010). Regional differences in neural crest morphogenesis. *Cell adhesion & migration, 4*, 567-585. doi:10.4161/cam.4.4.12890

Kurihara, Y., Kurihara, H., Suzuki, H., Kodama, T., Maemura, K., Nagai, R., . . . Yazaki, Y. (1994). Elevated blood pressure and craniofaclal abnormalities in mice deficient in endothelin-1. *Nature, 368*(6473), 703-710. doi:10.1038/368703a0

Kurjak, A., Azumendi, G., Andonotopo, W., & Salihagic-Kadic, A. (2007). Three- and four-dimensional ultrasonography for the structural and functional evaluation of the fetal face. *American Journal of Obstetrics and Gynecology, 196*(1), 16-28. doi:https://doi.org/10.1016/j.ajog.2006.06.090

Kwak, J., Park, O. K., Jung, Y. J., Hwang, B. J., Kwon, S.-H., & Kee, Y. (2013). Live image profiling of neural crest lineages in zebrafish transgenic lines. *Molecules and Cells, 35*(3), 255-260. doi:10.1007/s10059-013-0001-5

Lambert, P. R., & Dodson, E. E. (1996). Congenital malformations of the external auditory canal. *Otolaryngologic clinics of North America, 29*(5), 741-760. Retrieved from http://europepmc.org/abstract/MED/8893214

Lapsiwala, S. B., & Iskandar, B. J. (2004). The tethered cord syndrome in adults with spina bifida occulta. *Neurological Research, 26*(7), 735-740. doi:10.1179/016164104225017956

Larbuisson, A., Dalcq, J., Martial, J. A., & Muller, M. (2013). Fgf receptors Fgfr1a and Fgfr2 control the function of pharyngeal endoderm in late cranial cartilage development. *Differentiation, 86*(4), 192-206. doi:https://doi.org/10.1016/j.diff.2013.07.006

Lassi, Z. S., Kedzior, S. G. E., Tariq, W., Jadoon, Y., Das, J. K., & Bhutta, Z. A. (2020). Effects of Preconception Care and Periconception Interventions on Maternal Nutritional Status and Birth Outcomes in Low- and Middle-Income Countries: A Systematic Review. *Nutrients, 12*(3). doi:10.3390/nu12030606

Légaré, S., & Basik, M. (2016). Minireview: The Link Between ERα Corepressors and Histone Deacetylases in Tamoxifen Resistance in Breast Cancer. *Molecular endocrinology (Baltimore, Md.), 30*(9), 965-976. doi:10.1210/me.2016-1072

Lemay, P., De Marco, P., Emond, A., Spiegelman, D., Dionne-Laporte, A., Laurent, S., . . . Kibar, Z. (2017). Rare deleterious variants in GRHL3 are associated with human spina bifida. *Hum Mutat, 38*(6), 716-724. doi:https://doi.org/10.1002/humu.23214

Leslie, Elizabeth J., Liu, H., Carlson, Jenna C., Shaffer, John R., Feingold, E., Wehby, G., . . . Marazita, Mary L. (2016). A Genome-wide Association Study of Nonsyndromic Cleft Palate Identifies an Etiologic Missense Variant in GRHL3. *The American Journal of Human Genetics, 98*(4), 744-754. doi:https://doi.org/10.1016/j.ajhg.2016.02.014

Leslie, E. J., & Marazita, M. L. (2013). Genetics of cleft lip and cleft palate. *American journal of medical genetics. Part C, Seminars in medical genetics, 163C*(4), 246-258. doi:10.1002/ajmg.c.31381

Leslie, E. J., Standley, J., Compton, J., Bale, S., Schutte, B. C., & Murray, J. C. (2013). Comparative analysis of IRF6 variants in families with Van der Woude syndrome and popliteal pterygium syndrome using public whole-exome databases. *Genetics in Medicine, 15*(5), 338-344. doi:10.1038/gim.2012.141

Litingtung, Y., & Chiang, C. (2000). Control of Shh activity and signaling in the neural tube. *Developmental Dynamics, 219*(2), 143-154. doi:https://doi.org/10.1002/1097-0177(2000)9999:9999<::AID-DVDY1050>3.0.CO;2-Q

Liu, J. A. J., Wu, M.-H., Yan, C. H., Chau, B. K. H., So, H., Ng, A., . . . Cheung, M. (2013). Phosphorylation of Sox9 is required for neural crest delamination and is regulated downstream of BMP and canonical Wnt signaling. *Proceedings of the National Academy of Sciences, 110*(8), 2882. doi:10.1073/pnas.1211747110

Lough, K. J., Spitzer, D. C., Bergman, A. J., Wu, J. J., Byrd, K. M., & Williams, S. E. (2020). Disruption of the nectin-afadin complex recapitulates features of the human cleft lip/palate syndrome CLPED1. *Development, 147*(21). doi:10.1242/dev.189241

Luo, Z., Zhang, L., Li, Z., Li, X., Li, G., Yu, H., . . . Li, G. (2012). An in silicoanalysis of dynamic changes in microRNA expression profiles in stepwise development of nasopharyngeal carcinoma. *BMC Medical Genomics, 5*(1), 3. doi:10.1186/1755-8794-5-3

Mackay, D. R., Hu, M., Li, B., Rhéaume, C., & Dai, X. (2006). The mouse Ovol2 gene is required for cranial neural tube development. *Developmental Biology, 291*(1), 38-52. doi:https://doi.org/10.1016/j.ydbio.2005.12.003

Malik, S., Cleves, M. A., Honein, M. A., Romitti, P. A., Botto, L. D., Yang, S., & Hobbs, C. A. (2008). Maternal Smoking and Congenital Heart Defects. *Pediatrics, 121*(4), e810. doi:10.1542/peds.2007-1519

Mangold, E., Böhmer, Anne C., Ishorst, N., Hoebel, A.-K., Gültepe, P., Schuenke, H., . . . Ludwig, Kerstin U. (2016). Sequencing the GRHL3 Coding Region Reveals Rare Truncating Mutations and a Common Susceptibility Variant for Nonsyndromic Cleft Palate. *The American Journal of Human Genetics, 98*(4), 755-762. doi:https://doi.org/10.1016/j.ajhg.2016.02.013

Mathiyalagan, N., Miles, L. B., Anderson, P. J., Wilanowski, T., Grills, B. L., McDonald, S. J., . . . Dworkin, S. (2019). Meta-Analysis of Grainyhead-Like Dependent Transcriptional Networks: A Roadmap for Identifying Novel Conserved Genetic Pathways. *Genes, 10*(11), 876. doi:10.3390/genes10110876

McDonald-McGinn, D. M., & Sullivan, K. E. (2011). Chromosome 22q11.2 Deletion Syndrome (DiGeorge Syndrome/Velocardiofacial Syndrome). *Medicine, 90*(1). Retrieved from https://journals.lww.com/md-journal/Fulltext/2011/01000/Chromosome_22q11_2_Deletion_Syndrome__DiGeorge.1.aspx

McGreevy, E. M., Vijayraghavan, D., Davidson, L. A., & Hildebrand, J. D. (2015). Shroom3 functions downstream of planar cell polarity to regulate myosin II distribution and cellular organization during neural tube closure. *Biology Open, 4*(2), 186-196. doi:10.1242/bio.20149589

McMahon, J. A., Takada, S., Zimmerman, L. B., Fan, C. M., Harland, R. M., & McMahon, A. P. (1998). Noggin-mediated antagonism of BMP signaling is required for growth and patterning of the neural tube and somite. *Genes Dev, 12*(10), 1438-1452. doi:10.1101/gad.12.10.1438

Mehrazarin, S., Chen, W., Oh, J. E., Liu, Z. X., Kang, K. L., Yi, J. K., . . . Kang, M. K. (2015). The p63 Gene Is Regulated by Grainyhead-like 2 (GRHL2) through Reciprocal Feedback and Determines the Epithelial Phenotype in Human Keratinocytes. *J Biol Chem, 290*(32), 19999-20008. doi:10.1074/jbc.M115.659144

Miles, L. B., Darido, C., Kaslin, J., Heath, J. K., Jane, S. M., & Dworkin, S. (2017). Mis-expression of grainyhead-like transcription factors in zebrafish leads to defects in enveloping layer (EVL) integrity, cellular morphogenesis and axial extension. *Scientific Reports, 7*(1), 17607. doi:10.1038/s41598-017-17898-7

Miles, L. B., Dworkin, S., & Darido, C. (2017). Alternative splicing and start sites: Lessons from the Grainyhead-like family. *Developmental Biology, 429*(1), 12-19. doi:https://doi.org/10.1016/j.ydbio.2017.06.018

Miller, C. T., Schilling, T. F., Lee, K., Parker, J., & Kimmel, C. B. (2000). sucker encodes a zebrafish Endothelin-1 required for ventral pharyngeal arch development. *Development, 127*(17), 3815-3828. doi:10.1242/dev.127.17.3815

Miller, C. T., Yelon, D., Stainier, D. Y. R., & Kimmel, C. B. (2003). Two endothelin effectors, hand2 and bapx1, pattern ventral pharyngeal cartilage and the jaw joint. *Development, 130*(7), 1353. doi:10.1242/dev.00339

Minoux, M., & Rijli, F. M. (2010). Molecular mechanisms of cranial neural crest cell migration and patterning in craniofacial development. *137*(16), 2605-2621. doi:10.1242/dev.040048 %J Development

Mlacki, M., Darido, C., Jane, S. M., & Wilanowski, T. (2014). Loss of Grainy head-like 1 is associated with disruption of the epidermal barrier and squamous cell carcinoma of the skin. *PLoS One, 9*(2), e89247. doi:10.1371/journal.pone.0089247

Mollo, M. R., Antonini, D., Mitchell, K., Fortugno, P., Costanzo, A., Dixon, J., . . . Missero, C. (2015). p63-dependent and independent mechanisms of nectin-1 and nectin-4 regulation in the epidermis. *Experimental Dermatology, 24*(2), 114-119. doi:https://doi.org/10.1111/exd.12593

Mongera, A., Singh, A. P., Levesque, M. P., Chen, Y. Y., Konstantinidis, P., & Nüsslein-Volhard, C. (2013). Genetic lineage labeling in zebrafish uncovers novel neural crest contributions to the head, including gill pillar cells. *Development, 140*(4), 916-925. doi:10.1242/dev.091066

Mork, L., & Crump, G. (2015). Chapter Ten - Zebrafish Craniofacial Development: A Window into Early Patterning. In Y. Chai (Ed.), *Current Topics in Developmental Biology* (Vol. 115, pp. 235-269): Academic Press.

Moussian, B., & Uv, A. E. (2005). An ancient control of epithelial barrier formation and wound healing. *BioEssays, 27*(10), 987-990. doi:https://doi.org/10.1002/bies.20308

Mukherjee, A., Hollern, D. P., Williams, O. G., Rayburn, T. S., Byrd, W. A., Yates, C., & Jones, J. D. (2018). A Review of FOXI3 Regulation of Development and Possible Roles in Cancer Progression and Metastasis. *Frontiers in Cell and Developmental Biology, 6*(69). doi:10.3389/fcell.2018.00069

Mulligan, M. L., Felton, S. K., Riek, A. E., & Bernal-Mizrachi, C. (2010). Implications of vitamin D deficiency in pregnancy and lactation. *American Journal of Obstetrics and Gynecology, 202*(5), 429.e421-429.e429. doi:https://doi.org/10.1016/j.ajog.2009.09.002

Nakajima, A., F. Shuler, C., Gulka, A. O. D., & Hanai, J.-i. (2018). TGF-β Signaling and the Epithelial-Mesenchymal Transition during Palatal Fusion. *International Journal of Molecular Sciences, 19*(11). doi:10.3390/ijms19113638

Nanni, M., Ranieri, D., Persechino, F., Torrisi, M. R., & Belleudi, F. (2019). The Aberrant Expression of the Mesenchymal Variant of FGFR2 in the Epithelial Context Inhibits Autophagy. *Cells, 8*(7). doi:10.3390/cells8070653

Nasevicius, A., & Ekker, S. C. (2000). Effective targeted gene 'knockdown' in zebrafish. *Nature Genetics, 26*(2), 216-220. doi:10.1038/79951

Nawshad, A. (2008). Palatal seam disintegration: To die or not to die? that is no longer the question. *Developmental Dynamics, 237*(10), 2643-2656. doi:https://doi.org/10.1002/dvdy.21599

Nguyen, V. H., Trout, J., Connors, S. A., Andermann, P., Weinberg, E., & Mullins, M. C. (2000). Dorsal and intermediate neuronal cell types of the spinal cord are established by a BMP signaling pathway. *Development, 127*(6), 1209-1220.

Nie, X., Luukko, K., & Kettunen, P. (2006). BMP signalling in craniofacial development. *Int J Dev Biol, 50*(6), 511-521. doi:10.1387/ijdb.052101xn

Nishino, H., Takano, S., Yoshitomi, H., Suzuki, K., Kagawa, S., Shimazaki, R., . . . Ohtsuka, M. (2017). Grainyhead-like 2 (GRHL2) regulates epithelial plasticity in pancreatic cancer progression. *Cancer medicine, 6*(11), 2686-2696. doi:10.1002/cam4.1212

Nissen, R. M., Amsterdam, A., & Hopkins, N. (2006). A zebrafish screen for craniofacial mutants identifies wdr68 as a highly conserved gene required for endothelin-1 expression. *BMC Developmental Biology, 6*(1), 28. doi:10.1186/1471-213X-6-28

Northrup, H., & Volcik, K. A. (2000). Spina bifida and other neural tube defects. *Current Problems in Pediatrics, 30*(10), 317-332. doi:https://doi.org/10.1067/mpp.2000.112052

Oberoi, S., & Vargervik, K. (2005). Hypoplasia and Hypodontia in Van der Woude Syndrome. *The Cleft Palate-Craniofacial Journal, 42*(5), 459-466. doi:10.1597/04-028.1

Oster, M. E., Lee, K. A., Honein, M. A., Riehle-Colarusso, T., Shin, M., & Correa, A. (2013). Temporal Trends in Survival Among Infants With Critical Congenital Heart Defects. *131*(5), e1502-e1508. doi:10.1542/peds.2012-3435 %J Pediatrics

Parker, S. E., Mai, C. T., Canfield, M. A., Rickard, R., Wang, Y., Meyer, R. E., . . . Network, f. t. N. B. D. P. (2010). Updated national birth prevalence estimates for selected birth defects in the United States, 2004–2006. *88*(12), 1008-1016. doi:10.1002/bdra.20735

Petrof, G., Nanda, A., Howden, J., Takeichi, T., McMillan, James R., Aristodemou, S., . . . McGrath, John A. (2014). Mutations in GRHL2 Result in an Autosomal-Recessive Ectodermal Dysplasia Syndrome. *The American Journal of Human Genetics, 95*(3), 308-314. doi:https://doi.org/10.1016/j.ajhg.2014.08.001

Peyrard-Janvid, M., Leslie, Elizabeth J., Kousa, Youssef A., Smith, Tiffany L., Dunnwald, M., Magnusson, M., . . . Schutte, Brian C. (2014a). Dominant Mutations in GRHL3 Cause Van der Woude Syndrome and Disrupt Oral Periderm Development. *The American Journal of Human Genetics, 94*(1), 23-32. doi:https://doi.org/10.1016/j.ajhg.2013.11.009

Peyrard-Janvid, M., Leslie, E. J., Kousa, Y. A., Smith, T. L., Dunnwald, M., Magnusson, M., . . . Schutte, B. C. (2014b). Dominant mutations in GRHL3 cause Van der Woude Syndrome and disrupt oral periderm development. *American journal of human genetics, 94*(1), 23-32. doi:10.1016/j.ajhg.2013.11.009

Pitkin, R. M. (2007). Folate and neural tube defects. *The American Journal of Clinical Nutrition, 85*(1), 285S-288S. doi:10.1093/ajcn/85.1.285S

Pla, P., Moore, R., Morali, O. G., Grille, S., Martinozzi, S., Delmas, V., & Larue, L. (2001). Cadherins in neural crest cell development and transformation. *Journal of Cellular Physiology, 189*(2), 121-132. doi:10.1002/jcp.10008

Ramos-Vara, J. A., Webster, J. D., DuSold, D., & Miller, M. A. (2013). Immunohistochemical Evaluation of the Effects of Paraffin Section Storage on Biomarker Stability. *Veterinary Pathology, 51*(1), 102-109. doi:10.1177/0300985813476067

Ranieri, D., Rosato, B., Nanni, M., Magenta, A., Belleudi, F., & Torrisi, M. R. (2016). Expression of the FGFR2 mesenchymal splicing variant in epithelial cells drives epithelial-mesenchymal transition. *Oncotarget, 7*(5), 5440-5460. doi:10.18632/oncotarget.6706

Refsum, H. (2001). Folate, vitamin B12 and homocysteine in relation to birth defects and pregnancy outcome. *British Journal of Nutrition, 85*(S2), S109-S113. doi:10.1049/BJN2000302

Richardson, S., Krishna, S., & Khandeparker, R. V. (2018). A comprehensive management protocol to treat cleft maxillary hypoplasia. *Journal of Cranio-Maxillofacial Surgery, 46*(2), 356-361. doi:https://doi.org/10.1016/j.jcms.2017.12.005

Rifat, Y., Parekh, V., Wilanowski, T., Hislop, N. R., Auden, A., Ting, S. B., . . . Jane, S. M. (2010). Regional neural tube closure defined by the Grainy head-like transcription factors. *Developmental Biology, 345*(2), 237-245. doi:https://doi.org/10.1016/j.ydbio.2010.07.017

Riobo, N. A., Haines, G. M., & Emerson, C. P., Jr. (2006). Protein kinase C-delta and mitogen-activated protein/extracellular signal-regulated kinase-1 control GLI activation in hedgehog signaling. *Cancer Res, 66*(2), 839-845. doi:10.1158/0008-5472.Can-05-2539

Rivera-Pérez, J. A., Mallo, M., Gendron-Maguire, M., Gridley, T., & Behringer, R. R. (1995). Goosecoid is not an essential component of the mouse gastrula organizer but is required for craniofacial and rib development. *Development, 121*(9), 3005-3012.

Robinson, A., Escuin, S., Doudney, K., Vekemans, M., Stevenson, R. E., Greene, N. D. E., . . . Stanier, P. (2012). Mutations in the planar cell polarity genes CELSR1 and SCRIB are associated with the severe neural tube defect craniorachischisis. *Hum Mutat, 33*(2), 440-447. doi:https://doi.org/10.1002/humu.21662

Roca, H., Hernandez, J., Weidner, S., McEachin, R. C., Fuller, D., Sud, S., . . . Pienta, K. J. (2013). Transcription factors OVOL1 and OVOL2 induce the mesenchymal to epithelial transition in human cancer. *PLoS One, 8*(10), e76773. doi:10.1371/journal.pone.0076773

Salih, M. A. M., Murshid, W. R., Mohamed, A. G., Ignacio, L. C., de Jesus, J. E., Baabbad, R., & El Bushra, H. M. (2014). Risk factors for neural tube defects in Riyadh City, Saudi Arabia: Case-control study. *Sudanese journal of paediatrics, 14*(2), 49-60. Retrieved from https://pubmed.ncbi.nlm.nih.gov/27493405

https://www.ncbi.nlm.nih.gov/pmc/articles/PMC4949798/

Satishchandran, A., Ambade, A., Rao, S., Hsueh, Y.-C., Iracheta-Vellve, A., Tornai, D., . . . Szabo, G. (2018). MicroRNA 122, Regulated by GRLH2, Protects Livers of Mice and Patients From Ethanol-Induced Liver Disease. *Gastroenterology, 154*(1), 238-252.e237. doi:https://doi.org/10.1053/j.gastro.2017.09.022

Sato, T., Kurihara, Y., Asai, R., Kawamura, Y., Tonami, K., Uchijima, Y., . . . Kurihara, H. (2008). An endothelin-1 switch specifies maxillomandibular identity. *Proceedings of the National Academy of Sciences, 105*(48), 18806. doi:10.1073/pnas.0807345105

Schneider, R. A., & Helms, J. A. (2003). The Cellular and Molecular Origins of Beak Morphology. *299*(5606), 565-568. doi:10.1126/science.1077827 %J Science

Schoen, C., Aschrafi, A., Thonissen, M., Poelmans, G., Von den Hoff, J. W., & Carels, C. E. L. (2017). MicroRNAs in Palatogenesis and Cleft Palate. *Front Physiol, 8*, 165. doi:10.3389/fphys.2017.00165

Sela-Donenfeld, D., & Kalcheim, C. (1999). Regulation of the onset of neural crest migration by coordinated activity of BMP4 and Noggin in the dorsal neural tube. *Development, 126*(21), 4749-4762. doi:10.1242/dev.126.21.4749

Selleck, M. A., Garcia-Castro, M. I., Artinger, K. B., & Bronner-Fraser, M. (1998). Effects of Shh and Noggin on neural crest formation demonstrate that BMP is required in the neural tube but not ectoderm. *Development, 125*(24), 4919-4930. doi:10.1242/dev.125.24.4919

Setó-Salvia, N., & Stanier, P. (2014). Genetics of cleft lip and/or cleft palate: Association with other common anomalies. *European Journal of Medical Genetics, 57*(8), 381-393. doi:https://doi.org/10.1016/j.ejmg.2014.04.003

Shah, N. M., & Anderson, D. J. (1997). Integration of multiple instructive cues by neural crest stem cells reveals cell-intrinsic biases in relative growth factor responsiveness. *94*(21), 11369-11374. doi:10.1073/pnas.94.21.11369 %J Proceedings of the National Academy of Sciences

Shukla, V., Coumoul, X., Wang, R.-H., Kim, H.-S., & Deng, C.-X. (2007). RNA interference and inhibition of MEK-ERK signaling prevent abnormal skeletal phenotypes in a mouse model of craniosynostosis. *Nature Genetics, 39*(9), 1145-1150. doi:10.1038/ng2096

Sieber, C., Kopf, J., Hiepen, C., & Knaus, P. (2009). Recent advances in BMP receptor signaling. *Cytokine & Growth Factor Reviews, 20*(5), 343-355. doi:https://doi.org/10.1016/j.cytogfr.2009.10.007

Siismets, E. M., & Hatch, N. E. (2020). Cranial Neural Crest Cells and Their Role in the Pathogenesis of Craniofacial Anomalies and Coronal Craniosynostosis. *Journal of Developmental Biology, 8*(3). doi:10.3390/jdb8030018

Skromne, I., & Prince, V. E. (2008). Current perspectives in zebrafish reverse genetics: Moving forward. *Developmental Dynamics, 237*(4), 861-882. doi:https://doi.org/10.1002/dvdy.21484

Smith, W. C. (1999). TGFβ inhibitors: new and unexpected requirements in vertebrate development. *Trends in Genetics, 15*(1), 3-5. doi:https://doi.org/10.1016/S0168-9525(98)01641-2

Snyder-Warwick, A. K., Perlyn, C. A., Pan, J., Yu, K., Zhang, L., & Ornitz, D. M. (2010). Analysis of a gain-of-function FGFR2 Crouzon mutation provides evidence of loss of function activity in the etiology of cleft palate. *Proceedings of the National Academy of Sciences of the United States of America, 107*(6), 2515-2520. doi:10.1073/pnas.0913985107

Son, Y., Lee, B., Choi, Y. J., Jeon, S. A., Kim, J. H., Lee, H. K., . . . Cho, J. Y. (2016). Nectin-2 (CD112) Is Expressed on Outgrowth Endothelial Cells and Regulates Cell Proliferation and Angiogenic Function. *PLoS One, 11*(9), e0163301. doi:10.1371/journal.pone.0163301

Steventon, B., Araya, C., Linker, C., Kuriyama, S., & Mayor, R. (2009). Differential requirements of BMP and Wnt signalling during gastrulation and neurulation define two steps in neural crest induction. *Development, 136*(5), 771-779. doi:10.1242/dev.029017

Stottmann, R. W., Berrong, M., Matta, K., Choi, M., & Klingensmith, J. (2006). The BMP antagonist Noggin promotes cranial and spinal neurulation by distinct mechanisms. *Developmental Biology, 295*(2), 647-663. doi:https://doi.org/10.1016/j.ydbio.2006.03.051

Stuhlmiller, T. J., & García-Castro, M. I. (2012). FGF/MAPK signaling is required in the gastrula epiblast for avian neural crest induction. *Development, 139*(2), 289-300. doi:10.1242/dev.070276

Swartz, M. E., Sheehan-Rooney, K., Dixon, M. J., & Eberhart, J. K. (2011). Examination of a palatogenic gene program in zebrafish. *Dev Dyn, 240*(9), 2204-2220. doi:10.1002/dvdy.22713

Talbot, J. C., Johnson, S. L., & Kimmel, C. B. (2010). hand2 and Dlx genes specify dorsal, intermediate and ventral domains within zebrafish pharyngeal arches. *Development, 137*(15), 2507-2517. doi:10.1242/dev.049700

Tang, J., Song, M., Wang, Y., Fan, X., Xu, H., & Bai, Y. (2009). Noggin and BMP4 co-modulate adult hippocampal neurogenesis in the APPswe/PS1ΔE9 transgenic mouse model of Alzheimer's disease. *Biochemical and Biophysical Research Communications, 385*(3), 341-345. doi:https://doi.org/10.1016/j.bbrc.2009.05.067

Ţarcă, E., Roșu, S. T., Cojocaru, E., Trandafir, L., Luca, A. C., Rusu, D., & Ţarcă, V. (2021). Socio-Epidemiological Factors with Negative Impact on Infant Morbidity, Mortality Rates, and the Occurrence of Birth Defects. *Healthcare, 9*(4). doi:10.3390/healthcare9040384

Teddy, J. M., & Kulesa, P. M. (2004). In vivo evidence for short- and long-range cell communication in cranial neural crest cells. *Development, 131*(24), 6141-6151. doi:10.1242/dev.01534

Tehranchi, A., Behnia, H., Nadjmi, N., Yassaee, V. R., Ravesh, Z., & Mina, M. (2017). Multidisciplinary management of a patient with van der Woude syndrome: A case report. *International Journal of Surgery Case Reports, 30*, 142-147. doi:https://doi.org/10.1016/j.ijscr.2016.11.032

Tian, T., Wang, L., Shen, Y., Zhang, B., Finnell, R. H., & Ren, A. (2018). Hypomethylation of GRHL3 gene is associated with the occurrence of neural tube defects. *Epigenomics, 10*(7), 891-901. doi:10.2217/epi-2018-0016

Ting, S. B., Wilanowski, T., Auden, A., Hall, M., Voss, A. K., Thomas, T., . . . Jane, S. M. (2003). Inositol- and folate-resistant neural tube defects in mice lacking the epithelial-specific factor Grhl-3. *Nature Medicine, 9*(12), 1513-1519. doi:10.1038/nm961

Tobin, J. L., Di Franco, M., Eichers, E., May-Simera, H., Garcia, M., Yan, J., . . . Beales, P. L. (2008). Inhibition of neural crest migration underlies craniofacial dysmorphology and Hirschsprung's disease in Bardet-Biedl syndrome. *Proc Natl Acad Sci U S A, 105*(18), 6714-6719. doi:10.1073/pnas.0707057105

Turksen, K., & Troy, T.-C. (2001). Claudin-6: A novel tight junction molecule is developmentally regulated in mouse embryonic epithelium. *Developmental Dynamics, 222*(2), 292-300. doi:https://doi.org/10.1002/dvdy.1174

van der Loos, C. M. (2007). A focus on fixation. *Biotechnic & Histochemistry, 82*(3), 141-154. doi:10.1080/10520290701375302

Van Laer, L., Van Eyken, E., Fransen, E., Huyghe, J. R., Topsakal, V., Hendrickx, J.-J., . . . Van Camp, G. (2007). The grainyhead like 2 gene (GRHL2), alias TFCP2L3, is associated with age-related hearing impairment. *Human Molecular Genetics, 17*(2), 159-169. doi:10.1093/hmg/ddm292

Venkatesan, K., McManus, H. R., Mello, C. C., Smith, T. F., & Hansen, U. (2003). Functional conservation between members of an ancient duplicated transcription factor family, LSF/Grainyhead. *Nucleic acids research, 31*(15), 4304-4316. doi:10.1093/nar/gkg644

Wada, N., Javidan, Y., Nelson, S., Carney, T. J., Kelsh, R. N., & Schilling, T. F. (2005). Hedgehog signaling is required for cranial neural crest morphogenesis and chondrogenesis at the midline in the zebrafish skull. *Development, 132*(17), 3977. doi:10.1242/dev.01943

Wald, N. (1991). Prevention of neural tube defects: results of the Medical Research Council Vitamin Study. MRC Vitamin Study Research Group. *Lancet, 338*(8760), 131-137.

Wang, D., Weng, Y., Guo, S., Qin, W., Ni, J., Yu, L., . . . Ma, J. (2019). microRNA-1 Regulates NCC Migration and Differentiation by Targeting sec63. *International journal of biological sciences, 15*(12), 2538-2547. doi:10.7150/ijbs.35357

Wang, Y., Sun, Y., Huang, Y., Pan, Y., Jia, Z., Ma, L., . . . Shi, B. (2016). Association study between Van der Woude Syndrome causative gene GRHL3 and nonsyndromic cleft lip with or without cleft palate in a Chinese cohort. *Gene, 588*(1), 69-73. doi:https://doi.org/10.1016/j.gene.2016.04.045

Warzecha, C. C., Shen, S., Xing, Y., & Carstens, R. P. (2009). The epithelial splicing factors ESRP1 and ESRP2 positively and negatively regulate diverse types of alternative splicing events. *RNA Biology, 6*(5), 546-562. doi:10.4161/rna.6.5.9606

Webb, J. F. (1963). CANADIAN THALIDOMIDE EXPERIENCE. *Canadian Medical Association journal, 89*(19), 987-992. Retrieved from https://pubmed.ncbi.nlm.nih.gov/14076167

https://www.ncbi.nlm.nih.gov/pmc/articles/PMC1921912/

Weisinger, K., Kayam, G., Missulawin-Drillman, T., & Sela-Donenfeld, D. (2010). Analysis of expression and function of FGF-MAPK signaling components in the hindbrain reveals a

central role for FGF3 in the regulation of Krox20, mediated by Pea3. *Developmental Biology, 344*(2), 881-895. doi:https://doi.org/10.1016/j.ydbio.2010.06.001

Werner, J. M., Negesse, M. Y., Brooks, D. L., Caldwell, A. R., Johnson, J. M., & Brewster, R. M. (2021). Hallmarks of primary neurulation are conserved in the zebrafish forebrain. *Communications Biology, 4*(1), 147. doi:10.1038/s42003-021-01655-8

Xiang, J., Fu, X., Ran, W., & Wang, Z. (2017). Grhl2 reduces invasion and migration through inhibition of TGFβ-induced EMT in gastric cancer. *Oncogenesis, 6*(1), e284-e284. doi:10.1038/oncsis.2016.83

Xu, J., Kochanek, K. D., Murphy, S. L., & Arias, E. (2014). Mortality in the United States, 2012. *NCHS Data Brief*(168), 1-8.

Yagnik, G., Ghuman, A., Kim, S., Stevens, C. G., Kimonis, V., Stoler, J., . . . Boyadjiev, S. A. (2012). ALX4 gain-of-function mutations in nonsyndromic craniosynostosis. *Hum Mutat, 33*(12), 1626-1629. doi:10.1002/humu.22166

Yu, X., An, J., Hua, Y., Li, Z., Yan, N., Fan, W., & Su, C. (2017). MicroRNA-194 regulates keratinocyte proliferation and differentiation by targeting Grainyhead-like 2 in psoriasis. *Pathol Res Pract, 213*(2), 89-97. doi:10.1016/j.prp.2016.11.020

Zeisberg, M., Hanai, J., Sugimoto, H., Mammoto, T., Charytan, D., Strutz, F., & Kalluri, R. (2003). BMP-7 counteracts TGF-beta1-induced epithelial-to-mesenchymal transition and reverses chronic renal injury. *Nat Med, 9*(7), 964-968. doi:10.1038/nm888

Zhao, N., Han, D., Liu, Y., Li, Y., Zeng, L., Wang, Y., & Feng, H. (2016). DLX3 negatively regulates osteoclastic differentiation through microRNA-124. *Experimental Cell Research, 341*(2), 166-176. doi:https://doi.org/10.1016/j.yexcr.2016.01.018

Zhou, C. J., Ji, Y., Reynolds, K., McMahon, M., Garland, M. A., Zhang, S., . . . Iwasa, J. (2020). Non-neural surface ectodermal rosette formation and F-actin dynamics drive mammalian neural tube closure. *Biochemical and Biophysical Research Communications, 526*(3), 647-653. doi:https://doi.org/10.1016/j.bbrc.2020.03.138